Doctoral Dissertation

Finely Designed Porphyrinoids: Metallocorrinoid Catalysts for Small Molecule Activation and a Porphycene Chromophore with Near-infrared Absorption

(精密に構造設計されたポルフィリノイド：小分子活性化を促進する金属コリノイド触媒および近赤外光吸収能を有するポルフィセンの創製)

January 2019

Ayumu Ogawa

Graduate School of Engineering,
Osaka University

Contents

General Introduction

Porphyrin

Many important reactions in biological systems are performed by metal complexes of tetrapyrrolic macrocycles. In particular, porphyrins (Chart 1a) and the corresponding metal complexes (metalloporphyrins) have attracted great interests because of the various functions in biological events. For example, an Fe(II) complex of protoporphyrin IX (Chart 1b) is widely found in proteins, such as hemoglobin,[1] myoglobin,[2] cytochrome P450[3] and catalase[4] (Figure 1). The former two proteins function as an oxygen-binding/transporting protein, cytochrome P450 is responsible for hydroxylation of C−H bonds in a variety of hydrocarbons, and catalase promotes the disproportionation of hydrogen peroxide to water and dioxygen. As seen in these proteins, porphyrin is one of the most important pigments in biological processes and hence referred to as the "pigment of life".[5] These functions of proteins are derived from the excellent intrinsic properties of porphyrin framework.

Porphyrin is an 18π-conjugated macrocycle, leading to a small HOMO-LUMO gap and strong absorption in UV-vis region. In addition, porphyrin is capable of constructing complexes with a variety of metal ions owing to the large N4 core in the framework. Being inspired by the natural functions and these intrinsic properties, a huge number of researches have gone into employing porphyrins and metalloporphyrins as catalysts and electrochemical/photochemical materials.

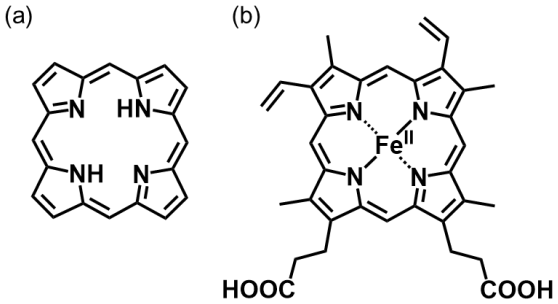

Chart 1. Chemical structure of (a) porphyrin and (b) Fe(II) complex of protoporphyrin IX.

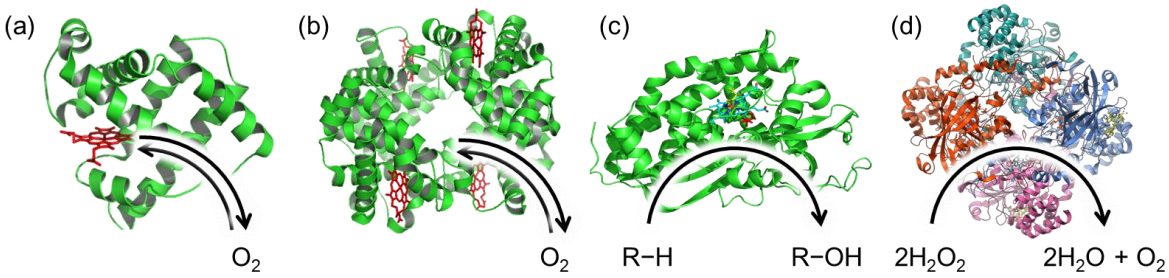

Figure 1. Crystal structures and functions of (a) myoglobin (PDB ID: 1MBN), (b) hemoglobin (PDB ID: 1HGA), (c) cytochrome P450 (PDB ID: 1W0E) and (d) catalase (PDB ID: 1DGB).

Modification of porphyrin

To employ a porphyrin framework as a component of catalysts and materials, modification of macrocycle structure is a promising strategy (Figure 2a). Two common approaches are available: (i) insertion of metal ions into the macrocycle and (ii) introduction of substituents at *meso*-positions and *β*-positions of pyrrole moieties. These synthetically simple and effective strategies are expected to achieve unique physicochemical properties and reactivities. Over the last few decades, porphyrins and metalloporphyrins have been employed in a wide variety of fields by appropriate modification. Figure 2b shows the recent representative examples of functionalized porphyrins as an oxidation catalyst, a reduction catalyst and a photosensitizer. Groves *et al.* reported that a site-selective oxidative fluorination reaction of various simple alkanes and substituted alkanes as well as larger natural-product molecules is achieved with catalytic amounts of a Mn(III) porphyrin complex.[6] In the study, an electron-rich porphyrin ligand activates the high-valent manganese species to promote the oxidation reaction, and the bulky mesityl substituents at the *meso*-positions control the site-selectivity. As a reduction catalyst, Mayer *et al.* demonstrated that introduction of 2-pyridyl substituents to engineer an appropriate proton relay at each *meso*-position of the Fe(III) porphyrin complex enhances the catalytic activity toward electrochemical oxygen reduction reaction.[7] In the field of material chemistry, Nakamura *et al.* found that π-extended porphyrin works as an excellent donor molecule in organic photovoltaic devices.[8] Annulation of benzene molecules at each *β*-position of pyrrole moieties induces the strong absorption in visible region, and increases the crystallinity of the molecule. Besides these efforts, a lot of examples have been reported as the applications including a C−H bond activation catalyst,[9] a small molecule activation catalyst,[10] a photosensitizer of solar cells[11-12] and photodynamic therapy,[13] as well as a cofactor of artificial metalloenzymes.[14-16]

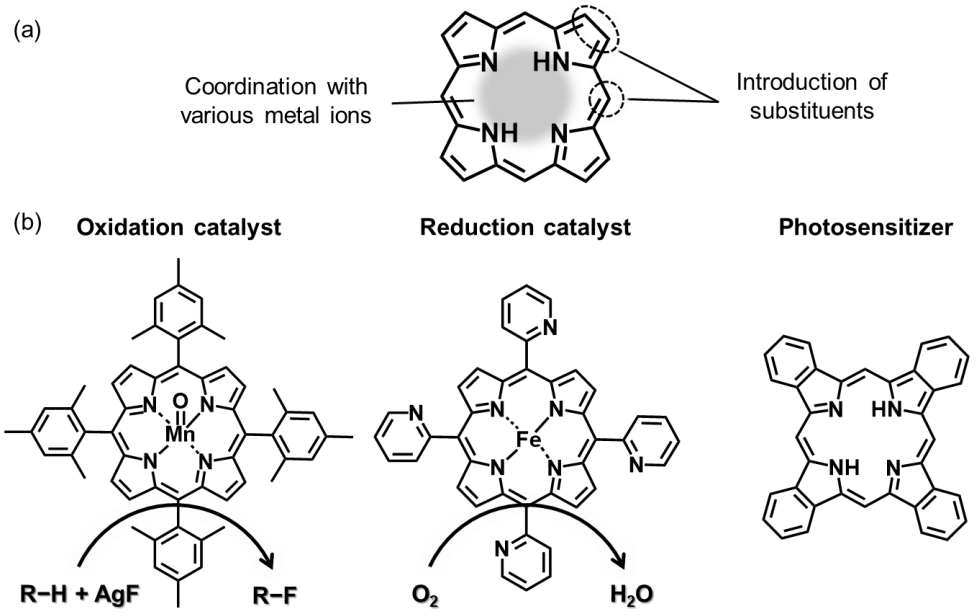

Figure 2. (a) Strategies for modification of the porphyrin framework and (b) representative examples of previous works that utilize functionalized porphyrins.

Porphyrin derivatives in nature

"Porphyrinoids", tetrapyrrolic macrocycles that structurally related to porphyrin, are also found in nature as the ligands of the metal complexes. For example, cobalamin consists of the Co(II) complex with a corrin framework (Figure 3a), which lacks one of the *meso*-position carbons as seen in the porphyrin framework and all *β*-positions of pyrrole moieties are saturated. This natural cofactor acts as a catalyst for essential reactions in biological events, such as methyl group transfer, 1,2-rearrangement and dehalogenation.[17-19] A low-valent cobalt species, a common key intermediate in the enzymatic reactions dependent on cobalamin, is stabilized by a monoanionic corrin framework, leading to regulation of the reactivity. Mg(II) complexes of chlorophylls, pigments in photosynthesis to absorb sunlight energy, contain a chlorin macrocycle in the structure (Figure 3b).[20,21] One of the *β*-positions of pyrrole moieties in the porphyrin framework is saturated in the macrocycle of chlorin. Owing to the partially saturated structure, chlorophylls show stronger absorption in longer wavelength region relative to porphyrin, which reaches absorption maximum in 800–900 nm. These natural systems demonstrate that modification of porphyrin backbone has a great potential to provide significant changes in physicochemical properties. These biological systems containing a series of porphyrinoid frameworks have encouraged researchers to synthesize artificial porphyrinoids, which are largely classified into two types: cobalamin-related porphyrinoids and constitutional isomers of porphyrin. To date, a number of efforts for syntheses, investigations of physicochemical property and reactivity of artificial porphyrinoids have been reported.

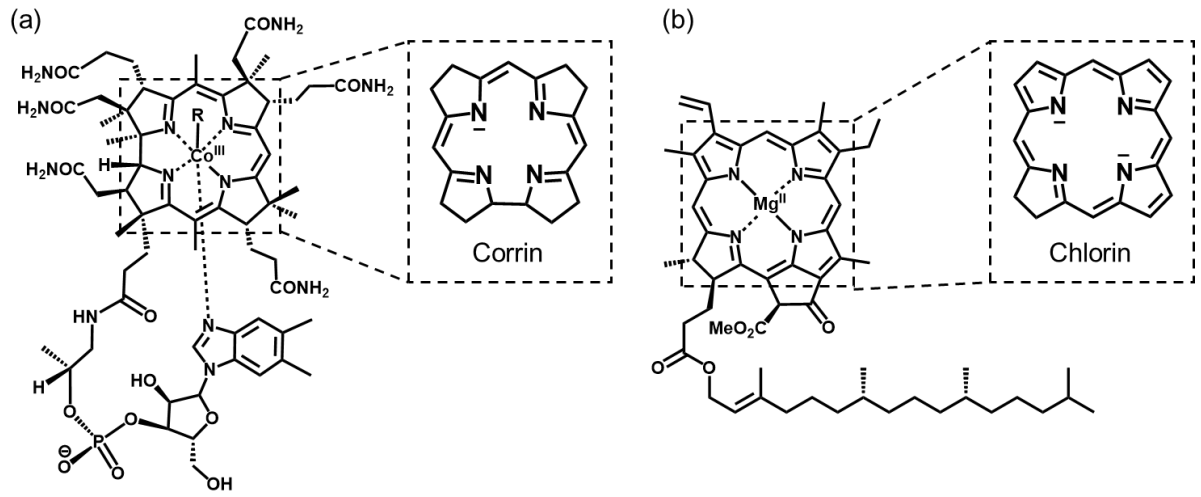

Figure 3. (a) Chemical structure of cobalamin and deprotonated structure of corrin. (b) Chemical structure of chlorophyll *a* and deprotonated structure of chlorin.

Cobalamin-related porphyrinoids

Corrole (Chart 2a) is one of the well-known porphyrinoids and possesses a similar structure to the corrin ring of cobalamin. Corrole lacks one carbon a tom at the *meso*-position compared to porphyrin and bears a direct pyrrole-pyrrole linkage, resulting in a trianionic ligand character. This structural feature provides fundamentally different coordination behavior relative to dianionic porphyrin ligand. In particular, a high-valent metal species in the metal complex of corrole is effectively stabilized by the trianionic corrole ligand owing to the high electron-donating ability. The first synthesis of corrole was achieved by Kay *et al.* in 1964,[22] and the growth of corrole chemistry has been accelerated since Gross *et al.*[23,24] and Paolesse *et al.*[25,26] reported efficient synthetic methods of *meso*-substituted corrole derivatives from the pyrrole and benzaldehyde precursors. The pioneering works have largely prompted optimizations of the corrole synthesis, [27-29] and recently a various *meso*-substituted corrole derivatives are synthesized by nearly one-pot procedure (Scheme 1a). Owing to the efficient synthesis and the unique coordination chemistry, corroles and the corresponding metal complexes have been well-studied and widely utilized in a variety of fields such as catalysis, sensing, dye-sensitized solar cells, photoactive arrays, and medicinal applications.[10,30-33] According to SciFinder®, over 1700 publications about corrole chemistry are now available.

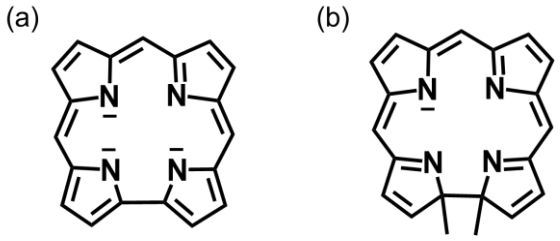

Chart 2. Deprotonated structures of (a) corrole and (b) tetradehydrocorrin as cobalamin-related porphyrinoids.

Another cobalamin-related porphyrinoid is 1,19-disubstituted tetradehydrocorrin (Chart 2b). Four β-positions of pyrrolic moieties of the corrin ring are unsaturated in tetradehydrocorrin, and thus the structure of tetradehydrocorrin is closely related to that of corrin. Due to the structural relationship, the freebase structure of tetradehydrocorrin possesses only one pyrrole-type hydrogen, leading to the monoanionic ligand character as similar to corrin. Therefore, tetradehydrocorrin is capable of stabilizing a low-valent metal species and thus cobalt complexes of tetradehydrocorrin derivatives are of particular interest as an analogue of cobalamin. The first synthesis of cobalt tetradehydrocorrin complex was demonstrated by Dolphin *et al.*,[34] and several studies focusing on the synthesis and physicochemical properties of cobalt and nickel tetradehydrocorrins have been reported.[35-38] Although interesting properties derived from the monoanionic ligand character are expected, the investigation of tetradehydrocorrin metal complexes toward its reactivity has been quite limited except for the artificial enzyme models reported by Hayashi *et al.*,[39,40] because of the multistep synthesis (Scheme 1b) and difficulty in functionalization at the *meso*-positions.

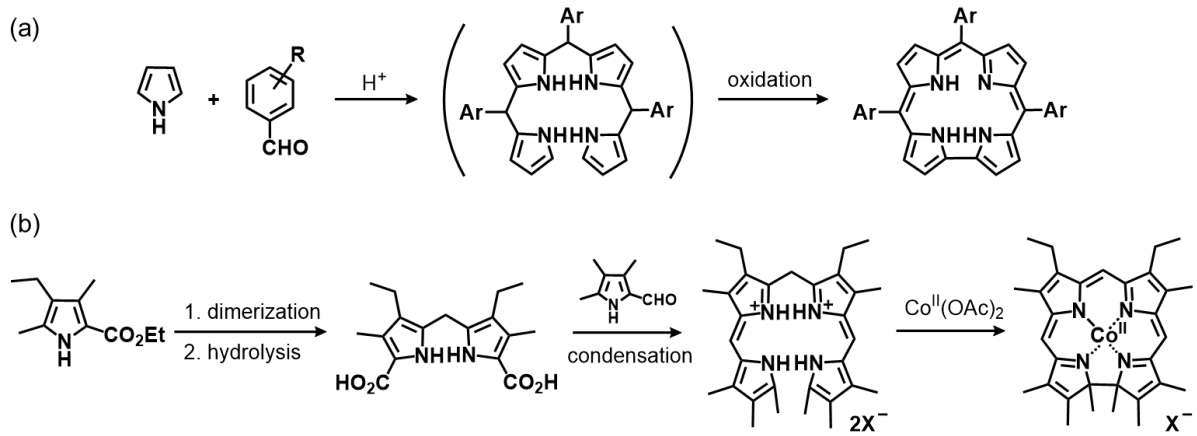

Scheme 1. (a) Synthesis of *meso*-substituted corrole reported by Gryko *et al*.[27] (b) Synthesis of tetradehydrocorrin cobalt complex reported by Dolphin *et al*.[35]

Constitutional isomers of porphyrin

Theoretically, porphyrin has seven constitutional isomers.[41] Previously, porphycene,[42] corrphycene,[43] hemiporphycene[44] and isoporphycene[45] have been successfully synthesized in contrast to other unstable three isomers (Figure 4).[41] However, the preparation of isoporphycene is achieved only via nickel or palladium-templated cyclization with quite low yield, resulting in the bottleneck of investigations.[46-48] Although several researches are available for corrphycene[49-52] and hemiporphycene,[48,52-55] porphycene and its derivatives are of particular interest among the porphyrin isomers owing to the attractive physicochemical properties, such as high stability, strong absorption in visible region, and coordination ability with various metal ions. The unique properties of porphycene have prompted preparation of a variety of porphycene derivatives,[56] and investigations as a catalyst,[57,58] precursor of materials,[59] photosensitizer of photodynamic therapy,[60,61] as well as a cofactor of enzymes.[62-65] However, almost modifications of the porphycene framework in those works are performed at the β-positions of the pyrrole moieties. Although introduction of functional groups at the ethylene-bridged positions (*meso*-positions) promises further regulation of the properties, those examples are quite rare because of the synthetic difficulty.[66-68]

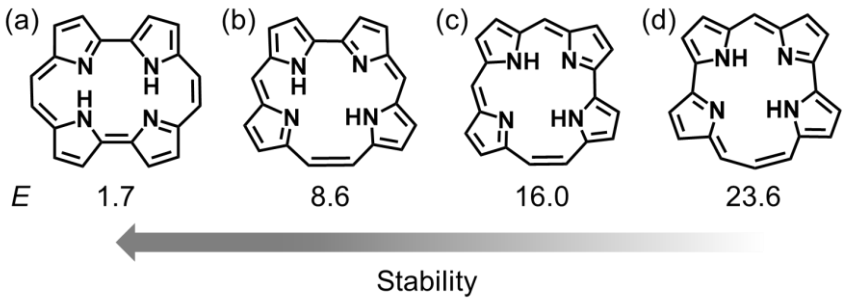

Figure 4. Chemical structures of (a) porphycene, (b) corrphycene (c) hemiporphycene and (d) isoporphycene as constitutional isomers of porphyrin with their energies relative to porphyrin (kcal·mol^{-1}).[41]

Outline of this thesis

According to the previous findings, the author has focused on tetradehydrocorrin and porphycene as potential candidates for unique characters by overcoming the synthetic difficulty in modification. Based on those frameworks, three molecules were designed and investigated. In Chapters 1 and 2, cobalt complexes of two types of monoanionic porphyrinoids were synthesized and employed as catalysts for small molecule activation. In Chapter 3, π-extended porphycene was synthesized and the physicochemical properties were evaluated.

Chapter 1: Synthesis of cobalt tetradehydrocorrin and evaluation of the reactivity of the low-valent species[69]

A *meso*-substituted cobalt(II) tetradehydrocorrin complex (**Co(II)TDHC**) has been synthesized and the reactivity of the low-valent species was investigated. Cyclic voltammetric measurements show that the $E_{1/2}$ of $Co^{II/I}$ redox couple in **Co(II)TDHC** is positively shifted by 0.75 V compared to cobalt(II) complex of dianionic tetraphenylporphyrin (**Co(II)TPP**), indicating that Co(I) species in **CoTDHC** is significantly stabilized by the monoanionic tetradehydrocorrin ligand. Controlled-potential electrolysis experiments under CO_2 in the presence of H_2O reveal that significantly stabilized Co(I) species promotes thermodynamically favored H_2 evolution rather than CO_2 reduction.

Chapter 2: Synthesis of cobalt bipyricorrole and electrochemical CO_2 reduction with a small overpotential value[70]

A cobalt(II) complex of a monoanionic bipyricorrole ligand (**Co(II)BIPC**) has been newly synthesized to improve the catalytic activity toward CO_2 reduction. Electrochemical measurements of **Co(II)BIPC** demonstrates that **Co(II)BIPC** promotes a selective CO_2-to-CO electroreduction owing to the reactive Co(I) species relative to **Co(II)TDHC**. Moreover, catalytic Tafel plots show that **Co(II)BIPC** catalyzes CO_2 reduction reaction with 0.35 V smaller overpotential than **Co(II)TPP**, indicating that the monoanionic ligand is useful as a component of CO_2 reduction catalyst.

Chapter 3: Synthesis, structure and chemical properties of *meso*-dibenzoporphycene[71]

meso-Dibenzoporphycene (**mDBPc**), possessing two benzene-fused *meso*-positions, has been synthesized and fully characterized. Electrochemical measurements indicate that **mDBPc** has significantly small HOMO-LUMO gap, resulting in 418 nm of bathochromic shift of Q-band compared to unsubstituted porphycene in UV-vis-NIR spectra. Furthermore, it is notable that X-ray photoelectron spectroscopic measurement and theoretical study support the presence of a *cis* tautomeric form in the ground state of **mDBPc**, despite the fact that all known porphycene derivatives adopt the *trans* tautomeric form.

References

1. M. F. Perutz, M. G. Rossmann, A. F. Cullis, H. Muirhead and G. Will, *Nature* 1960, **185**, 416-422.
2. J. C. Kendrew, G. Bodo, H. M. Dintzis, R. G. Parrish and H. Wyckoff, *Nature* 1958, **181**, 662-666.
3. P. R. Ortiz de Montellano, *Chem. Rev*. 2010, **110**, 932-948.
4. I. Fita and M. G. Rossmann, *J. Mol. Biol*. 1985, **185**, 21-37.
5. A. R. Battersby, C. J. R. Fookes, G. W. J. Matcham and E. Mcdonald, *Nature* 1980, **285**, 17-21.
6. W. Liu, X. Huang, M.-J. Cheng, R. J. Nielsen, W. A. Goddard III and J. T. Groves, *Science* 2012, **337**, 1322-1326.
7. B. D. Matson, C. T. Carver, A. V. Ruden, J. Y. Yang, S. Raugei and J. M. Mayer, *Chem. Commun*. 2012, **48**, 11100-11102.
8. Y. Matsuo, Y. Sato, T. Niinomi, I. Soga, H. Tanaka and E. Nakamura, E. *J. Am. Chem. Soc*. 2009, **131**, 16048-16050.
9. H. Lu and X. P. Zhang, *Chem. Soc. Rev.* 2011, **40**, 1899-1909.
10. W. Zhang, W. Lai and R. Cao, *Chem. Rev*. 2017, **117**, 3717-3797.
11. L.-L. Li and W.-G. Diau, *Chem. Soc. Rev*. 2013, **42**, 291-304.
12. M. Urbani, M. Grätzel, M. K. Nazeeruddin and T. Torres, *Chem. Rev*. 2014, **114**, 12330-12396.
13. M. Ethirajan, Y. Chen, P. Joshi and R. K. Pandey, *Chem. Soc. Rev*. 2011, **40**, 340-362.
14. T. Hayashi, Y. Hitomi, T. Ando, T. Mizutani, Y. Hisaeda, S. Kitagawa and H. Ogoshi, *J. Am. Chem. Soc*. 1999, **121**, 7747-7750.
15. Y.-B. Cai, S.-Y. Yao, M. Hu, X. Liu and J.-L. Zhang, *Inorg. Chem. Front.* 2016, **3**, 1236-1244.
16. P. Dydio, H. M. Key, A. Nazarenko, J. Y.-E. Rha, V. Seyedkazemi, D. S. Clark and J. F. Hartwig, *Science* 2016, **354**, 102-107.
17. K. Gruber, B. Puffer and B. Kräutler, B. *Chem. Soc. Rev*. 2011, **40**, 4346-4363.
18. R. G. Matthews, *Acc. Chem. Res*. 2001, **34**, 681-689.
19. W. Buckel and B. T. Golding, *Chem. Soc. Rev*. 1996, **25**, 329-337.
20. R. B. Woodward, W. A. Ayer, J. M. Beaton, F. Bickelhaupt, R. Bonnett, P. Buchschacher, G. L. Closs, H. Dutler, J. Hannah, F. P. Hauck, S. Ito, A. Langemann, E. L. Goff, W. Leimgruber, W. Lwowski, J. Sauer, Z. Valenta and H. Volz, *Tetrahedron* 1990, **46**, 7599-7659.
21. G. McDermott, S. M. Price, A. A. Freer, A. M. Hawthornthwaite-Lawless, M. Z. Papiz, R. J. Cogdell and N. W. Isaacs, *Nature* 1995, **374**, 517-521.
22. A. W. Johnson and I. T. Kay, *Proc. Chem. Soc.* 1964, 89-90.
23. Z. Gross, N. Galili, L. Simkhovich, I. Saltman, M. Botoshansky, D. Bläser, R. Boese and I. Goldberg, *Org. Lett.* 1999, **1**, 599-602.
24. Z. Gross, N. Galili and I. Saltsman, *Angew. Chem., Int. Ed.* 1999, **38**, 1427-1429.
25. R. Paolesse, L. Jaquinod, D. J. Nurco, S. Mini, F. Sagone, T. Boschi and K. M. Smith, *Chem. Commun.* 1999,

1307-1308.

26. R. Paolesse, S. Nardis, F. Sagone and R. G. Khoury, *J. Org. Chem*. 2001, **66**, 550-556.
27. B. Koszarna and D. T. Gryko, *J. Org. Chem*. 2006, **71**, 3707-3717.
28. C. R. Geier III, J. F. B. Chick, J. B. Callinan, C. G. Reid and W. P. Auguscinski, *J. Org. Chem.* 2004, **69**, 4159-4169.
29. J.-W. Ka, W.-S. Cho and C.-H. Lee, *Tetrahedron Lett.* 2000, **41**, 8121-8125.
30. T. Matsuo, A. Hayashi, M. Abe, T. Matsuda, Y. Hisaeda and T. Hayashi, *J. Am. Chem. Soc.* **2009**, *131*, 15124-15125.
31. I. Aviv and Z. Gross, *Chem. Commun*. 2007, 1987-1999.
32. L. Flamigni and D. T. Gryko, *Chem. Soc. Rev.* 2009, **38**, 1635-1646.
33. A. Haber and Z. Gross, *Chem. Commun*. 2015, **51**, 5812.
34. D. Dolphin, R. L. N. Harris, J. L. Huppatz, A. W. Johnson and I. T. Kay, *J. Chem. Soc. C*. 1966, 30-40.
35. C.-J. Liu, A. Thompson and D. Dolphin, *J. Inorg. Biochem.* 2001, **83**, 133-138.
36. Y. Murakami, Y. Aoyama and K. Tokunaga, *J. Am. Chem. Soc*. 1980, **102**, 6736-6744.
37. Y. Murakami, K. Sakata, Y. Tanaka and T. Matsuo, *Bull. Chem. Soc. J*. 1975, **48**, 3622-3630.
38. N. S. Hush, I. S. Woolsey, *J. Am. Chem. Soc*. 1972, **94**, 4107-4114.
39. Y. Morita, K. Oohora, A. Sawada, T. Kamachi, K. Yoshizawa, T. Hayashi, *Inorg. Chem*. 2017, **56**, 1950-1955.
40. Y. Morita, K. Oohora, A. Sawada, K. Doitomi, J. Ohbayashi, T. Kamachi, K. Yoshizawa, Y. Hisaeda, T. Hayashi, *Dalton Trans*. 2016, **45**, 3277-3284.
41. E. Vogel, M. Bröring, J. Fink, D. Rosen, H. Schmickler, J. Lex, K. W. K. Chan, Y.-D. Wu, D. A. Plattner, M. Nendel and K. N. Houk, *Angew. Chem. Int. Ed*. 1995, **34**, 2511-2514.
42. E. Vogel, M. Köcher, H. Schmickler and J. Lex, *Angew. Chem. Int. Ed.* 1986, **25**, 257-259.
43. J. L. Sessler, E. A. Brucker, S. J. Weghorn, M. Kisters, M. Schäfer, J. Lex and E. Vogel, *Angew. Chem. Int. Ed*. 1994, **33**, 2308-2312.
44. E. Vogel, M. Bröring, S. J. Weghorn, P. Scholz, R. Deponte, J. Lex, H. Schmickler, K. Schaffner, S. E. Braslavsky, M. Müller, S. Pörting, C. J. Fowler and J. L. Sessler, *Angew. Chem. Int. Ed*. 1997, **36**, 1651-1654.
45. E. Vogel, M. Bröring, C. Erben, R. Demuth, J. Lex, M. Nendel and K. N. Houk, *Angew. Chem. Int. Ed*. 1997, **36**, 353-357.
46. E. Vogel, P. Scholz, R. Demuth, C. Erben, M. Bröring, H. Schmickler, J. Lex, G. Hohlneicher, D. Bremm and Y.-D. Wu, *Angew. Chem. Int. Ed*. **1999**, *38*, 2919-2923.
47. D. Bremm, J. Lex and G. Hohlneicher, *J. Mol. Struct.: THEOCHEM* 2007, **802**, 45-52.
48. J. P. Gisselbrecht, M. Gross, E. Vogel, P. Scholz, M. Bröring and J. L. Sessler, *J. Electroanal. Chem.* 2001, **507**, 244-249.
49. S. Neya, K. Imai, Y. Hiramatsu, T. Kitagawa, T. Hoshino, M. Hata and N. Funasaki, *Inorg. Chem*. 2006, **45**, 4238-4242.

50. S. Neya, T. Hoshino, M. Hata and N. Funasaki, *Chem. Lett*. 2004, **33**, 114-115.
51. M. Fujitsuka, H. Shimakoshi, Y. Tei, K. Noda, S. Tojo, Y. Hisaeda and T. Majima, *Phys. Chem. Chem. Phys*. 2013, **15**, 5677-5683.
52. C. J. Fowler, J. L. Sessler, V. M. Lynch, J. Waluk, A. Gebauer, J. Lex, A. Heger, F. Zuniga-y-Rivero and E. Vogel, *Chem. Eur. J*. 2002, **8**, 3485-3496.
53. S. Neya, K. Imai, H. Hori, H. Ishikawa, K. Ishimori, D. Okuno, S. Nagatomo, T. Hoshino, M. Hata and N. Funasaki, *Inorg, Chem.* 2003, **42**, 1456-1461.
54. Y. Fang, F. Mandoj, S. Nardis, G. Pomarico, M. Stefanelli, D. O. Cicero, S. Lentini, A. Vecchi, Y. Cui, L. Zeng, K. M. Kadish and R. Paolesse, *Inorg. Chem.* 2014, **53**, 7404-7415.
55. M. Fujitsuka, H. Shimakoshi, S. Tojo, L. Cheng, D. Maeda, Y. Hisaeda and T. Majima, *J. Phys. Chem. A* 2010, **114**, 4156-4162.
56. D. Sánchez-Garcia and J. L. Sessler, *Chem. Soc. Rev*. 2008, **37**, 215-232.
57. T. Hayashi, K. Okazaki, N. Urakawa, H. Shimakoshi, J. L. Sessler, E. Vogel and Y. Hisaeda, *Organometallics* 2001, **20**, 3074-3078.
58. W.-C. Lo, C.-M. Che, K.-F. Cheng and T. C. W. Mak, *Chem. Commun.* 1997, 1205-1206.
59. J.-M. Barbe, P. Richard, M. A. Aukauloo, C. Lecomte, P. Petit and R. Guilard, *J. Chem. Soc. Chem. Commun*. 1994, 2757-2758.
60. S. E. Braslavsky, M. Müller, D. O. Mártire, S. Pörting, S. G. Bertolotti, S. Chakravorti, G. Koç-Weier, B. Knipp and K. Schaffner, *J. Photochem. Photobiol. B* 1997, **40**, 191-198.
61. A. Rana and P. K. Panda, *Org. Lett.* 2014, **16**, 78-81.
62. T. Hayashi, H. Dejima, T. Matsuo, H. Sato, D. Murata and Y. Hisaeda, *J. Am. Chem. Soc*. 2002, **124**, 11226-11227.
63. K. Oohora, Y. Kihira, E. Mizohata, T. Inoue and T. Hayashi, *J. Am. Chem. Soc*. 2013, **135**, 17282-17285.
64. K. Oohora, H. Meichin, L. Zhao, M. W. Wolf, A. Nakayama, J. Hasegawa, N. Lehnert and T. Hayashi, *J. Am. Chem. Soc*. 2017, **139**, 17265-17268.
65. K. Oohora, H. Meichin, Y. Kihira, H. Sugimoto, Y. Shiro and T. Hayashi, *J. Am. Chem. Soc*. 2017, **139**, 18460-18463.
66. E. Vogel, M. Köcher, J. Lex and O. Ermer, *Isr. J. Chem*. 1989, **29**, 257-266.
67. D. Kuzuhara, H. Yamada, K. Yano, T. Okujima, S. Mori and H. Uno, *Chem. Eur. J*. 2011, **17**, 3376-3383.
68. K. S. Anju, S. Ramakrishnan, A. P. Thomas, E. Suresh and A. Srinivasan, *Org. Lett*. 2008, **10**, 5545-5548.
69. A. Ogawa, K. Oohora and T. Hayashi, *Inorg. Chem*. 2018, **57**, 14644-14652.
70. A. Ogawa, K. Oohora, W. Gu and T. Hayashi, *Chem. Commun*. In press. DOI: 10.1039/C8CC08876D
71. K. Oohora, A. Ogawa, T. Fukuda, A. Onoda, J. Hasegawa and T. Hayashi, *Angew. Chem. Int. Ed.* 2015, **54**, 6227-6230.

Chapter 1
Synthesis of cobalt tetradehydrocorrin and evaluation of the reactivity of the low-valent species

1-1. Introduction

Cobalamin plays important roles in biological systems as a cofactor of metalloenzymes which catalyze essential reactions such as methyl group transfer, 1,2-rearrangement and dehalogenation.[1-5] A low-valent cobalt species, a common key intermediate in the enzymatic reactions with cobalamin, is stabilized by a monoanionic macrocyclic corrin framework (Chart 1-1b), which lacks one of the *meso*-position carbons as seen in the dianionic porphyrin framework (Chart 1-1a). Tuning the valency of a series of porphyrinoid frameworks is an essential strategy used in regulation of the reactivity of the metal center, resulting in catalysis of a broad range of reactions in biological systems. Thus, it is of particular interest to synthesize a porphyrinoid-type monoanionic ligand and to study the reactivity of its cobalt complex. Previously, Dolphin demonstrated the synthesis of 1,19-disubstituted tetradehydrocorrin (Chart 1-1c) as an analog of cobalamin,[6] and several additional studies have been reported focusing on the synthesis and physicochemical properties of cobalt tetradehydrocorrin derivatives.[7] However, investigations of the reactivity of cobalt tetradehydrocorrin derivatives have been quite limited, except for the artificial enzyme models reported by our group.[8] In this context, the author attempted to evaluate the reactivity of the low-valent cobalt species using a structurally modified cobalt tetradehydrocorrin complex.

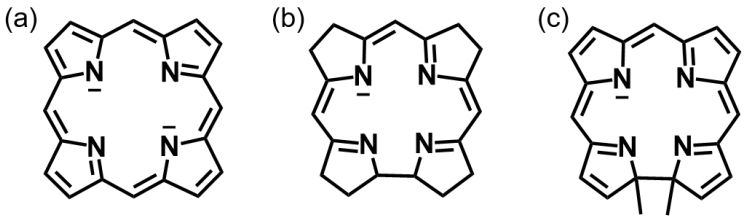

Chart 1-1. Deprotonated structures of (a) porphyrin, (b) corrin and (c) tetradehydrocorrin.

In order to evaluate the reactivity of the low-valent cobalt species, the author has focused on reductive catalytic conversions of small molecules such as carbon dioxide (CO_2) reduction and hydrogen (H_2) evolution. A variety of investigations into H_2 evolution have been carried out using cobalt macrocyclic complexes consisting of cobalt cyclams, cobaloxymes and cobalt porphyrins, among others.[9-13] It is known that cobalt complexes can function as useful and practical catalysts for CO_2 reduction because they are relatively inexpensive.[14-19] In particular, cobalt porphyrin complexes have been reported to function as CO_2 reduction catalysts.[20-22] Although cobalt complexes of

other porphyrinoids including phthalocyanine[23] and corrole[24] have also been evaluated as CO_2 reduction catalysts, significantly negative potentials to generate a low-valent metal species are required, and low product selectivities were observed for these catalysts due to competition between CO_2 and proton reductions. In contrast, a strategy to easily stabilize the low-valent metal species should provide important insights into achieving high catalytic activity and product selectivity. On this point, investigations of cobalamin and its derivatives as a homogeneous catalyst for CO_2 photoreduction have been demonstrated.[25] However, the catalytic reaction provides a mixture of H_2, CO and formic acid, and the dependency of catalytic activity and the product selectivity on the ligand valency has not yet been defined. Therefore, the author has focused on a monoanionic tetradehydrocorrin framework, which is able to further promote efficient formation of the low-valent cobalt species for small molecule activation, compared to cobalt complexes with highly saturated corrin frameworks or well-known porphyrins providing a typical dianionic ligand framework. In the present study, the author have designed, synthesized and characterized the *meso*-aryl substituted cobalt tetradehydrocorrin complex shown in Chart 1-2 to evaluate the electrochemical behavior under a CO_2 atmosphere.

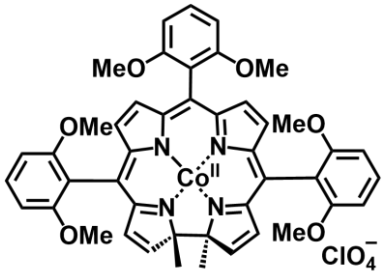

Co(II)TDHC
(+ enantiomer)

Chart 1-2. Chemical structure of **Co(II)TDHC**.

1-2. Results and discussion

Molecular design and synthesis of Co(II)TDHC

For achieving effective CO_2 reduction, it is necessary to design a finely tuned catalyst considering access of substrate,[26] facilitation of proton transfer,[27,28] and inhibition of catalyst dimerization.[29] To address these structural requirements, the author took advantage of the properties of the proximal methoxy group, employing it as a pendant Lewis base, because a similar pendant Lewis base is known to promote cleavage of a C–OH bond of protonated CO_2 in a reaction intermediate via engineering of a hydrogen bond between metallocarboxylic acid ($M–CO_2H$) and the methoxy group of the peripheral ligand substituent.[30] Based on this work, our group has recently designed a cobalt(II) tetradehydrocorrin (**Co(II)TDHC**) complex modified with 1,3-dimethoxybenzene moieties at the *meso*-positions (Chart 1-2). The synthesis of **Co(II)TDHC** is depicted in Scheme 1-1. The target molecule was achieved via 6 steps. First, commercially available 1,3-dimethoxybenzene was formylated and the subsequent reaction with

pyrrole in the presence of trifluoroacetic acid afforded dipyrromethane **2**. A Vilsmeier-Haack reaction of compound **2** gave mono-formylated compound **3**. Compound **4** was then obtained via a Wolf-Kishner reaction of compound **3**, and subsequent acid-catalyzed coupling with compound **1** afforded tetrapyrrole **5**. Finally, cobalt-templated oxidative cyclization of tetrapyrrole **5** produced **Co(II)TDHC** in an 18% yield. Typically, *meso*-unsubstituted or *meso*-methyl substituted tetradehydrocorrin derivatives have been synthesized through acid-catalyzed intermolecular coupling of the corresponding 2,2′-dicarboxybipyrromethane and 2-formylpyrrole followed by metal-templated cyclization.[6,7a] In the case of *meso*-aryl substituted tetradehydrocorrin, however, this method could not be applied to prepare the corresponding biladiene because of severe steric hindrance around the carbonyl group in the pyrrole precursor.[31] The author is unaware of any reports of synthesis of *meso*-aryl substituted tetradehydrocorrin derivatives despite the broad versatility available for functionalization of the tetradehydrocorrin framework. To the best of our knowledge, this is the first example of synthesis of a *meso*-aryl substituted tetradehydrocorrin. The author also attempted to prepare *meso*-phenyl substituted tetradehydrocorrin and *meso*-mesityl substituted tetradehydrocorrin as reference compounds, but was not successful because of their low stability to promote the spontaneous demetallation. Thus, the effect of proximal methoxy groups toward electrochemical reaction is not evaluated in this paper. However, 1,3-dimethoxybenzene moiety at *meso*-positions seems to be important to maintain the macrocyclic structure of *meso*-aryl substituted cobalt tetradehydrocorrins.

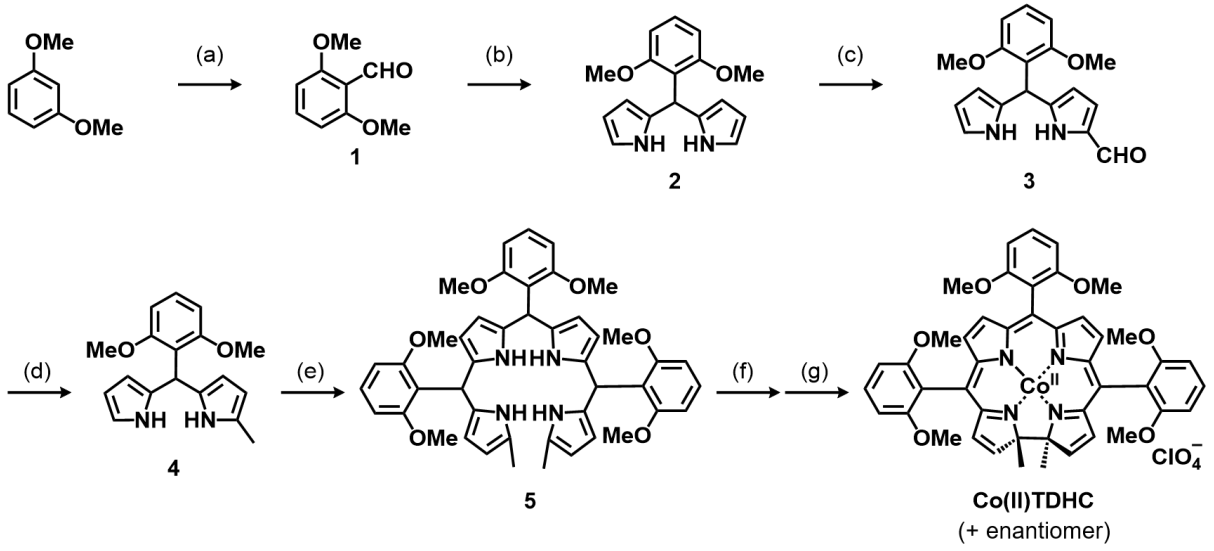

Scheme 1-1. Synthesis of **Co(II)TDHC**. (a) TMEDA, ^{n}BuLi, DMF, THF, 88%; (b) pyrrole, TFA, 71%; (c) $POCl_3$, DMF, 69%; (d) $H_2NNH_2{\cdot}H_2O$, KOH, ethylene glycol, 84%; (e) **1**, HCl, CH_3OH, H_2O, 47%; (f) $Co(OAc)_2{\cdot}4H_2O$, *p*-chloranil, CH_2Cl_2, CH_3OH; (g) $HClO_4$, H_2O, CH_2Cl_2, 18% in 2 steps. TMEDA = *N*,*N*,*N*′,*N*′-tetramethylethylenediamine, TFA = trifluoroacetic acid.

X-ray crystal structure

A single crystal of **Co(II)TDHC** was successfully obtained from a solution of hexane/CH_2Cl_2 (*v*/*v* = 1/1) by vapor diffusion. The structure of **Co(II)TDHC** was unambiguously revealed by single crystal X-ray analysis as depicted in Figure 1-1. The cobalt center has a pentacoordinated structure ligated by an oxygen atom of ethyl acetate as a neutral axial ligand and four nitrogen atoms from the tetradehydrocorrin ligand. Since **Co(II)TDHC** possesses two chiral sp^3 carbon atoms at the 1 and 19 positions, **Co(II)TDHC** is a mixture of (1*R*, 19*R*) and (1*S*, 19*S*) enantiomers with a relative population of approximately 0.8 and 0.2, respectively, in the crystal. This ratio is similar to previously reported ratio of a cobalt tetradehydrocorrin derivative.[7a] Furthermore, the aryl groups at the *meso*-positions are nearly perpendicular to the tetradehydrocorrin macrocycle, indicating that the methoxy substituents in the aryl groups are capable of interacting with an external substrate bound to the cobalt atom in the framework.

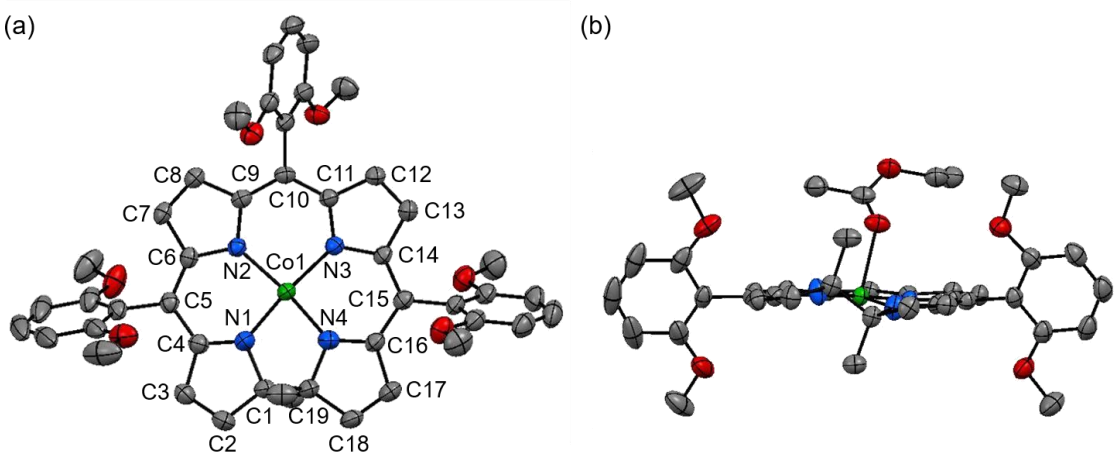

Figure 1-1. X-ray crystal structure of **Co(II)TDHC** with 50% thermal ellipsoid probability. (a) Top view and (b) side view. Hydrogen atoms and the nonbonding counteranion (ClO_4^-) are omitted for clarity and only the (1*R*,19*R*) enantiomer is shown as the major configuration of the disordered groups. Ethyl acetate as a neutral axial ligand in the top view and an aryl group at the 10-position in the side view are also omitted.

Electrochemical/spectroscopic characterization

The redox behaviors of **Co(II)TDHC** under an N_2 atmosphere were evaluated by cyclic voltammetry (CV) using a glassy carbon electrode as the working electrode. All potentials in this paper are reported relative to the Fe(III)/Fe(II) couple at 0.0 V using ferrocene (Fc). In a DMF solution of **Co(II)TDHC**, two reversible peaks were found with $E_{1/2}$ of −0.53 V and −1.70 V (Figure 1-2a). The redox couples are confirmed to be diffusion-controlled process by the CV measurements under the various scan rate conditions (Figures 1-2b – 1-2d). The first redox potential has a slightly positive shift compared to that of *meso*-unsubstituted cobalt tetradehydrocorrin ($E_{1/2}$ ~ −0.65 V).[7b] This result indicates that introduction of an aryl group at each *meso*-position stabilizes the π-electrons of the tetradehydrocorrin macrocycle, resulting in lower electron density, as previously reported for *meso*-tetraphenylporphyrin derivatives.[32-34]

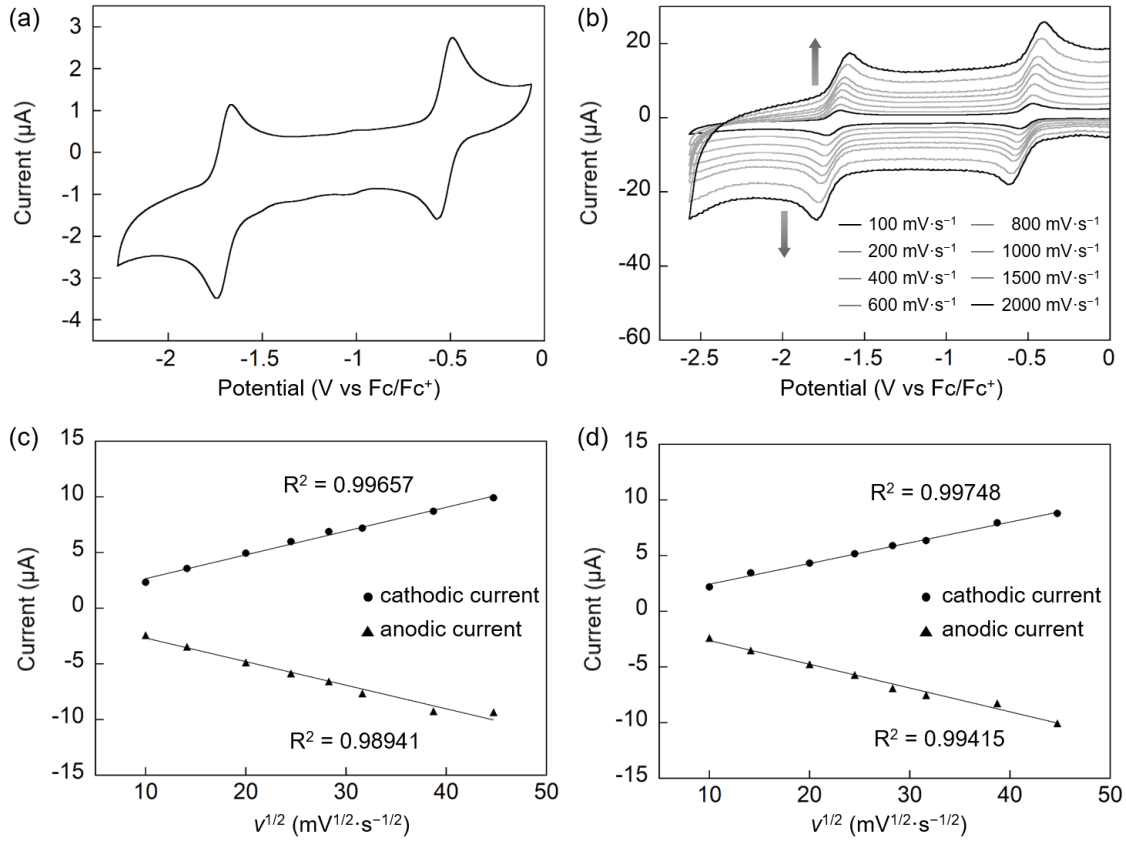

Figure 1-2. (a) CV of **Co(II)TDHC** (0.5 mM) in anhydrous DMF with 0.1 M $TBAPF_6$ at a scan rate of 100 $mV \cdot s^{-1}$ under an N_2 atmosphere. (b) CVs of **Co(II)TDHC** (0.5 mM) in anhydrous DMF with 0.1 M $TBAPF_6$ under an N_2 atmosphere upon increasing a scan rate from 100 to 2000 $mV \cdot s^{-1}$. Plots of (c) first and (d) second redox peak currents against $v^{1/2}$ in the cyclic voltammograms in anhydrous DMF with 0.1 M $TBAPF_6$ under an N_2 atmosphere.

In order to characterize the species generated by one-electron reduction at −0.53 V, the titration experiment with cobaltocene was performed under anaerobic conditions. Cobaltocene is a one-electron reductant with a reduction potential of −1.3 V, which is between the first and second redox potentials of **Co(II)TDHC**.[35] It is known that cobalt tetradehydrocorrin derivatives display significant absorption changes depending on the valency of the cobalt ion.[7a] The UV-vis spectrum of **Co(II)TDHC** shows characteristic absorption peaks at 510 and 615 nm (Figure 1-3a, black dotted line), whereas a new absorption peak at 573 nm appears upon addition of cobaltocene with a concomitant decrease of absorption peaks at 510 and 615 nm via several isosbestic points (Figure 1-3a, black solid line). These changes are similar to those observed in the reduction of the previously reported Co(II) tetradehydrocorrin to Co(I) tetradehydrocorrin.[7a] The reduction of **Co(II)TDHC** using $NaBH_4$ as a reductant was also monitored with the same spectral changes (Figure 1-3b).

EPR spectra of **Co(II)TDHC** were measured at 100 K. Eight hyperfine lines were observed due to the interaction with the Co nucleus ($I = 7/2$) with $g_{//} = 1.99$, supporting the presence of a Co(II) species with the unpaired electron of the Co atom in a low-spin d^7 configuration (Figure 1-3c).[7c,7d] Upon addition of excess $NaBH_4$, the signals

derived from the Co(II) species completely disappear, indicating formation of the Co(I) species (Figure 1-3d).[7d] These results suggest that $NaBH_4$ is capable of reducing **Co(II)TDHC** to **Co(I)TDHC**. The chemical reductions of **Co(II)TDHC** monitored by UV-vis and EPR spectra indicate that the reduction event observed at −0.53 V is attributed to the $[Co^{II}]^+/[Co^{I}]$ couple ($[Co^{II}]$ = **Co(II)TDHC**). Compared to the cobalt complex formed by dianionic tetraphenylporphyrin (**CoTPP**), the redox potential of **Co(II)TDHC** is positively shifted by 750 mV ($E_{1/2}(Co^{II/I})$ of **CoTPP** is −1.28 V) due to the monoanionic ligand. **Co(I)TDHC** is highly stable and can be maintained for a few days even under aerobic conditions. Next, the redox peak at −1.70 V is considered to be attributed not to reduction of the Co(I) species to form the Co(0) species but to reduction of the tetradehydrocorrin ligand to generate $[Co^{I}]^{\bullet-}$, and/or $[Co^{II}]^{-}$ after the one-electron transfer from Co(I) to the ligand, according to a previous report.[7d]

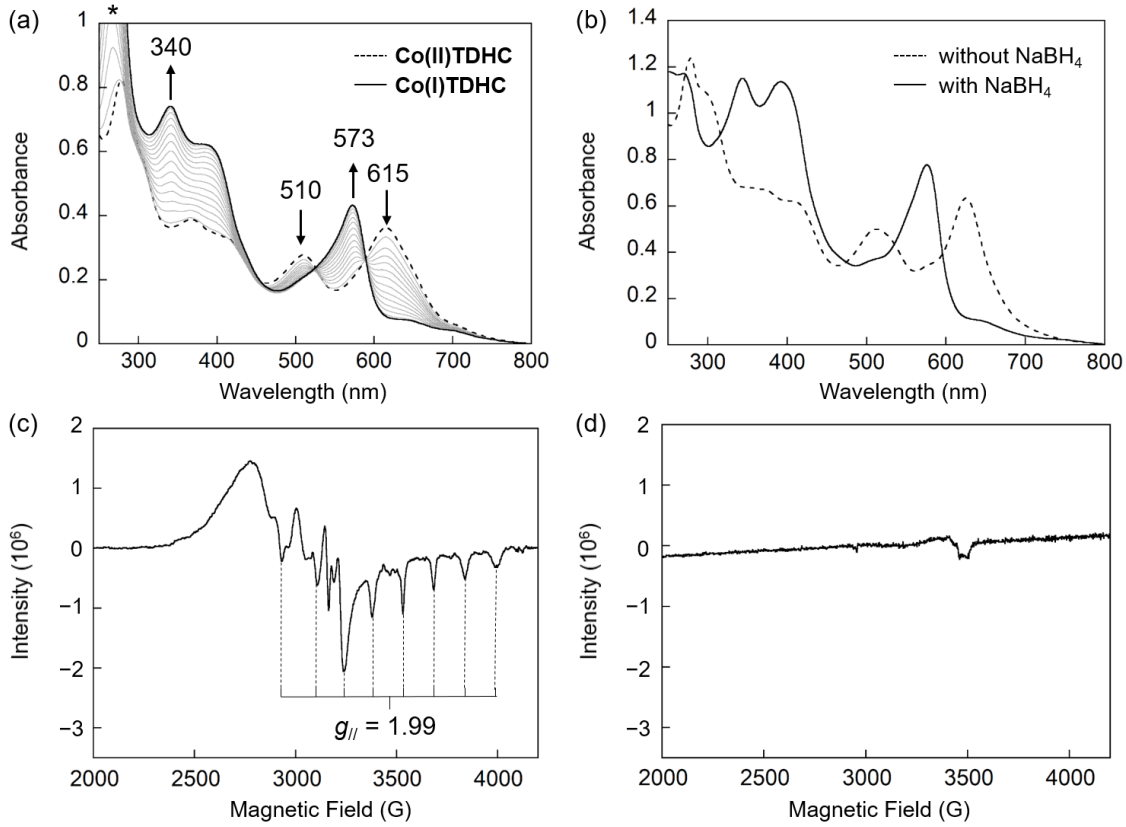

Figure 1-3. (a) Changes in UV-vis absorption spectra of **Co(II)TDHC** (50 μM in CH_2Cl_2) upon addition of cobaltocene ranging from 0 mM (black dashed line) to 0.84 mM (black solid line). Asterisk (*) shows an absorption peak of cobaltocene and cobaltocenium. The absorption peak of cobaltocene at 365 nm was negligible because of the strong absorptions of **Co(II)TDHC** and **Co(I)TDHC**.[35] (b) UV-vis absorption spectra of **Co(II)TDHC** in the absence (dashed line) and presence (solid line) of $NaBH_4$ in THF. (c) EPR spectrum of **Co(II)TDHC** in THF at 100 K. (d) EPR spectrum of **Co(I)TDHC** in THF at 100 K with an excess amount of $NaBH_4$.

Electrochemistry under a CO_2 atmosphere

To investigate the activity of **Co(II)TDHC** for CO_2 reduction, CV measurements were conducted in dry and wet CO_2-saturated DMF ([CO_2] ~ 0.23 M) containing 0.1 M $TBAPF_6$ under a CO_2 atmosphere. As shown in Figure 1-4a, only a small increase of current was observed in an electrochemical solution saturated by CO_2. Under a CO_2 atmosphere, the addition of H_2O to the solution clearly enhances the current after the second reduction process. This result indicates that reductive catalysis occurs in the presence of CO_2 and H_2O after the two-electron reduction of **Co(II)TDHC**. Further addition of H_2O, however, does not cause an increase in current, indicating that the reaction rate of reductive electrolysis does not depend on the concentration of H_2O in the presence of > 5 M H_2O (Figure 1-4b). As a proton source, 2,2,2-trifluoroethanol (TFE) or CH_3OH was also employed. In the case of TFE, a large enhancement of the current was observed in the CV experiment even under an N_2 atmosphere, indicating the H_2 evolution (Figure 1-5). In contrast, addition of CH_3OH under a CO_2 atmosphere also enhanced the current in the CV experiment, whereas negligible increase in the current was observed upon addition of CH_3OH under an N_2 atmosphere (Figure 1-6).[36]

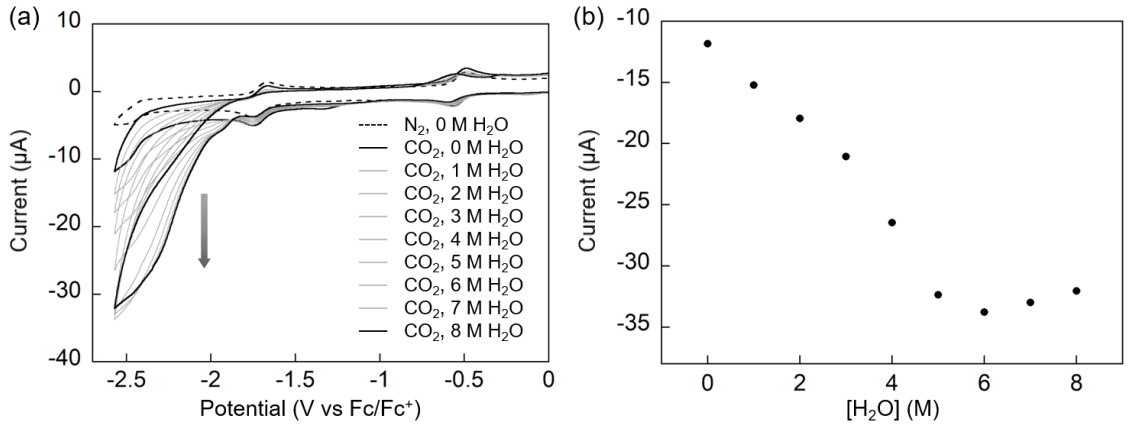

Figure 1-4. (a) CVs of **Co(II)TDHC** (0.5 mM) in dry DMF with 0.1 M $TBAPF_6$ at a scan rate of 100 $mV \cdot s^{-1}$ under an N_2 atmosphere (black dashed line) and upon addition of H_2O under a CO_2 atmosphere: [H_2O] = 0, 1, 2, 3, 4, 5, 6, 7 and 8 M. (b) Relationship between the concentration of H_2O and current at −2.57 V in cyclic voltammetry.

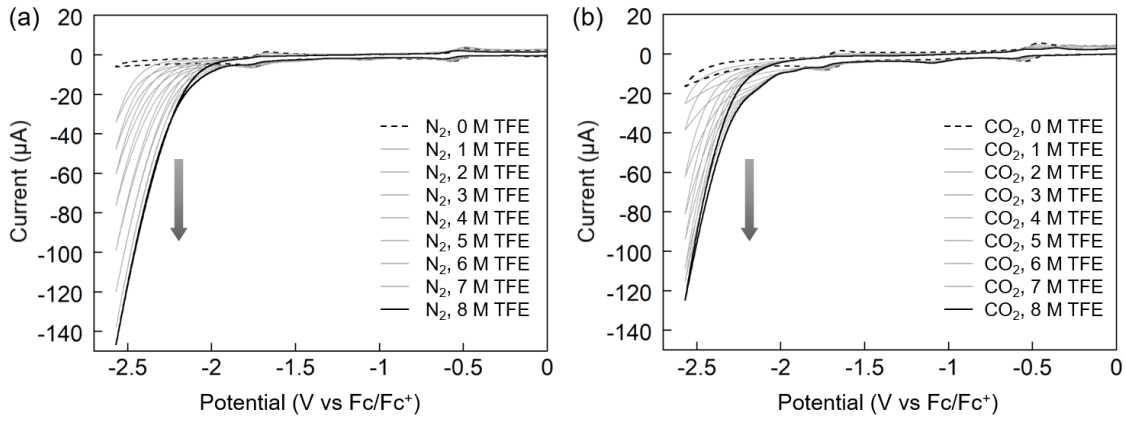

Figure 1-5. CVs of **Co(II)TDHC** (0.5 mM) in DMF with 0.1 M $TBAPF_6$ at a scan rate of 100 $mV \cdot s^{-1}$ under (a) an N_2 atmosphere and (b) a CO_2 atmosphere upon addition of 2,2,2-trifluoroethanol (TFE) ranging from 0 M (black dashed line) to 8 M (black solid line).

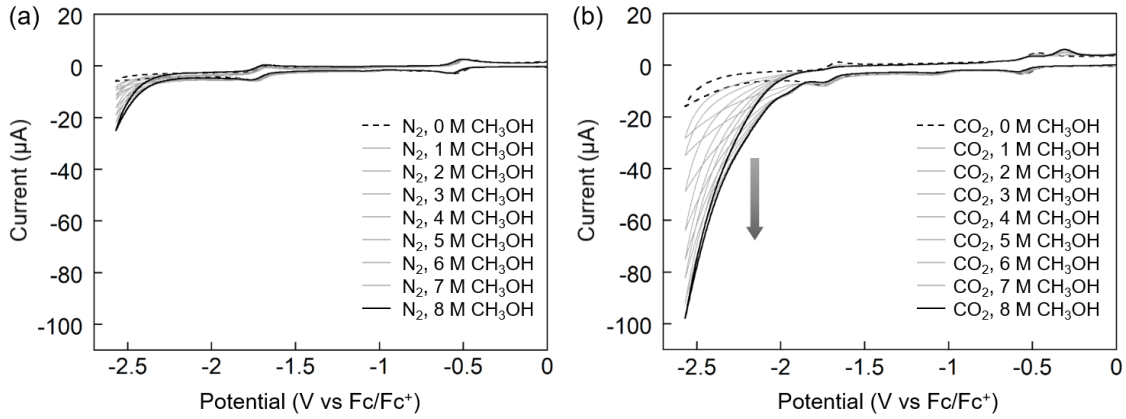

Figure 1-6. CVs of **Co(II)TDHC** (0.5 mM) in DMF with 0.1 M $TBAPF_6$ at a scan rate of 100 $mV \cdot s^{-1}$ under (a) an N_2 atmosphere and (b) a CO_2 atmosphere upon addition of CH_3OH ranging from 0 M (black dashed line) to 8 M (black solid line).

To evaluate the product(s) generated by the electrocatalysis, controlled-potential electrolysis (CPE) experiments were carried out at a potential of −2.11 V for 1 h in a CO_2-saturated DMF solution in the presence of various amounts of H_2O, and the Faradaic efficiencies were determined from the quantification of gaseous and liquid products by gas chromatography and ion chromatography analyses, respectively (Figure 1-7). In the CO_2-saturated dry DMF solution, small amounts of CO and H_2 were detected in the gas phase and the formation of formic acid was not observed in the liquid phase. Upon addition of H_2O, H_2 was dominantly generated and only a small amount of CO was produced. Under each set of conditions, no formic acid was detected in the liquid phase. In particular, in the presence of 2 M H_2O, the Faradaic efficiency of H_2 generation reached 70%, while the Faradaic efficiency of CO production as a CO_2 reduction product was only 5%. The CPE results suggest that enhancement of current in CV measurements is caused by H_2 generation catalyzed by two-electron reduced species of **Co(II)TDHC** rather than CO_2 reduction.

Further addition of H_2O results in decomposition of **Co(II)TDHC** during electrolysis. To ensure that the catalytic activity was not derived from electrodeposition on the electrode surface, a rinse test was performed after the CPE experiments. In the presence of less than 2 M H_2O, a negligible increase in current was observed, suggesting that the catalyst remains homogeneous during the electrolysis (Figure 1-8a). In contrast, the largely increased current in the presence of 3 M H_2O compared to a fresh working electrode suggests the formation of active and adsorbable decomposed materials (Figure 1-8b). CPE experiments were also carried out at more negative (−2.34 V) and at more positive (−2.00 V) potentials in the presence of 2 M H_2O. Electrolysis at −2.34 V resulted in H_2 and CO generation with the Faradaic efficiencies of 39.2% and 7.8%, respectively. However, CPE under this condition led to the formation of decomposed materials of the catalyst to adsorb on the working electrode as confirmed by the rinse test. In contrast, CPE at −2.00 V gave only a trace amount of H_2 with the Faradaic efficiency of 0.5% and no CO generation was detected. Thus, the electrolysis potential of −2.11 V is found to be appropriate in our system.

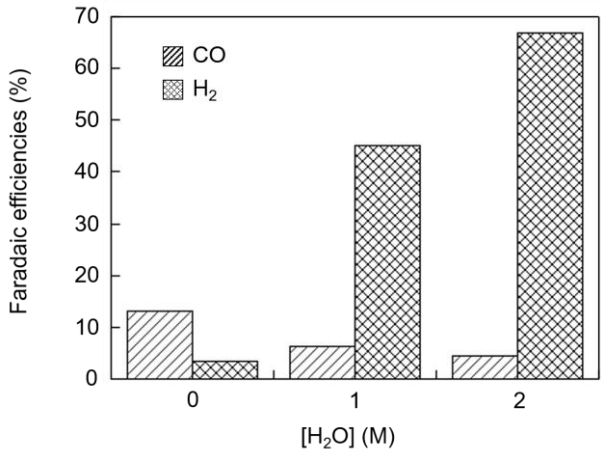

Figure 1-7. Faradaic efficiencies of CO and H_2 generations in the presence of various concentrations of H_2O after 1 h of electrolysis at −2.11 V under CO_2-saturated conditions.

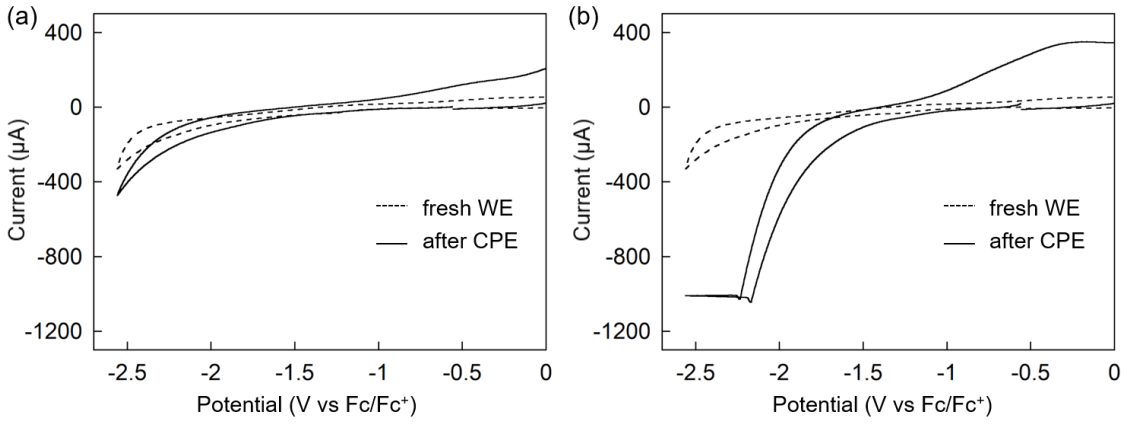

Figure 1-8. CVs of the glassy carbon plate electrode (5.8 cm^2 surface area) without catalyst before (dashed line) and after (solid line) a controlled-potential electrolysis with (a) 2 M H_2O and (b) 3 M H_2O in wet DMF + 0.1 M $TBAPF_6$ solution at a scan rate of 100 $mV \cdot s^{-1}$ under a CO_2 atmosphere.

Electrochemistry under an N_2 atmosphere in the presence of buffer solution

To determine whether the H_2 evolution reaction is caused by acidification of DMF/H_2O co-solvent under CO_2-saturated conditions, a buffer solution was used to regulate a pseudo-pH value of the electrochemical solution. The buffer solution is a mixture containing 15 mM each of 2-(*N*-morpholino)ethanesulfonic acid (MES), *N*-tris(hydroxymethyl)methyl-3-aminopropanesulfonic acid (TAPS), 4-(2-hydroxyethyl)-1-piperazineethanesulfonic acid (HEPES) and *N*-cyclohexyl-2-aminoethanesulfonic acid (CHES).[37] The author has employed the buffer solution for our experiments, and the pseudo-pH values of N_2-saturated DMF/buffer solutions were found to be similar to those of CO_2-saturated DMF/H_2O solutions.[38] Figure 1-9 shows the effect of addition of the buffer solution on the CV profiles under an N_2 atmosphere. Using the buffer solution, a comparable catalytic current to H_2O containing the CO_2-saturated solution was observed after generation of the two-electron reduced species. Further addition of the buffer solution did not show any effect on the enhancement of current (Figure 1-9b), which is consistent with the results obtained from addition of H_2O under a CO_2 atmosphere (*vide supra*). As a control experiment, the electrochemical behavior upon addition of H_2O under an N_2 atmosphere was also evaluated and no enhancement of current was observed, suggesting that moderate acidification of the electrochemical solution is essential for the reductive catalysis (Figure 1-10).

To obtain further evidence, the CPE experiments with the buffer solution under an N_2 atmosphere were conducted. H_2 generation was observed and the Faradaic efficiencies were found to be generally consistent with the Faradaic efficiencies measured in CO_2-saturated DMF solution containing H_2O (Figure 1-11). These results suggest that acidification of the bulk solution by the saturation of CO_2 generates a sufficient amount of protons to promote electrocatalytic H_2 generation by **Co(II)TDHC**.

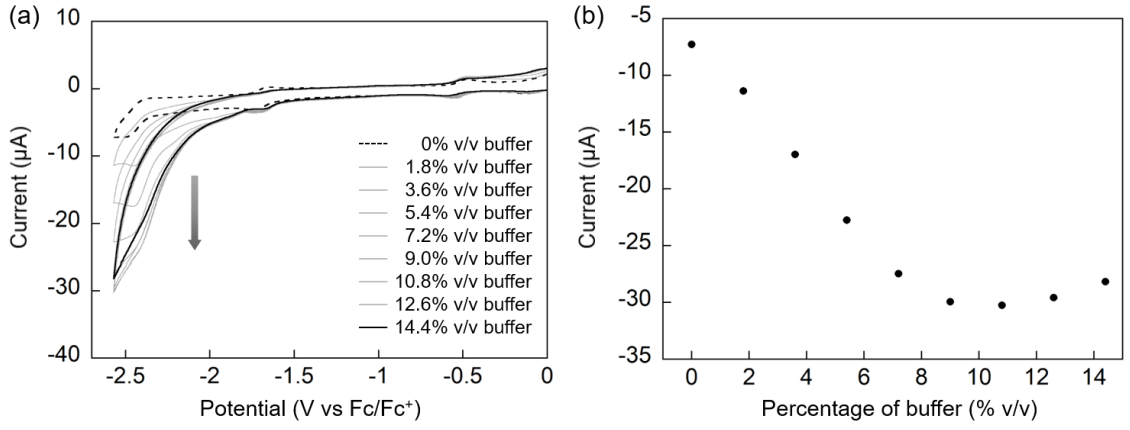

Figure 1-9. (a) CVs of **Co(II)TDHC** (0.5 mM) in DMF with 0.1 M $TBAPF_6$ at a scan rate of 100 $mV \cdot s^{-1}$ upon addition of buffer solution under an N_2 atmosphere ranging from 0% v/v (black dashed line) to 14.4% v/v (black solid line). (b) Relationship between the percentage of buffer solution and current at −2.57 V in cyclic voltammetry.

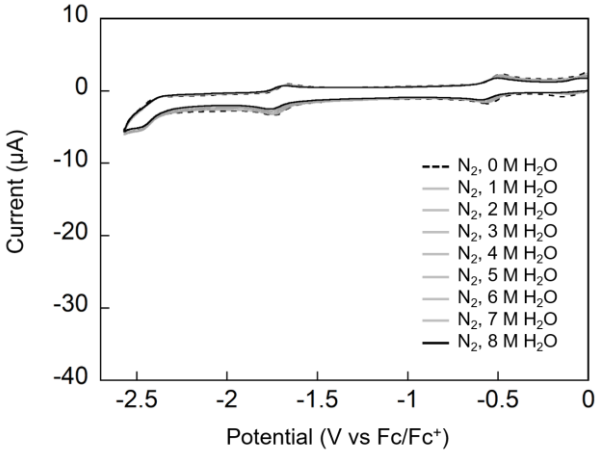

Figure 1-10. CVs of **Co(II)TDHC** (0.5 mM) in dry DMF with 0.1 M $TBAPF_6$ at a scan rate of 100 $mV \cdot s^{-1}$ under an N_2 atmosphere upon addition of H_2O ranging from 0 M (black dashed line) to 8 M (black solid line).

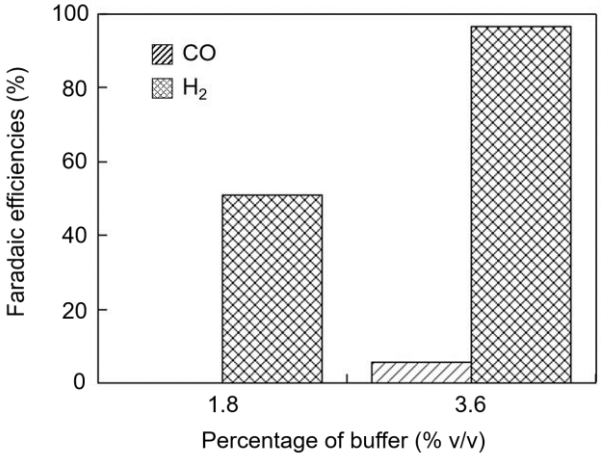

Figure 1-11. Faradaic efficiencies of CO and H_2 generations with 1.8 and 3.6% v/v of buffer solution after 1 h of electrolysis at −2.11 V under an N_2-saturation conditions. CO generated in the presence of 3.6% v/v buffer solution is derived from the decomposition of the catalyst or degradation of DMF/buffer components.

A plausible mechanism for electrocatalysis promoted by **Co(II)TDHC** toward H_2 evolution and CO_2 reduction is as follows: The one-electron reduction species of **Co(II)TDHC**, **Co(I)TDHC**, is inert toward both CO_2 reduction and H_2 evolution, which was confirmed by UV-vis absorption spectroscopic measurements where exposure of a THF solution of **Co(I)TDHC** to CO_2 and H_2O did not show any change in absorption spectra (Figure 1-12). This behavior is distinctly different from behavior exhibited by a series of Co(I) species of normal porphyrin which promote H_2 evolution via a Co(III)–H species.[10,11] In fact, no CO and H_2 evolution was observed in the CPE experiment conducted at –1.3 V. These findings suggest that the **Co(I)TDHC** seems to be stabilized by the monoanionic tetradehydrocorrin framework to the extent that it cannot overcome the activation energy of the reaction with CO_2. The $E_{1/2}$(Co(II)/Co(I)) of **Co(II)TDHC** is −0.53 V, which is 750 mV more positive than that of **CoTPP**. In contrast, under the two-electron reduction conditions carried out at –2.11 V, two-electron reduced species of **Co(II)TDHC** works as a catalyst toward H_2 evolution and CO_2 reduction. In particular, the plausible

intermediate $[Co(I)]^{\bullet-}$ and/or $[Co(II)]^{-}$ then may easily form thermodynamically favored Co–H species resulting in H_2 evolution. Even though **Co(II)TDHC** has poor activity toward CO_2, the author has found that **Co(II)TDHC** catalyzes H_2 generation under relatively mild conditions (pH ~ 8) compared to the previously reported porphyrinoid-type H_2 generating catalysts which require the addition of a strong Brønsted acid.[9-11]

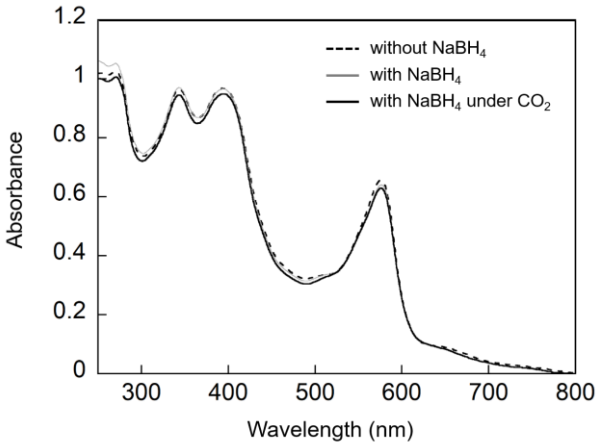

Figure 1-12. UV-vis absorption spectra of **Co(I)TDHC** generated by $NaBH_4$ reduction under an N_2 atmosphere (black dashed line), under a CO_2 atmosphere (gray solid line) and with 1 M H_2O under a CO_2 atmosphere (black solid line) in THF.

1-3. Summary

This work is the first example of introduction of an aryl group into the *meso*-positions of the tetradehydrocorrin framework to functionalize the corresponding cobalt complex. In contrast to unstable *meso*-phenyl and *meso*-mesityl substituted cobalt tetradehydrocorrins, it was figured out that 1,3-dimethoxybenzene moiety at *meso*-positions is essential to maintain the structure of *meso*-aryl substituted cobalt tetradehydrocorrins. **Co(II)TDHC** shows an enhancement of current in CV measurements under a CO_2 atmosphere upon addition of H_2O as a proton source. In CPE experiments conducted at –2.11 V for **Co(II)TDHC**, however, the author found that **Co(II)TDHC** dominantly catalyzes H_2 evolution rather than CO_2 reduction. CPE with buffer solution under an N_2 atmosphere offers evidence that H_2 evolution is promoted by moderate acidification of the electrochemical solution. In the present study, the author has demonstrated that the highly stabilized Co(I) species is inert for the reactions, whereas one more reduced species $[Co(I)]^{\bullet-}$ and/or $[Co(II)]^{-}$ promotes thermodynamically favored H_2 evolution, since **Co(II)TDHC** works as a catalyst under relatively mild conditions (pH ~ 8) with nearly 100% Faradaic efficiency. Moreover, the author has succeeded in demonstrating that the monoanionic ligand is useful for generating an electrocatalytically active low-valent metal species at much more positive potentials than dianionic porphyrinoid ligands. Efforts to design new catalysts to achieve CO_2-selective reduction with low overpotential are now underway in our laboratory.

1-4. Experimental section

Materials and methods

NMR spectra were recorded on a Bruker DPX 400 (400 MHz) and Bruker Avance III HD (400 MHz) spectrometers at 298 K. Chemical shifts are reported in ppm relative to the residual solvent resonances. ESI-TOF MS analyses were performed on a Bruker micrOTOF-II mass spectrometer. UV-vis spectral measurements were carried out with a Shimadzu UV-3600 Plus double-beam spectrophotometer with a thermostated cell holder. EPR spectroscopy was performed with a Bruker EMXmicro spectrometer at the X-band (9.66 GHz) microwave frequency with 151.7 mW microwave power and 5.00 G of modulation amplitude. During EPR measurements, the sample temperature was maintained at 100 K using liquid N_2 vapor. Tetrabutylammonium hexafluorophosphate ($TBAPF_6$, >98%) was purchased from Tokyo Chemical Industry Co., Ltd. and recrystallized from heated ethanol and dried under vacuum before use. Distilled water was demineralized using a Millipore Integral 3 apparatus. All other reagents of the highest guaranteed grade available were obtained from commercial sources and were used as received unless otherwise indicated.

2,6-Dimethoxybenzaldehyde (1)

To a flame dried flask was added 2,6-dimethoxybenzene (5.1 mL, 39.0 mmol), *N,N,N′,N′*-tetramethylethylenediamine (6.6 mL, 44.3 mmol) and THF (60 mL). The solution was cooled to 0 °C and then 1.6 M ^{n}BuLi hexane solution (29.3 mL, 46.9 mmol) was added dropwise. After stirring for 1 h at 0 °C, DMF (4.5 mL, 58.0 mmol) was added and the mixture was further stirred for 1 h at 0 °C. The solution was allowed to warm up to room temperature and the reaction was quenched by addition of 4 *N* $HCl_{aq.}$ (12 mL). The reaction mixture was extracted with ethyl acetate, washed with sat. $NaCl_{aq.}$, dried over Na_2SO_4, and the solvent was evaporated. The target compound **1** was obtained by re-precipitation in a hexane/CH_2Cl_2 solution as a white powder (5.69 g, 88%). ^{1}H NMR (400 MHz, $CDCl_3$) δ: 3.87 (s, 6H, OC*H*$_3$); 6.55 (d, *J* = 8.4 Hz, 2H, Ar-*H*); 7.43 (t, *J* = 8.4 Hz, 1H, Ar-*H*); 10.49 (s, 1H, C*H*O). ^{13}C NMR (100 MHz, $CDCl_3$) δ:56.14, 103.92, 114.34, 136.05, 162.27, 189.53. ESI-TOF MS: *m/z* = 189.0521 $[M + Na]^+$, calculated for $C_9H_{10}O_3Na$ 189.0522.

2,2′-((Dimethoxyphenyl)methylene)bis(1*H*-pyrrole) (2)

The mixture of compound **1** (1.00 g, 6.02 mmol) and pyrrole (10.5 mL, 0.151 mol) was treated with trifluoroacetic acid (50 µL, 0.65 mmol) and stirred for 5 min at room temperature. After stirring, the mixture was quenched by 0.1 M $NaOH_{aq.}$ (100 mL) and the organic layer was separated with ethyl acetate, washed with sat. $NaCl_{aq.}$, dried over Na_2SO_4, and the solvent was evaporated. Purification was carried out by SiO_2 column chromatography (hexane/ethyl acetate = 4/1) followed by recrystallization with hexane to yield compound **2** as a white powder (1.21 g, 71%). ^{1}H NMR (400 MHz, $CDCl_3$) δ: 3.76 (s, 6 H, OC*H*$_3$); 5.96 (m, 2H, pyrrole *βH*); 6.14 (m, 2H, pyrrole *βH*); 6.22 (s, 1H, *meso-H*); 6.65 (m, 2H, pyrrole *αH*); 6.66 (d, *J* = 8.4 Hz, 2H, Ar-*H*); 7.23 (t, *J* = 8.4 Hz, 1H, Ar-*H*); 8.54 (s, 2H, N*H*). ^{13}C NMR (100 MHz, $CDCl_3$) δ: 32.66, 56.51, 105.91, 107.78, 116.19, 119.64,

128.24, 133.06, 158.26. ESI-TOF MS: *m/z* = 305.1250 $[M + Na]^+$, calculated for $C_{17}H_{18}N_2O_2Na$ 305.1260.

5-((2,6-Dimethoxyphenyl)(1*H*-pyrrol-2-yl)methyl)-1*H*-pyrrole-2-carbaldehyde (3)

DMF (4.5 mL, 58.1 mmol) was treated with $POCl_3$ (0.67 mL, 7.38 mmol) at 0 ºC and the resulting solution was stirred for 1 h to give the Vilsmeier reagent. To a solution of compound **2** (0.96 g, 3.41 mmol) in DMF (11.3 mL) at 0 ºC, the freshly prepared Vilsmeier reagent (2.5 mL) was added dropwise and stirred for 2 h at 0 ºC. Then the reaction mixture was treated with sat. $CH_3COONa_{aq.}$ (36 mL) for 4 h at room temperature and the mixture was extracted with ethyl acetate, washed with sat. $NaCl_{aq.}$, dried over Na_2SO_4, and the solvent was evaporated. Purification was carried out by SiO_2 column chromatography (hexane/ethyl acetate = 3/2) to afford compound **3** (0.74 g, 69%). ^{1}H NMR (400 MHz, $CDCl_3$) δ: 3.75 (s, 6H, OC*H*$_3$); 5.92 (m, 1H, pyrrole *βH*); 6.10-6.13 (m, 2H, pyrrole *αH*, *βH*); 6.16 (s, 1H, *meso-H*); 6.62 (d, *J* = 8.4 Hz, 2H, Ar-*H*); 6.69 (m, 1H, pyrrole *βH*); 6.85 (m, 1H, pyrrole *βH*); 7.22 (t, *J* = 8.4 Hz, 1H, Ar-*H*); 8.83 (s, 1H, N*H*); 9.08 (s, 1H, N*H*); 9.33 (s, 1H, C*H*O). ^{13}C NMR (100 MHz, $CDCl_3$) δ: 33.02, 56.46, 105.77, 107.69, 108.09, 109.45, 117.59, 117.78, 129.09, 130.25, 131.51, 144.66, 158.03, 178.12. ESI-TOF MS: *m/z* = 333.1221 $[M + Na]^+$, calculated for $C_{18}H_{18}N_2O_3Na$ 333.1210.

2-((2,6-Dimethoxyphenyl)(1*H*-pyrrol-2-yl)methyl)-5-methyl-1*H*-pyrrole (4)

The mixture of compound **3** (735 mg, 2.37 mmol), KOH (456 mg, 8.13 mmol) in ethylene glycol (3.5 mL) was treated with hydrazine hydrate (0.48 mL, 9.71 mmol) and refluxed for 1 h. After cooling to room temperature, ethyl acetate was added and the mixture was washed with sat. $NaCl_{aq.}$, dried over Na_2SO_4, and the solvent was evaporated. Purification was carried out with SiO_2 column chromatography (hexane/ethyl acetate = 3/2) to yield compound **4** (590 mg, 84%). ^{1}H NMR (400 MHz, $CDCl_3$) δ: 2.20 (s, 3H, C*H*$_3$); 3.75 (s, 6H, OC*H*$_3$); 5.74 (m, 1H, pyrrole *βH*); 5.79 (m, 1H, pyrrole *βH*); 5.90 (m, 1H, pyrrole *βH*); 6.10 (m, 1H, pyrrole *βH*); 6.13 (s, 1H, *meso-H*); 6.63 (d, *J* = 8.4 Hz, 2H, Ar-*H*); 6.64 (m, 1H, pyrrole *αH*); 7.19 (t, *J* = 8.4 Hz, 1H, Ar-*H*); 8.21 (s, 1H, N*H*); 8.51 (s, 1H, N*H*). ^{13}C NMR (100 MHz, $CDCl_3$) δ: 13.23, 32.71, 56.48, 105.27, 105.61, 106.11, 107.73, 115.98, 119.74, 126.18, 128.09, 131.29, 133.38, 158.30. ESI-TOF MS: *m/z* = 319.1418 $[M + Na]^+$, calculated for $C_{18}H_{20}N_2O_2Na$ 319.1417.

5,5'-((2,6-Dimethoxyphenyl)methylene)bis(2-((2,6-dimethoxyphenyl)(5-methyl-1*H*-pyrrol-2-yl)methyl)-1*H*-pyrrole) (5)

To a mixture of compound **4** (483 mg, 1.63 mmol), compound **1** (135 mg, 0.81 mmol) and methanol (82 mL), HCl (4.0 mL) in H_2O (82 mL) was added and stirred for 12 h at room temperature with light protection. The reaction mixture was extracted with CH_2Cl_2, washed with sat. $NaCl_{aq.}$, dried over Na_2SO_4, and the solvent was evaporated. Purification was carried out by Al_2O_3 (neutral, grade III) column chromatography (CH_2Cl_2) followed by re-precipitation (CH_2Cl_2/CH_3OH) to give compound **5** as a pale yellow powder (283 mg, 47%). ESI-TOF MS: *m/z* = 763.3465 $[M + Na]^+$, calculated for $C_{45}H_{58}N_4O_6Na$ 763.3466.

5,10,15-Tri(2,6-dimethoxyphenyl)-1,19-dimethyltetradehydrocorrinato cobalt(II) perchlorate (Co(II)TDHC)

A mixture of compound **5** (50.0 mg, 67.5 µmol) and $Co(OAc)_2 \cdot 4H_2O$ (50.4 mg, 0.202 mmol) in CH_2Cl_2 (17 mL) and methanol (17 mL) was treated with *p*-chloranil (8.3 mg, 33.8 µmol) for 2 h at room temperature. After stirring, solvents were evaporated and crude product was re-dissolved in CH_2Cl_2. To this mixture was added 0.7% $HClO_{4aq.}$ and the mixture was stirred for 30 min at room temperature. The reaction mixture was extracted with ethyl acetate, washed with H_2O, dried over Na_2SO_4 and the solvent was evaporated. The crude product was purified by SiO_2 column chromatography (CH_2Cl_2/acetone = 4/1) followed by further purification by Al_2O_3 (basic, grade IV) column chromatography (CH_2Cl_2/acetone = 4/1) and the blue fraction was collected. Evaporation of the solvent afforded a black solid of **Co(II)TDHC** as a racemic mixture of (1*R*,19*R*) and (1*S*,19*S*) enantiomers (11 mg, 18%). ESI-TOF MS: *m/z* = 792.2357 $[M]^+$, calculated for $C_{45}H_{41}CoN_4O_6$ 792.2353. Elemental analysis: C 60.51, H 4.85, N 5.30. Calcd. for $C_{49}H_{49}ClCoN_4O_{12}$ C 60.03, H 5.04, N 5.72.

X-ray crystallography

The single crystal X-ray diffraction studies were carried out with Rigaku XtaLAB synergy. The structure was refined on F^2 by full-matrix least-squares method, using SHELXL-2016/6. Hydrogen atoms were included in the refinement on calculated positions riding on their carrier atoms.

Electrochemistry

Electrochemical studies were performed using a potentiostat (CompactStat, Ivium Technologies). A single-compartment cell was used for all cyclic voltammetry (CV) experiments with a polished glassy carbon working electrode (3 mm in diameter from ALS Co., Ltd. was used unless otherwise indicated.), a Pt wire counter electrode, and an Ag|AgCl reference electrode (3 M $NaCl_{aq.}$, from ALS Co., Ltd.). All experiments were referenced relative to the $Fe^{III/II}$ couple at 0.00 V using ferrocene (Fc) as an internal standard. All electrochemical experiments were performed with 0.1 M $TBAPF_6$ as a supporting electrolyte. All solutions were purged with N_2 or CO_2 before CVs were measured. Pseudo-pH values were measured with an F-72 Horiba pH meter equipped with a 9615-10D Horiba electrode.

Controlled-potential electrolysis

Controlled-potential electrolysis (CPE) experiments were carried out in a custom-made single compartment cell designed in our laboratory with a custom silicon top to hold each electrode and a joint for sealing with septa and gas sampling. This apparatus included a glassy carbon plate (5.8 cm^2 surface area, from ALS Co., Ltd.) as a working electrode, a Pt wire counter electrode separated from the bulk solution by a porous glass frit (from EC FRONTIER Co., Ltd.), and an Ag|AgCl reference electrode (3 M $NaCl_{aq}$) separated from the solution by a Vycor tip (from ALS Co., Ltd.). A potentiostat (CompactStat, Ivium Technologies) was used to apply potentials and record

current. The CPE experiments were performed in DMF with various amounts of proton source and 0.1 M $TBAPF_6$. CPE solutions were purged with N_2 or CO_2 for 20 min prior to electrolysis. The potential drift during the electrolysis experiments was negligible, which was confirmed by measuring the redox potential of ferrocene before and after the electrolysis. Gaseous products after CPE experiments were analyzed using 50 μL sample aliquots taken from the headspace of the electrochemical cell and injected on a Shimadzu BID-2010 plus series gas chromatograph with a 250 m×0.5 mm ID micropacked column with helium as a carrier gas at a flow rate of 3.0 mL/min. For the liquid products, a 1 mL sample solution was diluted twice with H_2O, filtered and analyzed with a Shimadzu ion chromatography system equipped with a Shodex IC SI-35 4D column equilibrated with a 1.8 mM Na_2CO_3 aqueous solution as eluent at a flow rate of 0.3 mL/min. Faradaic efficiencies were determined by dividing the measured amount of H_2 and CO by the expected amount of H_2 and CO calculated based on the charge passed during the CPE experiments. The CPE experiments were performed at least twice, and the reported Faradaic efficiencies are average values. As a rinse test, the glassy carbon electrode was removed from the bulk solution after CPE and washed carefully with DMF. Then the working electrode was immersed in a catalyst-free CO_2-saturated DMF/H_2O co-solution with 0.1 M $TBAPF_6$ and CV measurements were obtained.

References and notes

1. K. Gruber, B. Puffer, and B. Kräutler, *Chem. Soc. Rev*. 2011, **40**, 4346-4363.
2. R. G. Matthews, *Acc. Chem. Res*. 2001, **34**, 681-689.
3. K. L. Brown, *Chem. Rev*. 2005, **105**, 2075-2149.
4. C. L. Drennan, S. Huang, J. T. Drummond, R. G. Matthews and M. L. Ludwig, *Science* 1994, **266**, 1669-1674.
5. W. Buckel and B. T. Golding, *Chem. Soc. Rev*. 1996, **25**, 329-337.
6. D. Dolphin, R. L. N. Harris, J. L. Huppatz, A. W. Johnson and I. T. Kay, *J. Chem. Soc. C* 1966, 30-40.
7. (a) C.-J. Liu, A. Thompson and D. Dolphin, *J. Inorg. Biochem.* 2001, **83**, 133-138. (b) Y. Murakami, Y. Aoyama and K. Tokunaga, *J. Am. Chem. Soc*. 1980, **102**, 6736-6744. (c) Y. Murakami, K. Sakata, Y. Tanaka and T. Matsuo, *Bull. Chem. Soc. J*. 1975, **48**, 3622-3630. (d) N. S. Hush and I. S. Woolsey, I. S. *J. Am. Chem. Soc*. 1972, **94**, 4107-4114.
8. (a) Y. Morita, K. Oohora, A. Sawada, T. Kamachi, K. Yoshizawa and T. Hayashi, T. *Inorg. Chem*. 2017, **56**, 1950-1955. (b) Y. Morita, K. Oohora, A. Sawada, K. Doitomi, J. Ohbayashi, T. Kamachi, K. Yoshizawa, Y. Hisaeda, and T. Hayashi, *Dalton Trans*. 2016, **45**, 3277-3284.
9. V. S. Thoi, Y. Sun, J. R. Long and C. J. Chang, *Chem. Soc. Rev.* 2013, **42**, 2388-2400.
10. R. M. Kellett and T. G. Spiro, *Inorg. Chem.* 1985, **24**, 2373-2377.
11. A. G. Maher, G. Passard, D. K. Dogutan, R. L. Halbach, B. L. Anderson, C. J. Gagliardi, M. Taniguchi, J. S. Lindsey and D. G. Nocera, *ACS Catal*. 2017, **7**, 3597-3606.
12. J. G. Kleingardner, B. Kandemir and K. L. Bren, *J. Am. Chem. Soc*. 2014, **136**, 4-7.

13. N. Kaeffer, M. Chavarot-Kerlidou and V. Artero, *Acc. Chem. Res*. 2015, **48**, 1286-1295.
14. A. Chapovetsky, T. H. Do, R. Haiges, M. K. Takase, S. C. Marinescu, *J. Am. Chem. Soc.* 2016, **138**, 5765-5768.
15. B. Fisher and R. Eisenberg, *J. Am. Chem. Soc.* 1980, **102**, 7361-7363.
16. S. Roy, B. Sharma, J. Pécaut, P. Simon, M. Fontecave, P. D. Tran, E. Derat and V. Artero, *J. Am. Chem. Soc.* 2017, **139**, 3685-3696.
17. J. Losada, I. Delpeso, L. Beyer, J. Hartung, V. Fernández and M. Möbius, *J. Electroanal. Chem.* 1995, **398**, 89-93.
18. H. Sheng and H. Frei, *J. Am. Chem. Soc.* 2016, **138**, 9959-9967.
19. C. Cometto, L. Chen, P.-K Lo, Z. Guo, K.-C. Lau, E. Anxolabéhère-Mallart, C. Fave, T.-C Lau and M. Robert, *ACS Catal*. 2018, **8**, 3411-3417.
20. D. Behar, T. Dhanasekaran, P. Neta, C. M. Hosten, D. Ejeh, P. Hambright and E. Fujita, *J. Phys. Chem. A* 1998, **102**, 2870-2877.
21. X.-M. Hu, M. H. Rønne, S. U. Pedersen, T. Skrydstrup and K. Daasbjerg, *Angew. Chem. Int. Ed.* 2017, **56**, 6468-6472.
22. J. Shen, R. Kortlever, R. Kas, Y. Y. Birdja, O. Diaz-Morales, Y. Kwon, I. Ledezma-Yanez, K. J. P. Schouten, G. Mul and M. T. M. Koper, M. T. M. *Nat. Commun*. 2015, **6**, 8177-8184.
23. J. Grodkowski, T. Dhanasekaran, P. Neta, P. Hambright, B. S. Brunschwig, K. Shinozaki and E. Fujita, *J. Phys. Chem. A* 2000, **104**, 11332-11339.
24. J. Grodkowski, P. Neta, E. Fujita, A. Mahammed, L. Simkhovich and Z. Gross, *J. Phys. Chem. A* 2002, **106**, 4772-4778.
25. J. Grodkowski and P. Neta, *J. Phys. Chem. A* 2000, **104**, 1848-1853.
26. Y. Okabe, S. K. Lee, M. Kondo and S. Masaoka, *J. Biol. Inorg. Chem*. 2017, **22**, 713-725.
27. C. Costentin, S. Drouet, M. Robert and J.-M. Savéant, *Science* 2012, **338**, 90-94.
28. A. Chapovetsky, M. Welborn, J. M. Luna, R. Haiges, T. F. Miller III and S. C. Marinescu, *ACS Cent. Sci.* 2018, **4**, 397-404.
29. M. D. Sampson and C. P. Kubiak, *J. Am. Chem. Soc.* 2016, **138**, 1386-1393.
30. K. T. Ngo, M. McKinnon, B. Mahanti, R. Narayanan, D. C. Grills, M. Z. Ertem and J. Rochford, *J. Am. Chem. Soc*. 2017, **139**, 2604-2618.
31. W.-S. Cho, H.-J. Kim, B. J. Littler, M. A. Miller, C.-H. Lee and J. S. Lindsey, *J. Org. Chem*. 1999, **64**, 7890-7901.
32. Y.-J. Tu, H. C. Cheng, I. Chao, C.-R. Cho, R.-J. Cheng and Y. O. Su, *J. Phys. Chem. A* 2012, **116**, 1632-1637.
33. C. Paliteiro and A. Sobral, *Electrochimica Acta*, 2005, **50**, 2445-2451.
34. K. M. Barkigia, M. W. Renner, L. R. Furenlid, C. J. Medforth, K. M. Smith and J. Fajer, *J. Am. Chem. Soc*. 1993, **115**, 3627-3635.

35. The absorption spectra of cobaltocene and cobaltocenium were previously reported: M. M. MacInnes, S. Hlynchuk, S. Acharya, N. Lehnert and S. Maldonado, *ACS. Appl. Mater. Interfaces* 2018, **10**, 2004-2015.
36. CPE experiments at −2.11 V in the presence of CH_3OH under CO_2-saturated conditions revealed that the current enhancement depicted in Figure 1-6b is attributed to a selective H_2 evolution. In particular, 83.7% of Faradaic efficiency was achieved by CPE with 2 M CH_3OH, whereas no CO generation was observed.
37. T. K. Mukhopadhyay, N. L. MacLean, L. Gan, D. C. Ashley, T. L. Groy, M.-H. Baik, A. K. Jones and R. J. Trovitch, *Inorg. Chem*. 2015, **54**, 4475-4482.
38. The pseudo-pH values of CO_2-saturated DMF solutions containing 1, 2, 3, 4, 5, 6, 7 and 8 M H_2O were determined to be 8.53, 8.37, 8.21, 8.03, 7.86, 7.73, 7.62 and 7.51, respectively, whereas the pseudo-pH values of N_2-saturated DMF solutions containing 1.8, 3.6, 5.4, 7.2, 9.0, 10.8, 12.6 and 14.4% v/v buffer were determined to be 8.33, 7.99, 7.84, 7.74, 7.66, 7.56, 7.50 and 7.44, respectively.

Chapter 2
Synthesis of cobalt bipyricorrole and electrochemical CO_2 reduction with a small overpotential value

Reproduced in part with permission from [*Chem. Commun.* 2019, **55**, 493-496.]

2-1. Introduction

Provision of effective conversion of carbon dioxide (CO_2) into various compounds including fuels and chemical materials by electrocatalysis has been recognized as one of the most important objectives for realization of an environmentally sustainable society.[1] Over the last three decades, a wide variety of homogenous metal complexes based on first-row transition metals such as Mn,[2] Fe,[3] Co[4] and Ni[5] have been reported as useful and practical CO_2 reduction electrocatalysts because they are relatively inexpensive and abundant. Porphyrin (Chart 2-1a) is a promising catalyst ligand because it has intrinsically high durability and excellent photochemical and electrochemical properties. Iron porphyrin complexes have been extensively studied and are highly effective in converting CO_2 into carbon monoxide (CO).[6] In contrast, investigations of cobalt porphyrin complexes have been quite limited despite their potential as CO_2 reduction catalysts.[7] Although cobalt complexes formed by other porphyrinoids such as phthalocyanine[8] and corrole[9] have been investigated as CO_2 reduction catalysts, a significantly negative electrochemical potential to generate an active low-valent intermediate is required. In this context, it is important to promote the generation of the low-valent species by tuning the ligand structure. Corrin (Chart 2-1b), a monoanionic porphyrinoid ligand, is the natural cofactor of cobalamin. This ligand stabilizes the low-valent species to induce formation of the Co(I) species, which serves as a key intermediate for a broad range of reactions in biological systems.[10] The tetradehydrocorrin derivatives shown in Chart 2-1c have been synthesized as simple analogs of cobalamin and physicochemical properties of their cobalt complexes have been previously investigated.[11] Our recent study, however, has demonstrated that a stabilized Co(I) species with a tetradehydrocorrin framework as a ligand promotes selective H_2 evolution rather than CO_2 reduction.[12] Thus, the author hypothesizes that suitable stabilization of the Co(I) species will be required to promote a selective CO_2 reduction reaction with a low overpotential value. Here, the author employs a bipyricorrole framework (Chart 2-1d),[13] because the stronger Lewis basicity of the nitrogen atoms in a bipyridine moiety of bipyricorrole relative to the corresponding imine-like nitrogen atoms in the bipyrrolic moiety of tetradehydrocorrin promises a more reactive Co(I) species in this metal complex. Therefore, the author has designed and investigated a Co(II) bipyricorrole (**Co(II)BIPC**) functionalized with a 2,6-dimethoxyphenyl group at a *meso*-position of the bipyrricorrole framework (Scheme 2-1).[14]

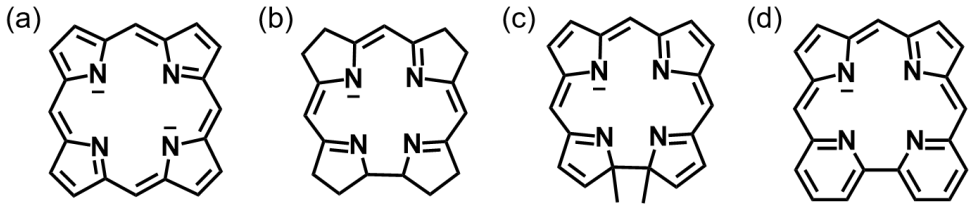

Chart 2-1. Deprotonated structures of (a) porphyrin, (b) corrin, (c) tetradehydrocorrin and (d) bipyricorrole frameworks.

2-2. Results and discussion

Synthesis of Co(II)BIPC

Co(II)BIPC was successfully synthesized according to Scheme 2-1. The target complex was achieved via acid-catalyzed intermolecular coupling of corresponding 5,5'-dicarboxydipyrromethane and 6,6'-diformyl-2,2'-bipyridine followed by cobalt insertion in a 25% yield. The zinc analog (**Zn(II)BIPC**) was also synthesized as a reference compound via the same procedure with **Co(II)BIPC** using $Zn(OAc)_2$ instead of $Co(OAc)_2{\cdot}4H_2O$ (see experimental section for details). **Zn(II)BIPC** was fully characterized by NMR spectroscopy (Figure 2-16 and Figure 2-17), in contrast to **Co(II)BIPC** which shows paramagnetic Co(II) behavior (*vide infra*).

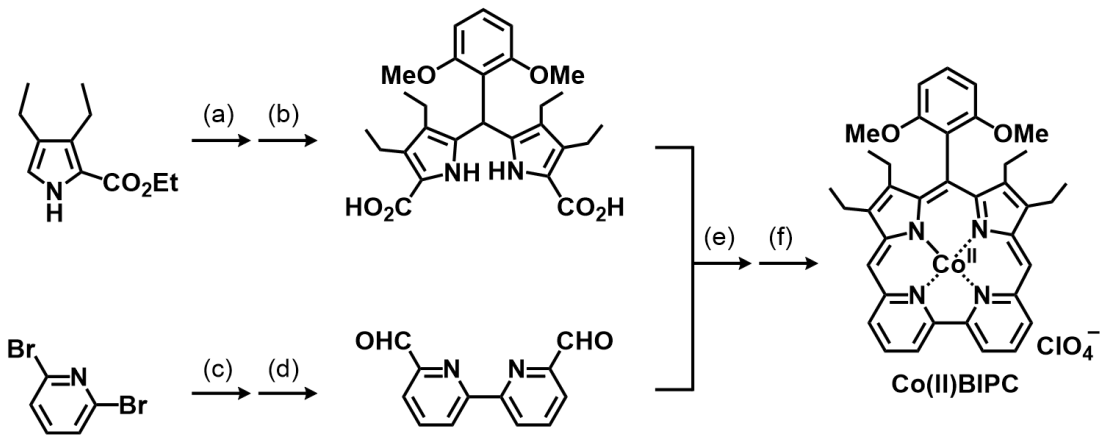

Scheme 2-1. Synthesis of **Co(II)BIPC**. (a) 2,6-dimethoxybenzaldehyde, HCl, H_2O, ethanol, 51%; (b) NaOH, ethanol, 81%; (c) ^{n}BuLi, $CuCl_2$, diethyl ether, 24%; (d) ^{n}BuLi, DMF, THF, 41%; (e) trifluoroacetic acid, THF; (f) $Co(OAc)_2{\cdot}4H_2O$, CH_3OH, CH_2Cl_2, then $NaClO_4{\cdot}H_2O$, H_2O, CH_3OH, 25% in 2 steps.

X-ray crystal structure

The structure of **Co(II)BIPC** was determined by X-ray crystallographic analysis. In the crystal, the macrocycle of bipyricorrole is nearly planar and the coordination site of the cobalt ion is open to allow entry of external substrates as shown in Figure 2-1. An aryl moiety linked to the C11 atom is close to being perpendicular to the macrocycle, indicating that the methoxy substituents in the aryl group are positioned to interact with the external substrate bound to the cobalt ion in the framework, in an arrangement which is similar to a Mn-based complex described in a previous report by Rochford.[15]

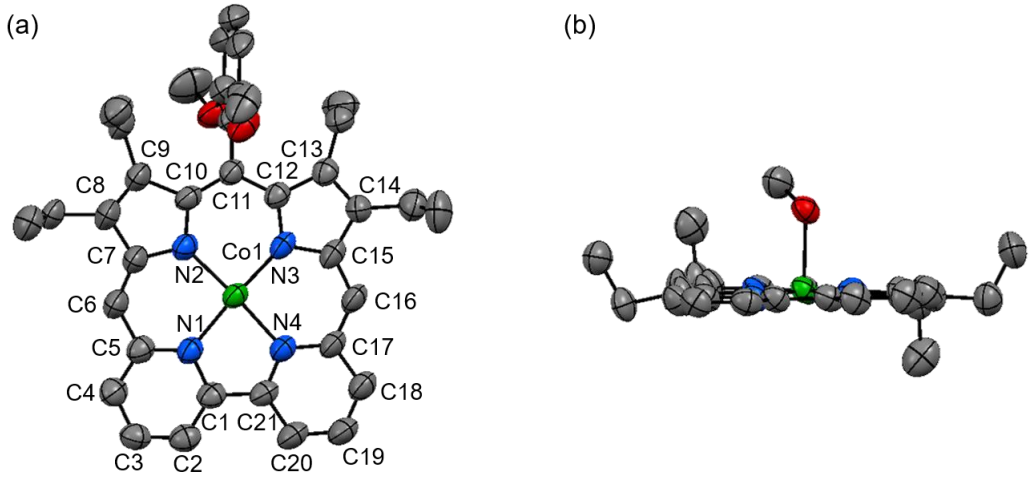

Figure 2-1. X-ray crystal structure of **Co(II)BIPC** with 50% thermal ellipsoid probability. (a) top view and (b) side view. Hydrogen atoms and the nonbonding counteranion (ClO_4^-) are omitted for clarity. Only the major configuration of the disordered groups is shown. Methanol as a neutral axial ligand in the top view and an aryl group in the side view are also omitted for clarity.

Electrochemical/spectroscopic characterization

Cyclic voltammetry (CV) of **Co(II)BIPC** in a DMF solution under an N_2 atmosphere displays two reversible peaks with $E_{1/2}$ of −0.87 V and −1.75 V (Figure 2-2a).[16] These redox couples are confirmed to be diffusion-controlled process by the CV measurements under the various scan rate conditions (Figures 2-2b – 2-2d). The first reduction event at −0.87 V was confirmed by EPR experiments to represent cobalt-based reduction of **Co(II)BIPC** to form **Co(I)BIPC** (Figure 2-3). Eight hyperfine peaks can be seen in Figure 2-3a due to the interaction with the Co nucleus (I = 7/2) with $g_{//}$ = 1.99, supporting the presence of a Co(II) species with the unpaired electron of the Co atom in a low-spin d^7 configuration. Upon addition of an excess amount of $NaBH_4$ as a one-electron reductant, the signals derived from the Co(II) species completely disappear (Figure 2-3b), suggesting the formation of the Co(I) species. The absorption change corresponding to [**Co(II)BIPC**]/[**Co(I)BIPC**] was also monitored using cobaltocene as a one-electron reductant, which has a reduction potential of −1.3 V (Figure 2-4). Furthermore, the absence of the redox peak at –0.87 V in the CV measurement of **Zn(II)BIPC** rules out a ligand-based reduction at the first reduction of **Co(II)BIPC**, whereas the presence of the redox peak at −1.75 V of **Zn(II)BIPC** indicates that the

second reduction of **Co(II)BIPC** is attributed to the ligand-based reduction (Figure 2-5). Compared to a Co(II) complex of dianionic tetraphenylporphyrin (**Co(II)TPP**, $E_{1/2}(Co^{II/I})$ = −1.28 V), the first redox potential of **Co(II)BIPC** is positively shifted by 0.41 V because of the significant stabilization of the Co(I) species by the monoanionic bipyricorrole ligand.

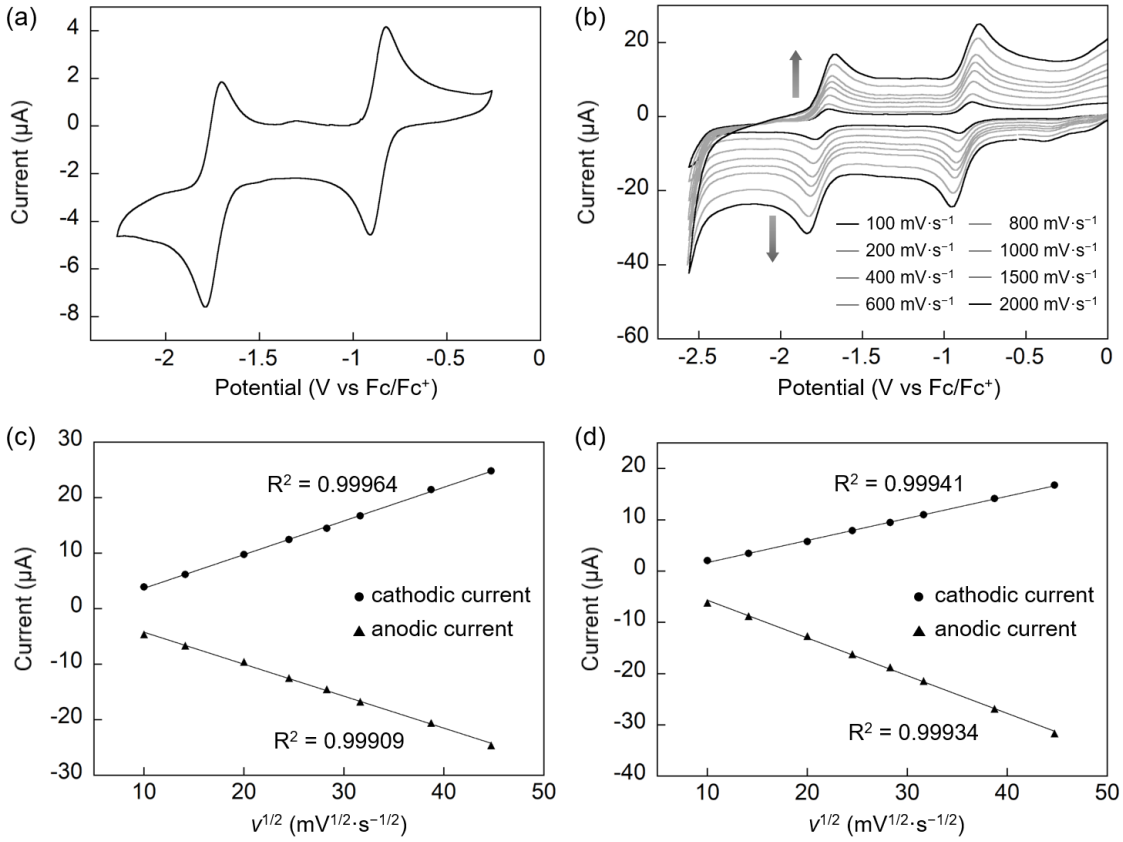

Figure 2-2. (a) CV of **Co(II)BIPC** (0.5 mM) in anhydrous DMF with 0.1 M $TBAPF_6$ at a scan rate of 100 mV·s^{-1} under an N_2 atmosphere. (b) CVs of **Co(II)BIPC** (0.5 mM) in anhydrous DMF with 0.1 M $TBAPF_6$ under an N_2 atmosphere upon increasing a scan rate from 100 to 2000 mV·s^{-1}. Plots of (c) first and (d) second redox peak currents against $v^{1/2}$ in the CV profiles in anhydrous DMF with 0.1 M $TBAPF_6$ under an N_2 atmosphere.

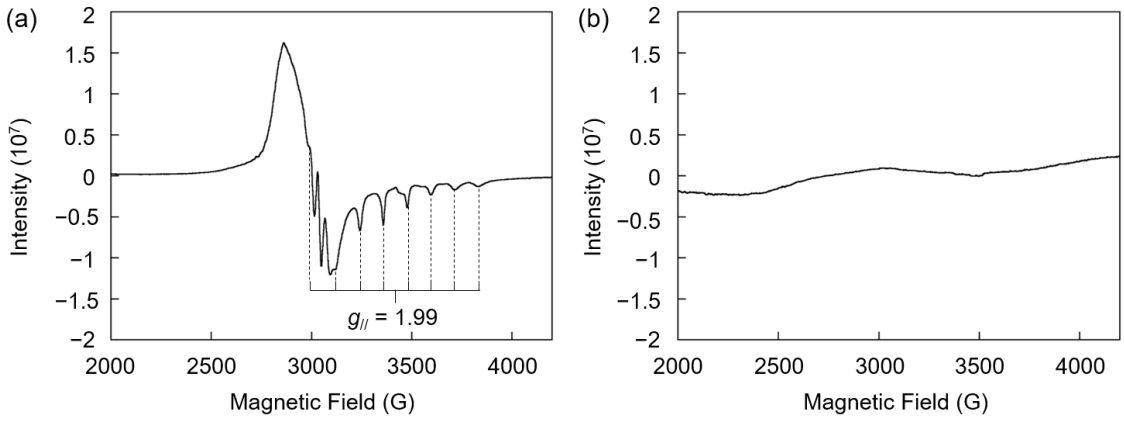

Figure 2-3. (a) EPR spectrum of **Co(II)BIPC** in THF at 100 K. (b) EPR spectrum of **Co(II)BIPC** in THF at 100 K with an excess amount of $NaBH_4$.

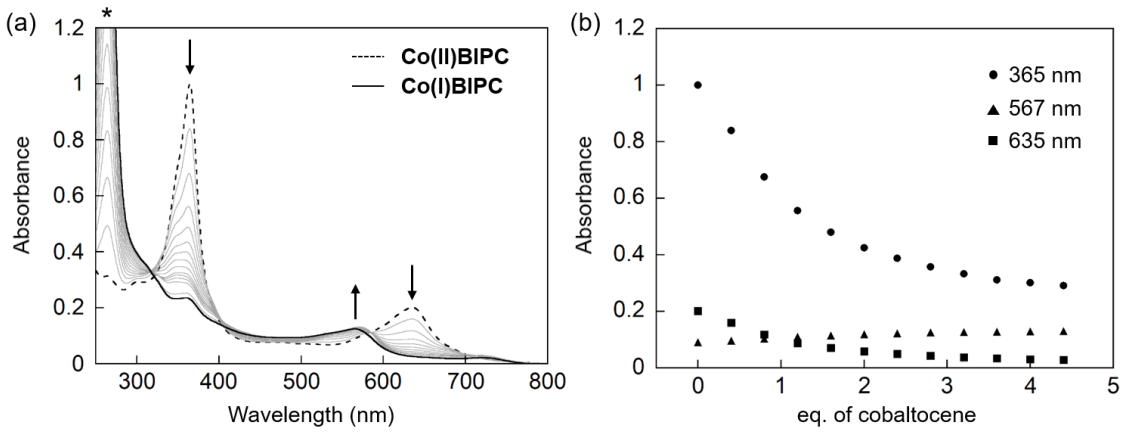

Figure 2-4. (a) UV-vis spectral changes of **Co(II)BIPC** (50 μM in CH_2Cl_2) upon addition of cobaltocene (from dashed line to solid line). Asterisk (*) shows an absorption peak of cobaltocene. (b) Absorbance changes of **Co(II)BIPC** upon addition of cobaltocene.

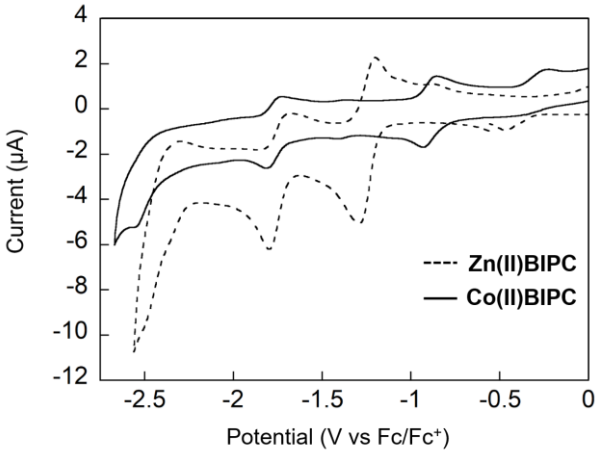

Figure 2-5. (a) CVs of **Co(II)BIPC** (0.5 mM, solid line) and **Zn(II)BIPC** (0.5 mM, dashed line) in anhydrous DMF with 0.1 M $TBAPF_6$ at a scan rate of 100 $mV \cdot s^{-1}$ under an N_2 atmosphere. Since Zn(II) is redox-innocent due to its fully occupied *d* orbitals, two reversible peaks of **Zn(II)BIPC** at −1.24 V and −1.75 V in the CV are both attributed to ligand-based reductions. The enhanced Coulomb repulsion between the additional electron and the neutral **Co(I)BIPC** complex relative to that between the electron and cationic **Zn(II)BIPC** seems to induce the negative shift of the first reduction potential of the macrocycle. The value of the potential shift is 0.51 V, which is similar to the previously reported value of 0.56 V observed in Zn(II) and Co(II) tetraphenylporphyrins.[17]

Electrochemical studies under a CO_2 atmosphere

The CV trace of **Co(II)BIPC** measured under a CO_2 atmosphere exhibits a significant current enhancement after the second reduction process (Figure 2-6). Addition of H_2O as a proton source results in a continuous increase in current at −2.17 V and the catalytic current reaches saturation with 5 M H_2O. The catalytic current was not observed upon addition of H_2O under an N_2 atmosphere (Figure 2-7). To determine the reaction corresponding to the current enhancement in the CV measurements, controlled-potential electrolysis (CPE) experiments for **Co(II)BIPC** were conducted at a potential of −2.17 V for 1 h in a CO_2-saturated DMF solution containing 5 M H_2O. Analysis of the gas phase by gas chromatography revealed selective CO production with Faradaic efficiency (FE) of 75%, whereas FE of a competing H_2 evolution was found to be 6% (Table 2-1, Entry 1). Formic acid in the liquid phase was not detected by ion chromatography. A rinse test performed after the CPE demonstrated negligible enhancement of the current compared to a fresh working electrode (Figure 2-8a). This indicates that the catalytic performance is not derived from an electrodeposition on the electrode. The UV-vis spectra of an aliquot of the electrochemical solution before and after the CPE experiments show that nearly 90% of the complex is maintained after 1 h of CPE, indicating that **Co(II)BIPC** has high durability in electrocatalysis (Figure 2-8b). The alternative proton source 2,2,2-trifluoroethanol (TFE) was also investigated. Upon addition of TFE under a CO_2 atmosphere, current enhancement was observed in the CV measurement, which reached a maximum when 5 M TFE was added (Figure 2-9). The CPE experiment conducted at −2.28 V in CO_2-saturated DMF with 5 M TFE revealed that the enhanced current in the CV measurement corresponds to a CO_2-to-CO reduction with FE of 77% along with the competing H_2 evolution with FE of 6% (Table 2-1, Entry 2).

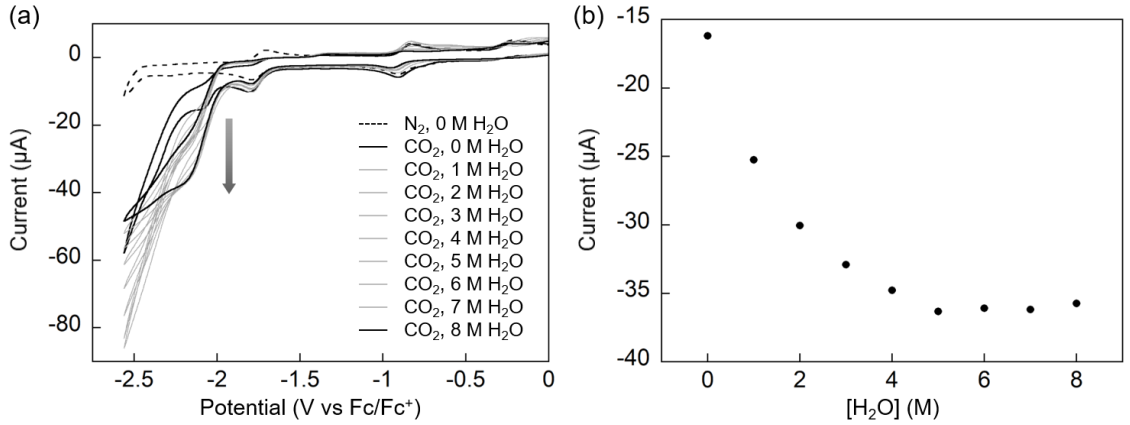

Figure 2-6. (a) CVs of **Co(II)BIPC** (0.5 mM) in dry DMF with 0.1 M $TBAPF_6$ at a scan rate of 100 $mV \cdot s^{-1}$ under an N_2 atmosphere (black dashed line) and upon addition of H_2O under a CO_2 atmosphere: [H_2O] = 0, 1, 2, 3, 4, 5, 6, 7 and 8 M. (b) Relationship between the concentration of H_2O and current at −2.17 V in CV measurements.

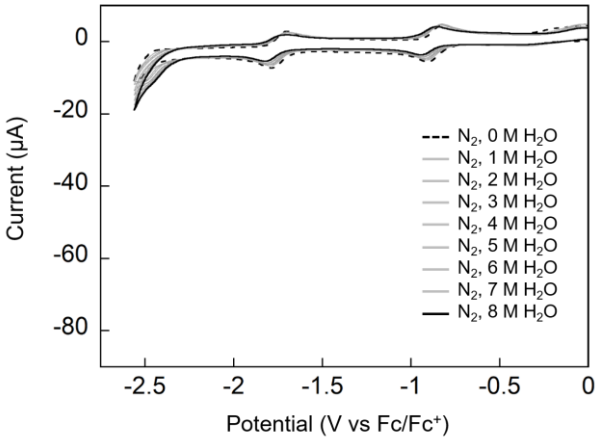

Figure 2-7. CVs of **Co(II)BIPC** (0.5 mM) in dry DMF with 0.1 M $TBAPF_6$ at a scan rate of 100 $mV \cdot s^{-1}$ under an N_2 atmosphere upon addition of H_2O ranging from 0 M (black dashed line) to 8 M (black solid line).

Table 2-1. Electrochemical data for **Co(II)BIPC.**

Entry	Atmosphere	Additive	FE(CO)/FE(H_2)[a]	i_{cat}/i_p[b]	k_{obs} (s^{-1})[c]
1	CO_2	5 M H_2O	75/6	6.3	7.8
2	CO_2	5 M TFE	77/6	-	-
3	N_2	9.0% v/v buffer	0/84	3.9	3.0

[a]CPE experiments in Entry 1 and 3 were performed at −2.17 V and CPE in Entry 2 was conducted at −2.28 V. [b]Calculated at −2.17 V [c]Determined as an apparent rate constant at −2.17 V at a scan rate of 100 $mV \cdot s^{-1}$ using the equation in ref 3a (see experimental section for details).

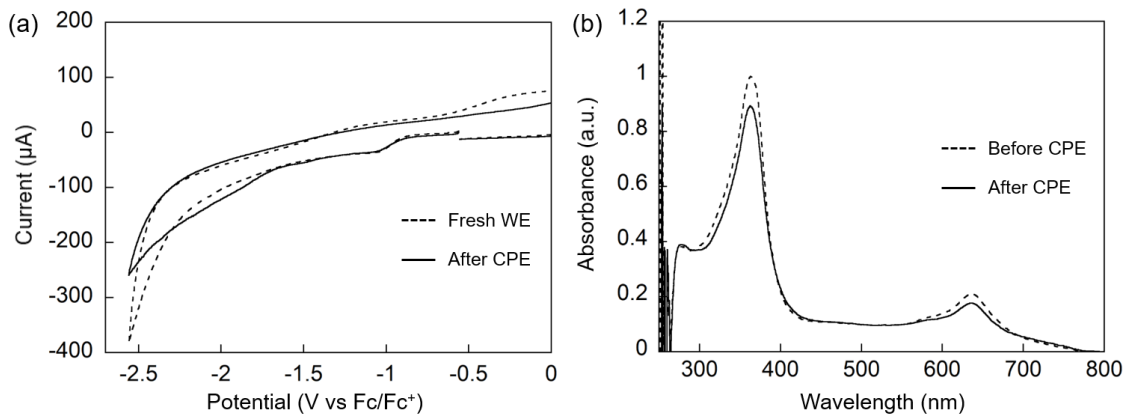

Figure 2-8. (a) CVs of a fresh glassy carbon plate electrode (dashed line) and the glassy carbon plate electrode after a controlled-potential electrolysis with 5 M H_2O (solid line) without catalyst in DMF with 0.1 M $TBAPF_6$ and 5 M H_2O at a scan rate of 100 $mV \cdot s^{-1}$ under a CO_2 atmosphere. (b) Normalized UV-vis absorption spectra of an aliquot of the electrochemical solution of **Co(II)BIPC** before (dashed line) and after (solid line) a controlled-potential electrolysis with 5 M H_2O in DMF.

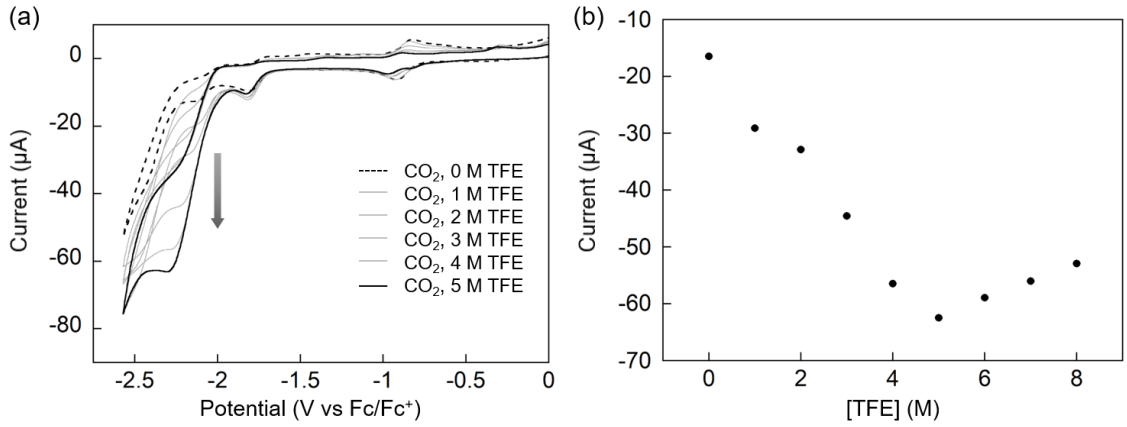

Figure 2-9. (a) CVs of **Co(II)BIPC** (0.5 mM) in DMF with 0.1 M $TBAPF_6$ at a scan rate of 100 $mV \cdot s^{-1}$ upon addition of 2,2,2-trifluoroethanol (TFE) under a CO_2 atmosphere (from black dashed line to black solid line): [TFE] = 0, 1, 2, 3, 4 and 5 M. (b) Relationship between the concentration of TFE and current at −2.28 V in CV measurements.

A proposed reaction mechanism based on the electrochemical results is shown in Figure 2-10. In the first step, (i) one-electron reduction of [**Co(II)BIPC**]$^{+}$ proceeds to generate [**Co(I)BIPC**] followed by (ii) further one-electron reduction to afford [**Co(I)BIPC**]$^{-}$. Next, (iii) CO_2 is bound to [**Co(I)BIPC**]$^{-}$ to form [**Co(II)BIPC**(CO_2H)] coupled with protonation, which is supported by the slight increase in current at the second reduction process of **Co(II)BIPC** under a CO_2 atmosphere relative to the current under an N_2 atmosphere. At the potential of *ca.* –1.98 V, which is consistent with the observed onset potential of the catalytic current, (iv) one-electron reduction occurs to produce [**Co(I)BIPC**(CO_2H)]$^{-}$ and (v) the subsequent C−OH bond cleavage by protonation affords [**Co(I)BIPC**(CO)]. (vi) Spontaneous dissociation of CO regenerates the starting complex [**Co(I)BIPC**] in the catalytic cycle. The proposed mechanism by **Co(II)BIPC** is slightly different from that performed by **Co(II)TPP**,[7b] whereas it is similar to that performed by a Mn complex reported by Kubiak.[2c]

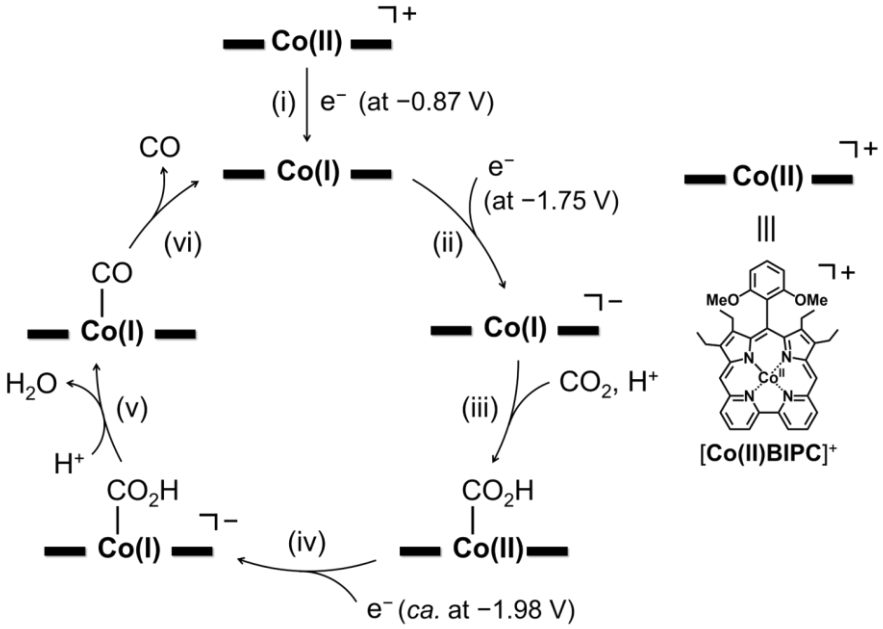

Figure 2-10. A proposed reaction mechanism of the catalytic CO_2 reduction by **Co(II)BIPC**.

Investigation of catalytic activity toward H_2 evolution by Co(II)BIPC

To investigate the competing H_2 evolution catalyzed by **Co(II)BIPC** in the presence of H_2O under a CO_2 atmosphere, pseudo-pH regulation experiments were conducted under CO_2-free conditions using a buffer solution containing a mixture of 15 mM each of MES, TAPS, HEPES and CHES.[18] The pseudo-pH values of N_2-saturated DMF/buffer solutions were found to be similar to those of CO_2-saturated DMF/H_2O solutions.[19] Addition of the buffer solution under N_2 resulted in a continuous increase of current in the CV measurements (Figure 2-11a). The CPE experiment with a 9.0% v/v buffer solution under an N_2 atmosphere, where the pseudo-pH value of the bulk solution is similar to that of a CO_2-saturated DMF solution containing 5 M H_2O, revealed selective H_2 evolution with FE of 84% (Table 2-1, Entry 3). These findings indicate that **Co(II)BIPC** is able to function both as a CO_2 reduction catalyst and an H_2 evolution catalyst under the same pseudo-pH conditions. However, the apparent catalytic rate constants (k_{obs}) of CO_2 reduction and H_2 evolution suggest that the reaction rates of CO_2 reduction are clearly faster than those of H_2 evolution in the range of pseudo-pH from 7.44 to 8.53 (Figure 2-11b).[20] In particular, the rate constant under CO_2 in the presence of 5 M H_2O is 2.6 times greater than the rate constant measured under N_2 in the presence of 9.0% v/v buffer solution (Table 2-1, Figure 2-11b). The difference in the reaction rates between CO_2 reduction and H_2 evolution supports the results of the selective CO_2 reduction by **Co(II)BIPC**.

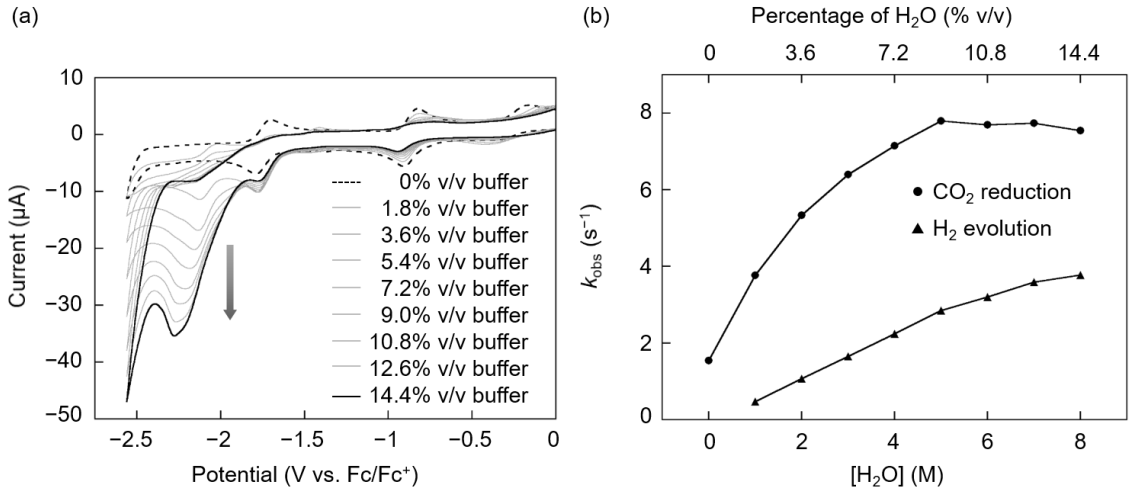

Figure 2-11. (a) CVs of **Co(II)BIPC** (0.5 mM) in DMF with 0.1 M $TBAPF_6$ under an N_2 atmosphere at a scan rate of 100 $mV \cdot s^{-1}$ upon addition of buffer solution ranging from 0% v/v (black dashed line) to 14.4% v/v (black solid line). (b) Reaction rate dependence upon addition of H_2O under a CO_2 atmosphere (circle) and upon addition of buffer solution under an N_2 atmosphere (triangle) determined at −2.17 V in the CV results with a scan rate of 100 $mV \cdot s^{-1}$.

Evaluation of the advantage of the monoanionic porphyrinoid ligand

The catalytic Tafel plots of **Co(II)BIPC** and **Co(II)TPP** clarify the electrochemical properties and give insights into the advantages of the monoanionic bipyricorrole ligand over the dianionic porphyrin ligand (Figure 2-12).[21] Each plot was obtained by determining the apparent catalytic rate constant values (k_{cat}) of **Co(II)BIPC** with 5 M H_2O, **Co(II)BIPC** with 5 M TFE[22] and **Co(II)TPP**[23] from the catalytic currents in the CV measurements, which gave k_{cat} of 7.8, 19.8 and 30.4 s^{-1}, respectively (Figures 2-13 – 2-16). Figure 2-12 reveals that **Co(II)BIPC** is capable of working as a CO_2 reduction catalyst with much smaller overpotential (η) than **Co(II)TPP** formed by the dianionic ligand, whereas the reaction rate of **Co(II)BIPC** is similar to that of **Co(II)TPP**. In particular, the maximum TOF (TOF_{max}) is achieved with η of 0.68 V by **Co(II)BIPC** with 5 M H_2O, which is 0.35 V more positive than **Co(II)TPP** in which the η for TOF_{max} is 1.03 V. This result unambiguously demonstrates the advantage of the monoanionic ligand as a component of a CO_2 reduction catalyst to decrease the overpotential in the electrochemical reaction.

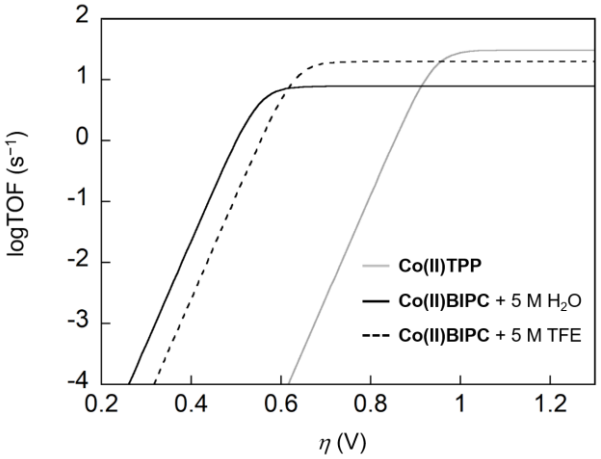

Figure 2-12. Catalytic Tafel plots of **Co(II)TPP** (gray solid line), **Co(II)BIPC** with 5 M H_2O (black solid line) and **Co(II)BIPC** with 5 M TFE (black dashed line).

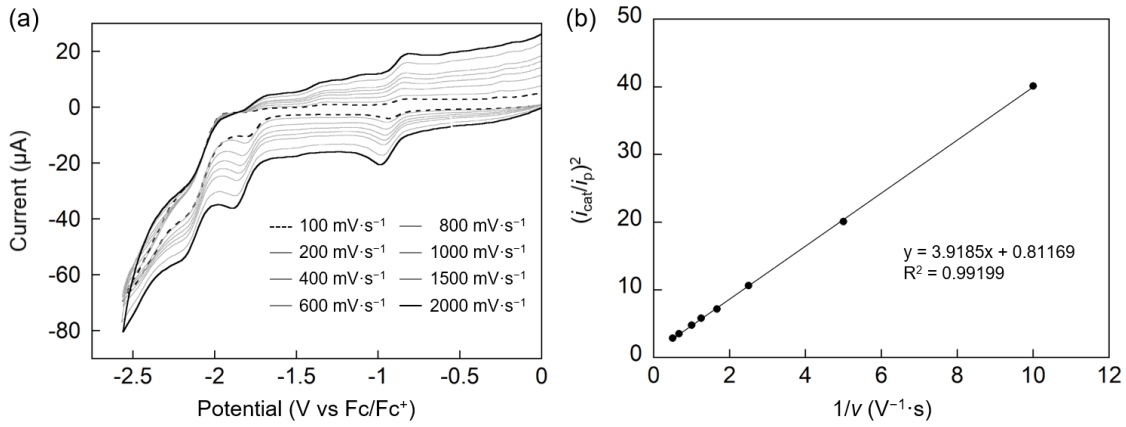

Figure 2-13. (a) CVs of **Co(II)BIPC** in CO_2-saturated DMF with 0.1 M $TBAPF_6$ and 5 M H_2O upon increasing a scan rate from 100 to 2000 $mV \cdot s^{-1}$. (b) Plots of $(i_{cat}/i_p)^2$ values against $1/v$. The apparent catalytic rate constant of **Co(II)BIPC** with 5 M H_2O was calculated from the slope using eq (4) (see experimental section for details).

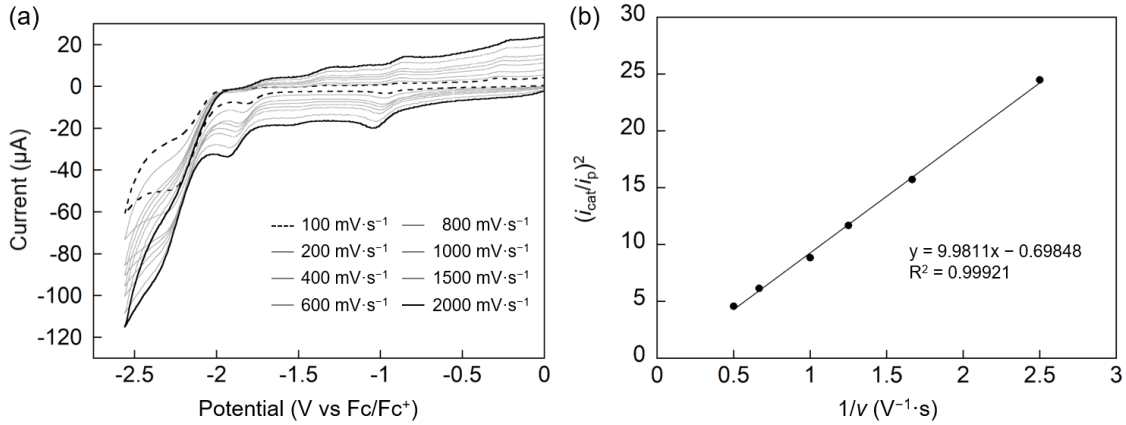

Figure 2-14. (a) CVs of **Co(II)BIPC** in CO_2-saturated DMF with 0.1 M $TBAPF_6$ and 5 M TFE upon increasing a scan rate from 100 to 2000 $mV \cdot s^{-1}$. The catalytic current was independent of the scan rates in the range of 400 $mV \cdot s^{-1}$ to 2000 $mV \cdot s^{-1}$. (b) Plots of $(i_{cat}/i_p)^2$ values against $1/v$ with the scan rates ranging from 400 to 2000 $mV \cdot s^{-1}$. The apparent catalytic rate constant of **Co(II)BIPC** with 5 M TFE was calculated from the slope using eq (4) (see experimental section for details).

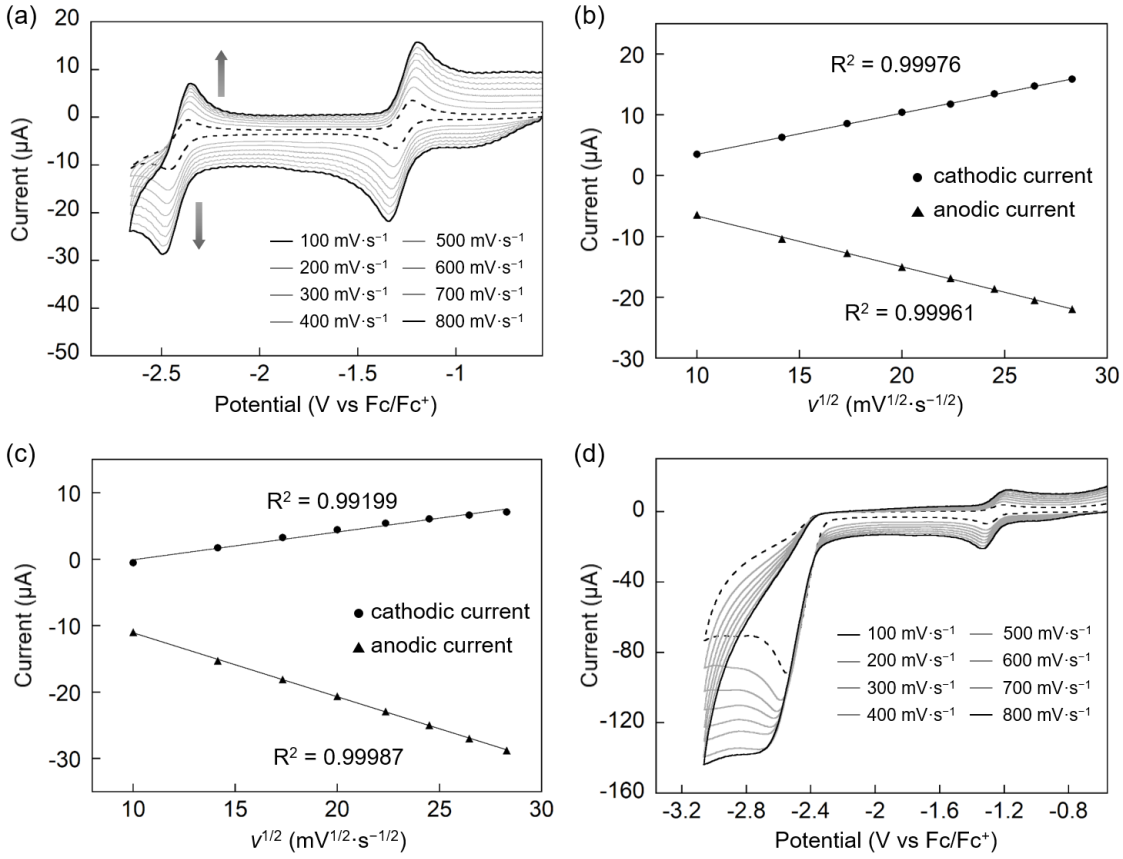

Figure 2-15. (a) CVs of **Co(II)TPP** in dry DMF with 0.1 M $TBAPF_6$ under an N_2 atmosphere upon increasing a scan rate from 100 to 800 $mV \cdot s^{-1}$. Plots of (b) first and (c) second redox peak current against $v^{1/2}$. The proportional dependence of the current on the square root of the scan rates indicates that the redox event is diffusion-controlled process. (d) CVs of **Co(II)TPP** in dry CO_2-saturated DMF with 0.1 M $TBAPF_6$ upon increasing a scan rate from 100 to 800 $mV \cdot s^{-1}$. The apparent catalytic rate constant of **Co(II)TPP** under CO_2-saturated conditions was calculated using the plateau current at a scan rate of 800 $mV \cdot s^{-1}$ using eq (3) (see experimental section for details).

2-3 Summary

In Chapter 2, **Co(II)BIPC**, which consists of the Co(II) complex with a monoanionic bipyricorrole ligand possessing a 2,6-dimethoxyphenyl group at the *meso*-position, catalyzes a selective CO_2 reduction reaction in the presence of proton sources, as confirmed by CPE experiments.[24] Although **Co(II)BIPC** was found to function both as a CO_2 reduction catalyst and an H_2 evolution catalyst under the same pseudo-pH conditions, the difference in reaction rates between CO_2 reduction and H_2 evolution leads to a selective CO_2-to-CO reduction under a CO_2 atmosphere. Furthermore, the author has demonstrated using catalytic Tafel plots that the monoanionic ligand is useful for generating an electrocatalytically active low-valent species at much more positive potentials than a dianionic porphyrinoid ligand. Compared to our previous work using a Co(II) complex of tetradehydrocorrin ($E_{1/2}(Co^{II/I}) = -0.53$ V) that promotes the selective H_2 evolution rather than CO_2 reduction, **Co(II)BIPC** exhibits a negatively shifted $E_{1/2}(Co^{II/I})$ at −0.87 V and catalyzes selective CO_2-to-CO reduction, indicating that the moderate stabilization of the Co(I) species is favorable to promote the selective CO_2 reduction reaction. The author believes that the present findings will contribute to the development of efficient CO_2 reduction catalysts with low overpotential.

2-4. Experimental section

Materials and methods

NMR spectra of compounds **6**-**9** and Zn(II) bipyricorrole (**Zn(II)BIPC**) were recorded on a Bruker Avance III HD (400 MHz) spectrometer at 298 K and Bruker Avance III (600 MHz) spectrometer at 305 K, respectively. Chemical shifts are reported in ppm relative to the residual solvent resonances. ESI-TOF MS analyses were performed on a Bruker micrOTOF-II mass spectrometer. UV-vis spectral measurements were carried out with a Shimadzu UV-3600 Plus double-beam spectrophotometer with a thermostated cell holder. EPR spectra were measured with a Bruker EMXmicro spectrometer at the X-band (9.61 GHz) microwave frequency with 20.0 mW microwave power and 10.0 G of modulation amplitude. During EPR measurements, the sample temperature was maintained at 100 K using liquid N_2 vapor. Co(II) tetraphenylporphyrin (**Co(II)TPP**) was prepared from the freebase tetraphenylporphyrin according to our previous method.[25] As buffer components, 2-(*N*-morpholino)ethanesulfonic acid (MES), *N*-tris(hydroxymethyl)methyl-3-aminopropanesulfonic acid (HEPES) and *N*-cyclohexyl-2-aminoethanesulfonic acid (CHES) were obtained from Dojindo Molecular Technologies, Inc. and 4-(2-hydroxyethyl)-1-piperazineethanesulfonic acid (TAPS) was purchased from Nacalai Tesque, Inc. Tetrabutylammonium hexafluorophosphate ($TBAPF_6$, >98%) from Tokyo Chemical Industry Co., Ltd. was recrystallized in heated ethanol and dried in vacuo before use. Distilled water was demineralized using a Merck Millipore Integral 3 apparatus. All other reagents of the highest guaranteed grade available were obtained from commercial sources and used as received unless otherwise indicated.

X-ray crystallography, electrochemistry and controlled-potential electrolysis

X-ray crystallographic data and electrochemical results were obtained with same methods as Chapter 1.

Calculation of catalytic rate constant from the results of cyclic voltammetry[3a]

The catalytic current i_{cat} is given by eq (1) when the catalysis proceeds via a two-electron transfer pathway:

$$i_{cat} = 2FA[cat]_0\sqrt{Dk_{cat}} \quad (1)$$

where F is Faraday's constant, A is the surface area of the electrode, $[cat]_0$ is the concentration of catalyst, and D is the diffusion coefficient of the catalyst. The one-electron diffusion current of the catalyst i_p is determined from eq (2),

$$i_p = 0.446FA[cat]_0\sqrt{\frac{FDv}{RT}} \quad (2)$$

where v is the scan rate in the cyclic voltammetry measurements, R is the universal gas constant, and T is temperature.

Dividing eq (1) by eq (2) avoids determining A and D, and leads to eq (3).

$$k_{cat} = \left(\frac{i_{cat}}{i_p}\right)^2 \times \frac{1}{(2 \times 2.24)^2} \times \frac{Fv}{RT} \quad (3)$$

Eq (3) is converted to eq (4),

$$\left(\frac{i_{cat}}{i_p}\right)^2 = \frac{(2 \times 2.24)^2 RT}{F} \times k_{cat} \times \frac{1}{v} \quad (4)$$

where $(i_{cat}/i_p)^2$ is obtained as a function of $1/v$.

The k_{cat} values in this work were determined as apparent catalytic rate constants using eq (3) with the plateau current in Figure 2-15d, and eq (4) with the plots in Figure 2-13d and Figure 2-14b.

According to ref 3a, Tafel plots that relate the turnover frequency (TOF) toward the overpotential η applied at the electrode were obtained using the following eq (5). In this equation,

$$\mathrm{TOF} = \frac{k_{cat}}{1 + \exp\left[\frac{F}{RT}(E^0_{\mathrm{CO_2/CO}} - E_{1/2})\right] \times \exp(-\frac{F}{RT}\eta)] } \qquad (5)$$

where, $E^0_{CO2/CO}$ is the standard potential for the conversion of CO_2 to CO (−0.69 V vs NHE),[6a] $E_{1/2}$ is the half-plateau wave potential in the CV measurement, where the potential measured in our conditions is converted to the NHE referenced value by adding 0.22 V for catalytic Tafel plots.

Synthesis of Co(II)BIPC and Zn(II)BIPC

The targets **Co(II)BIPC** and **Zn(II)BIPC** were synthesized through Scheme 2-2. Ethyl 3,4-diethyl-1*H*-pyrrole-2-carboxylate was prepared according to our previous report.[26]

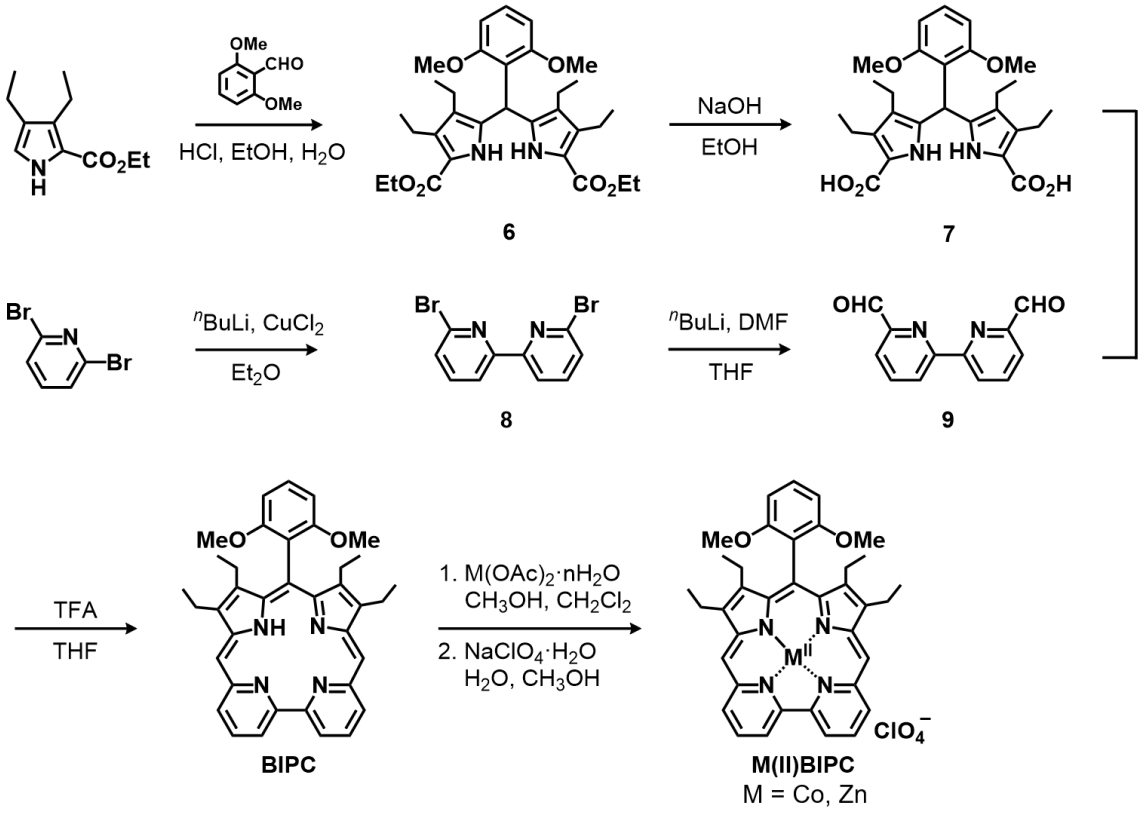

Scheme 2-2. Synthesis of **Co(II)BIPC** and **Zn(II)BIPC**.

Diethyl 5,5'-((2,6-dimethoxyphenyl)methylene)bis(3,4-diethyl-1*H*-pyrrole-2-carboxylate) (6)

To a stirred solution of ethyl 3,4-diethyl-1*H*-pyrrole-2-carboxylate (2.55 g, 15.4 mmol) and 2,6-dimethoxybenzaldehyde (6.00 g, 30.7 mmol) in ethanol (76.5 mL), conc. $HCl_{aq.}$ (1.3 mL) was added and the mixture was refluxed for 1.5 h. After cooling to 0 °C, precipitant was filtered and washed with cold methanol to give compound **6** as a white solid (4.24 g, 51%). ^{1}H NMR (400 MHz, $CDCl_3$) δ: 9.17 (s, 2H, N*H*); 7.19 (t, *J* = 8.4 Hz, 1H, *p*-$C_6H_3(OMe)_2$); 6.61 (d, *J* = 8.0 Hz, 2H, *m*-$C_6H_3(OMe)_2$); 6.25 (s, 1H, *meso-H*); 4.27 (q, *J* = 6.0 Hz, 4H, -$CO_2CH_2CH_3$); 3.80 (s, 6H, -OCH_3); 2.68 (q, *J* = 7.2 Hz, 4H, -CH_2CH_3); 2.31 (q, *J* = 7.6 Hz, 4H, -CH_2CH_3); 1.33 (t, *J* = 7.2 Hz, 6H, -$CO_2CH_2CH_3$); 1.12 (t, *J* = 7.2 Hz, 6H, -CH_2CH_3); 0.88 (t, *J* = 7.2 Hz, 6H, -CH_2CH_3). ^{13}C NMR (100 MHz, $CDCl_3$) δ: 161.58, 157.87, 133.35, 132.50, 128.77, 123.34, 118.14, 116.63, 105.74, 59.62, 56.30, 29.16, 18.49, 17.20, 16.02, 15.81, 14.61. ESI-TOF MS: *m/z* = 561.2955 $[M + Na]^+$, calculated for $C_{31}H_{42}N_2O_6Na$ 561.2935.

5,5'-((2,6-Dimethoxyphenyl)methylene)bis(3,4-diethyl-1*H*-pyrrole-2-carboxylic acid) (7)

A mixture of compound **6** (2.00 g, 3.72 mmol) and NaOH (1.25 g, 31.4 mmol) in ethanol (40 mL) was refluxed for 1 h. After cooling to room temperature, glacial acetic acid (20 mL) was added and the mixture was extracted with CH_2Cl_2, washed with sat. $NaCl_{aq.}$, dried over Na_2SO_4 and the solvent was evaporated. The target compound **7** was obtained by re-precipitation in a hexane/CH_2Cl_2 solution as a white powder (1.45 g, 81%). ^{1}H NMR (400 MHz, DMSO-d_6) δ: 12.09 (s, 2H, -COO*H*); 9.48 (s, 2H, N*H*); 7.25 (t, *J* = 8.4 Hz, 1H, *p*-$C_6H_3(OMe)_2$); 6.76 (d, *J* = 8.4 Hz, 2H, *m*-$C_6H_3(OMe)_2$); 6.18 (s, 1H, *meso-H*); 3.77 (s, 6H, -OCH_3); 2.60 (q, *J* = 7.2 Hz, 4H, -CH_2CH_3); 2.27 (q, *J* = 7.2 Hz, 4H, -CH_2CH_3); 1.04 (t, *J* = 7.2 Hz, 6H, -CH_2CH_3); 0.84 (t, *J* = 7.2 Hz, 6H, -CH_2CH_3). ^{13}C NMR (100 MHz, DMSO-d_6) δ: 161.86, 157.20, 131.68, 131.57, 128.88, 122.33, 117.42, 116.66, 105.94, 56.33, 28.24, 17.67, 16.60, 16.07, 15.76. ESI-TOF MS: *m/z* = 505.2300 $[M + Na]^+$, calculated for $C_{27}H_{34}N_2O_4Na$ 505.2309.

6,6'-Dibromo-2,2'-bipyridine (8)

A solution of 2,6-dibromopyridine (10.0 g, 50.6 mmol) in diethyl ether (39 mL) was cooled to −78 °C and 1.6 M ^{n}BuLi hexane solution (29.0 mL, 55.8 mmol) was added dropwise. After stirring for 1 h at −78 °C, $CuCl_2$ (2.84 g, 25.4 mmol) was added and the mixture was further stirred for 1 h at −78 °C. The equipment was then substituted and the mixture was stirred for 2 h under an O_2 atmosphere. After the reaction, the flask was substituted with N_2, and the reaction was quenched with 6 M $HCl_{aq.}$ (33 mL). The organic layer was separated with CH_2Cl_2, washed with sat. citric $acid_{aq.}$, dried over Na_2SO_4 and the solvent was evaporated. The resulting precipitant was washed with CH_3OH and subsequent filtration afforded compound **8** as a white powder (3.85 g, 24%). ^{1}H NMR (400 MHz, $CDCl_3$) δ: 8.40 (dd, *J* = 0.8 Hz, 7.6 Hz, 2H, *m*-NC_5H_3); 7.69 (t, *J* = 7.4 Hz, 2H, *p*-NC_5H_3); 7.53 (dd, *J* = 0.4 Hz, 7.8 Hz, 2H, *m*-NC_5H_3). ^{13}C NMR (100 MHz, $CDCl_3$) δ: 155.75, 141.74, 139.45, 128.74, 120.30. ESI-TOF MS: *m/z* = 334.8798 $[M + Na]^+$, calculated for $C_{10}H_6Br_2N_2Na$ 334.8790.

6,6'-Diformyl-2,2'-bipyridine (9)

To a THF solution of ^{n}BuLi (9.60 mmol, 66 mL) at −78 °C was added compound **8** (500 mg, 1.59 mmol) in THF (50 mL) and stirred for 45 min at −78 °C. The mixture was then treated with DMF (0.8 mL, 9.55 mmol) and allowed to warm to room temperature. After stirring for 3 h, the reaction was quenched with 4 M $HCl_{aq.}$ (20 mL) and the organic layer was separated with ethyl acetate. The water layer was treated with K_2CO_3 to increase the pH to 10 and then extracted with ethyl acetate. The organic layers were combined and dried over Na_2SO_4. After removal of solvent, cold CH_3OH was added and the precipitant was filtered to yield compound **9** as a white powder (140 mg, 41%). ^{1}H NMR (400 MHz, $CDCl_3$) δ: 10.19 (s, 2H, -C*H*O); 8.83 (d, *J* =7.2 Hz, 2H, *m*-NC_5H_3); 8.03-8.09 (m, 4H, *m*-NC_5H_3, *p*-NC_5H_3). ^{13}C NMR (100 MHz, $CDCl_3$) δ: 193.41, 155.52, 152.42, 138.21, 125.34, 122.03. ESI-TOF MS: *m/z* = 235.0472 $[M + Na]^+$, calculated for $C_{12}H_8N_2O_2Na$ 235.0478.

11-(2,6-Dimethoxyphenyl)bipyricorrole (BIPC)

To a mixture of compound **7** (1.36 g, 2.83 mmol) and compound **9** (600 mg, 2.83 mmol) in THF (960 mL), trifluoroacetic acid (65 mL) was added and the mixture was stirred for 14 h at room temperature. After removal of solvent, toluene was added and residual trifluoroacetic acid was removed by evaporation. After addition of triethylamine (6 mL) to a CH_2Cl_2 (20 mL) solution of the crude product, the mixture was washed with sat. $NaCl_{aq.}$, dried over Na_2SO_4 and the solvent was evaporated. Re-precipitation in a solution of hexane/CH_2Cl_2 afforded **BIPC** as a red powder and the crude product was used in the next step without further purification. ESI-TOF MS: *m/z* = 571.3042 $[M + H]^+$, calculated for $C_{37}H_{39}N_4O_2$ 571.3068.

11-(2,6-Dimethoxyphenyl)bipyricorrolatocobalt(II) perchlorate (Co(II)BIPC)

A solution of **BIPC** (500 mg) in CH_2Cl_2 (150 mL) and CH_3OH (150 mL) was treated with $Co(OAc)_2{\cdot}4H_2O$ (1.09 g, 4.38 mmol) for 5 h at room temperature. After stirring, the mixture was washed with sat. $NaCl_{aq.}$, dried over Na_2SO_4 and the solvent was evaporated. To a solution of the crude product in CH_3OH (10 mL), $NaClO_4{\cdot}H_2O$ (1.23 g, 8.76 mmol) in H_2O (30 mL) was added and stirred for 30 min at room temperature. The organic layer was separated with CH_2Cl_2, washed with H_2O, dried over Na_2SO_4 and the solvent was evaporated. Purification was carried out by SiO_2 column chromatography (CH_2Cl_2/acetone = 3/2) followed by re-precipitation in a diethyl ether/CH_2Cl_2 solution to give **Co(II)BIPC** as a green solid (49 mg, 25% from compound **7**). ESI-TOF MS: *m/z* = 628.2249 $[M]^+$, calculated for $C_{37}H_{37}CoN_4O_2$ 628.2243. UV-vis (CH_3OH) λ_{max}/nm (absorbance) = 367 (0.481), 639 (0.138). Elemental analysis: C 59.21, H 5.06, N 7.31, calculated for $C_{37}H_{39}ClCoN_4O_7$ C 59.56, H 5.27, N 7.51.

11-(2,6-Dimethoxyphenyl)bipyricorrolatozinc(II) perchlorate (Zn(II)BIPC)

To a stirred solution of **BIPC** (200 mg) in CH_2Cl_2 (50 mL) and CH_3OH (50 mL) was added $Zn(OAc)_2$ (0.32 g, 1.74 mmol) and the mixture was then stirred for 30 min at room temperature. After stirring, the solution was washed with sat. $NaCl_{aq.}$, dried over Na_2SO_4 and the solvent was evaporated. To a solution of crude product in CH_3OH (10 mL), $NaClO_4 \cdot H_2O$ (0.49 g, 3.49 mmol) in H_2O (20 mL) was added and the mixture was further stirred for 30 min at room temperature. The organic layer was separated with CH_2Cl_2, washed with H_2O, dried over Na_2SO_4 and the solvent was evaporated. The crude product was purified by SiO_2 column chromatography (CH_2Cl_2/acetone = 3/2) followed by further purification by SiO_2 column chromatography (CH_2Cl_2/CH_3OH = 5/1) and the blue fraction was collected. **Zn(II)BIPC** was obtained by re-precipitation in a diethyl ether/CH_3OH solution as a green powder (10 mg, 5% from compound **7**). ^{1}H NMR (600 MHz, DMSO-d_6, 305 K) δ: 9.20 (d, J = 7.8 Hz, 2H, *m*-NC_5H_3); 8.79 (d, J = 7.8 Hz, 2H, *m*-NC_5H_3); 8.72 (t, J = 7.8 Hz, 2H, *p*-NC_5H_3); 7.66 (s, 2H, *meso-H*); 7.61 (t, J = 9.0 Hz, 1H, *p*-$C_6H_3(OMe)_2$); 6.87 (d, J = 9.0 Hz, 2H, *m*-$C_6H_3(OMe)_2$); 3.64 (s, 6H, -OCH_3); 2.93 (q, J = 7.2 Hz, 4H, -CH_2CH_3); 1.99 (q, J = 7.8 Hz, 4H, -CH_2CH_3); 1.36 (t, J = 7.8 Hz, 6H, -CH_2CH_3); 0.76 (t, J = 7.8 Hz, 6H, -CH_2CH_3). ^{13}C NMR (150 MHz, DMSO-d_6, 305 K) δ: 164.08, 160.04, 153.55, 150.98, 148.54, 144.85, 144.69, 138.47, 130.77, 130.44, 119.28, 115.43, 106.26, 104.15, 55.33, 19.03, 17.62, 16.91, 15.20. ESI-TOF MS: m/z = 633.2188 $[M]^+$, calculated for $C_{37}H_{37}N_4O_2Zn$ 633.2202. UV-vis (CH_3OH) λ_{max}/nm (absorbance) = 367 (0.911), 635 (0.138), 690 (0.383). Elemental analysis: C 58.49, H 5.35, N 7.51, calculated for $C_{37}H_{39}ClN_4O_7Zn$ C 59.05, H 5.22, N 7.44.

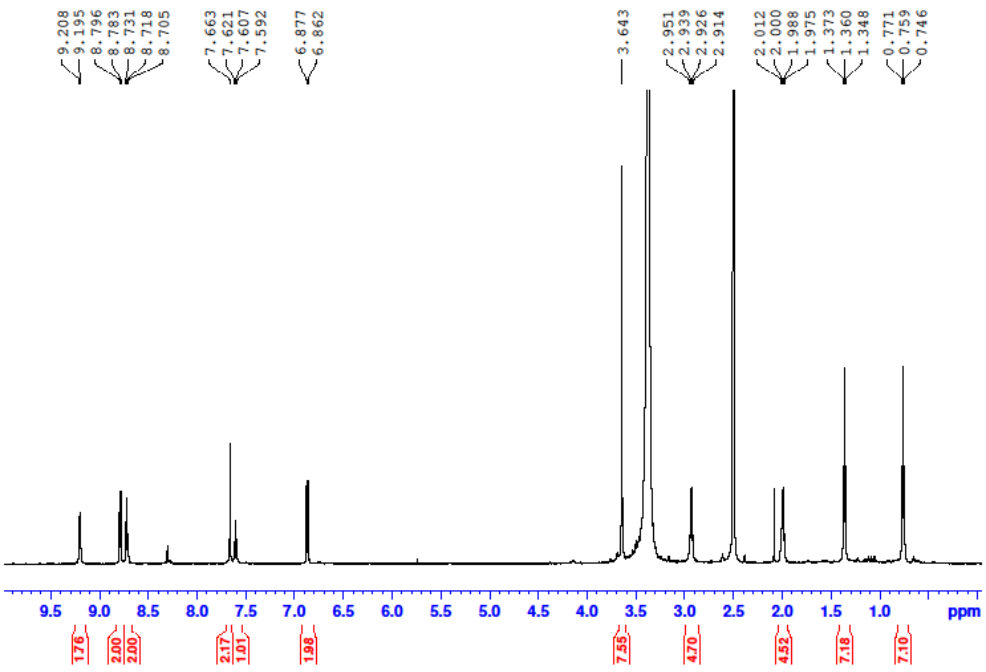

Figure 2-16. ^{1}H NMR spectrum (600 MHz, DMSO-d_6) of **Zn(II)BIPC**.

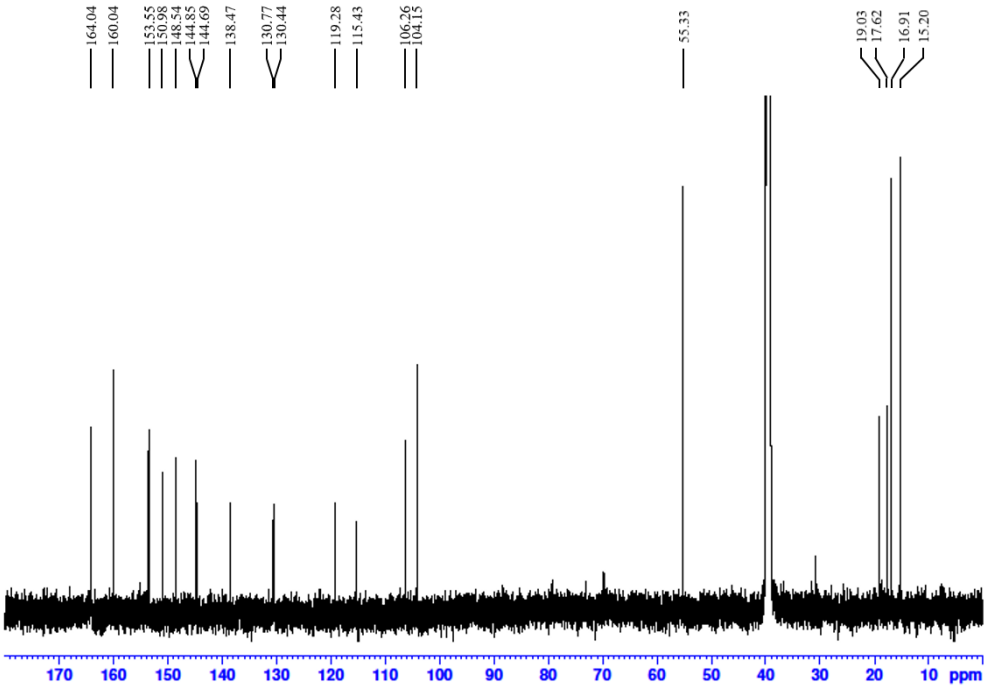

Figure 2-17. ^{13}C NMR spectrum (150 MHz, DMSO-d_6) of **Zn(II)BIPC**.

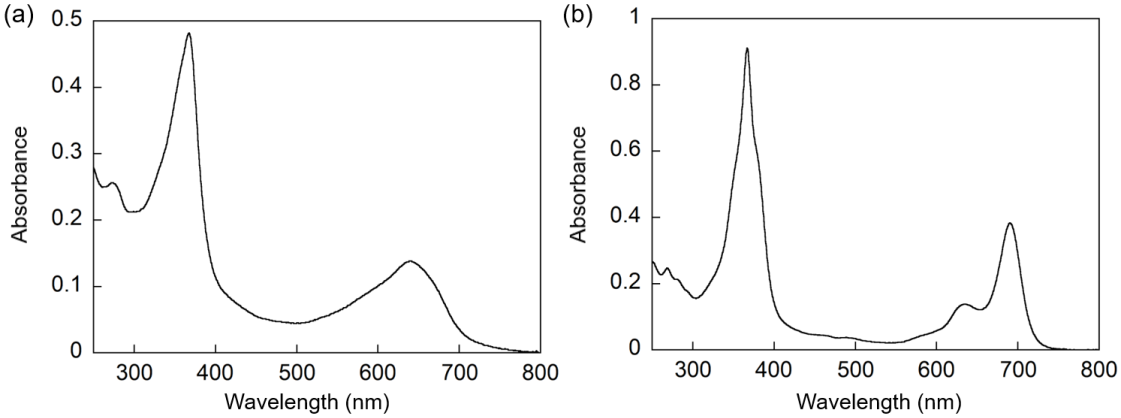

Figure 2-18. UV-vis absorption spectra of (a) **Co(II)BIPC** and (b) **Zn(II)BIPC** in CH_3OH.

11-(2,6-Dihydroxyphenyl)bipyricorrolatocobalt(II) perchlorate (demethylated Co(II)BIPC: Figure 2-19a)

To a solution of **Co(II)BIPC** (16 mg, 22.0 μmol) in CH_2Cl_2 (4.2 mL), 1 M BBr_3/CH_2Cl_2 solution (1.12 mL, 1.12 mmol) was added at room temperature, and the mixture was refluxed for 24 h. After quenching with sat. $NaHCO_{3aq.}$, the organic layer was washed with H_2O, dried over Na_2SO_4 and the solvent was evaporated. Purification was carried out by SiO_2 column chromatography (CH_2Cl_2/acetone/CH_3OH = 20/20/3) to afford demethylated **Co(II)BIPC** as a green solid (8 mg, 52%). ESI-TOF MS: *m/z* = 600.1914 $[M]^+$, calculated for $C_{35}H_{33}CoN_4O_2$ 600.1930.

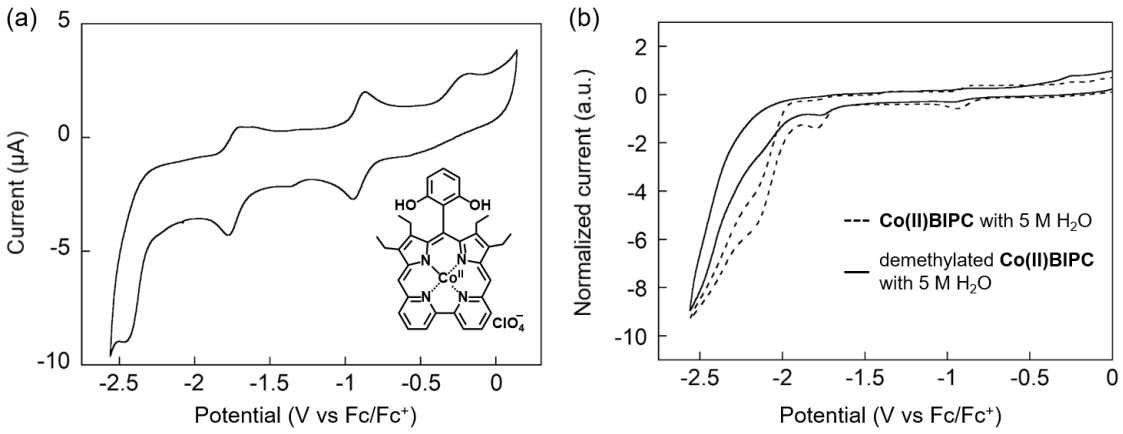

Figure 2-19. (a) CV of demethylated **Co(II)BIPC** (0.5 mM) in dry DMF with 0.1 M $TBAPF_6$ under an N_2 atmosphere. (b) Normalized CVs of **Co(II)BIPC** (0.5 mM, dashed line) and demethylated **Co(II)BIPC** (0.5 mM, solid line) in DMF containing 0.1 M $TBAPF_6$ with 5 M H_2O under a CO_2 atmosphere. Scan rate: 100 $mV \cdot s^{-1}$.

References and notes

1. (a) R. Francke, B. Schille and M. Roemelt, *Chem. Rev*. 2018, **118**, 4631-4701. (b) C. Costentin, M. Robert and J.-M. Savéant, *Chem. Soc. Rev.* 2013, **42**, 2423-2436. (c) E. E. Benson, C. P. Kubiak, A. J. Sathrum and J. M. Smieja, *Chem. Soc. Rev.* 2009, **38**, 89-99.
2. (a) T. E. Rosser, C. D. Windle and E. Reisner, *Angew. Chem. Int. Ed*. 2016, **55**, 7388-7392. (b) M. D. Sampson and C. P. Kubiak, *J. Am. Chem. Soc.* 2016, **138**, 1386-1393. (c) M. D. Sampson, A. D. Nguyen, K. A. Grice, C. E. Moore, A. L. Rheingold and C. P. Kubiak, *J. Am. Chem. Soc.* 2014, **136**, 5460. (d) B. Reuillard, K. H. Ly, T. E. Rosser, M. F. Kuehnel, I. Zebger and E. Reisner, *J. Am. Chem. Soc.* 2017, **139**, 14425-14435.
3. (a) C. Cometto, L. Chen, P.-K. Lo, Z. Guo, K.-C. Lau, E. Anxolabéhère-Mallart, C. Fave, T.-C. Lau and M. Robert, *ACS Catal*. 2018, **8**, 3411-3417. (b) S.-N. Pun, W.-H. Chung, K.-M. Lam, P. Guo, P.-H. Chan, K.-Y. Wong, C.-M. Che, T.-Y. Chen and S.-M. Peng, *J. Chem. Soc. Dalton Trans.* 2002, 575-583. (c) L. Chen, Z. Guo, X.-G. Wei, C. Gallenkamp, J. Bonin, E. Anxolabéhère-Mallart, K.-C. Lau, T.-C. Lau and M. Robert, *J.*

Am. Chem. Soc. 2015, **137**, 10918-10921.

4. (a) A. Chapovetsky, T. H. Do, R. Haiges, M. K. Takase and S. C. Marinescu, *J. Am. Chem. Soc.* 2016, **138**, 5765-5768. (b) S. Roy, B. Sharma, J. Pécaut, P. Simon, M. Fontecave, P. D. Tran, E. Derat and V. Artero, *J. Am. Chem. Soc.* 2017, **139**, 3685-3696. (c) J. Losada, I. del Peso, L. Beyer, J. Hartung, V. Fernández and M. Möbius, *J. Electroanal. Chem.* 1995, **398**, 89-83.
5. (a) J.-P. Collin, A. Jouaiti and J.-P. Sauvage, *Inorg. Chem.* 1988, **27**, 1986-1990. (b) T. Fogeron, T. K. Todorova, J.-P. Porcher, M. Gomez-Mingot, L.-M. Chamoreau, C. Mellot-Draznieks, Y. Li and M. Fontecave, *ACS Catal.* 2018, **8**, 2030-2038. (c) B. Fisher and R. Eisenberg, *J. Am. Chem. Soc.* 1980, **102**, 7361-7363.
6. (a) C. Costentin, S. Drouet, M. Robert and J.-M. Savéant, *Science* 2012, **338**, 90-94. (b) Z. N. Zahran, E. A. Mohamed and Y. Naruta, *Scientific Report* 2016, **6**, 1-12. (c) I. Azcarate, C. Costentin, M. Robert and J.-M. Savéant, *J. Am. Chem. Soc.* 2016, **138**, 16639-16644.
7. (a) D. Behar, T. Dhanasekaran, P. Neta, C. M. Hosten, D. Ejeh, P. Hambright and E. Fujita, *J. Phys. Chem. A* 1998, **102**, 2870-2877. (b) X.-M. Hu, M. H. Rønne, S. U. Pedersen, T. Skrydstrup and K. Daasbjerg, *Angew. Chem. Int. Ed.* 2017, **56**, 6468-6472. (c) J. Shen, R. Kortlever, R. Kas, Y. Y. Birdja, O. Diaz-Morales, Y. Kwon, I. Ledezma-Yanez, K. J. P. Schouten, G. Mul and M. T. M. Koper, *Nat. Commun*. 2015, **6**, 8177-8184.
8. J. Grodkowski, T. Dhanasekaran, P. Neta, P. Hambright, B. S. Brunschwig, K. Shinozaki and E. Fujita, *J. Phys. Chem. A* 2000, **104**, 11332-11339.
9. J. Grodkowski, P. Neta, E. Fujita, A. Mahammed, L. Simkhovich and Z. Gross, *J. Phys. Chem. A* 2002, **106**, 4772-4778.
10. (a) K. Gruber, B. Puffer and B. Kräutler, *Chem. Soc. Rev*. 2011, **40**, 4346-4363. (b) R. G. Matthews, *Acc. Chem. Res*. 2001, **34**, 681-689. (c) K. L. Brown, *Chem. Rev*. 2005, **105**, 2075-2149. (d) C. L. Drennan, S. Huang, J. T. Drummond, R. G. Matthews and M. L. Ludwig, *Science* 1994, **266**, 1669-1674. (e) W. Buckel and B. T. Golding, *Chem. Soc. Rev*. 1996, **25**, 329-337.
11. (a) D. Dolphin, R. L. N. Harris, J. L. Huppatz, A. W. Johnson and I. T. Kay, *J. Chem. Soc. C*. 1966, 30-40. (b) C.-J. Liu, A. Thompson and D. Dolphin, *J. Inorg. Biochem.* 2001, **83**, 133-138. (c) Y. Murakami, Y. Aoyama and K. Tokunaga, *J. Am. Chem. Soc*. 1980, **102**, 6736-6744. (d) Y. Murakami, K. Sakata, Y. Tanaka and T. Matsuo, *Bull. Chem. Soc. J*. 1975, **48**, 3622-3630. (e) N. S. Hush and I. S. Woolsey, *J. Am. Chem. Soc*. 1972, **94**, 4107-4114.
12. A. Ogawa, K. Oohora and T. Hayashi, *Submitted*.
13. B. Adinarayana, A. P. Thomas, P. Yadav, A. Kumar and A. Srinivasan, *Angew. Chem. Int. Ed*. 2016, **55**, 969-973.
14. The author also attempted to prepare a phenyl substituted Co(II) bipyricorrole instead of 2,6-dimethoxyphenyl substituted Co(II) bipyricorrole as a reference complex, but the synthesis was unsuccessful due to failure of the intermolecular coupling reaction of the corresponding bipyrromethane and bipyridine. Thus, the effect of the proximal methoxy group on the electrochemical reaction is not discussed in this paper.

15. K. T. Ngo, M. McKinnon, B. Mahanti, R. Narayanan, D. C. Grills, M. Z. Ertem and J. Rochford, *J. Am. Chem. Soc.* 2017, **139**, 2604-2618.
16. All potentials in this paper are reported relative to the $Fe^{III/II}$ couple of ferrocene (Fc).
17. R. H. Felton and H. Linschitz, *J. Am. Chem. Soc*. 1966, **88**, 1113-1116.
18. T. K. Mukhopadhyay, N. L. MacLean, L. Gan, D. C. Ashley, T. L. Groy, M.-H. Baik, A. K. Jones and R. J. Trovitch, *Inorg. Chem*. 2015, **54**, 4475-4482.
19. The pseudo-pH values of CO_2-saturated DMF solutions containing 1, 2, 3, 4, 5, 6, 7 and 8 M H_2O were determined to be 8.53, 8.37, 8.21, 8.03, 7.86, 7.73, 7.62 and 7.51, respectively, whereas the pseudo-pH values of N_2-saturated DMF solutions containing 1.8, 3.6, 5.4, 7.2, 9.0, 10.8, 12.6 and 14.4% v/v buffer were determined to be 8.33, 7.99, 7.84, 7.74, 7.66, 7.56, 7.50 and 7.44, respectively.
20. Each k_{obs} value was determined using the catalytic current at −2.17 V in the CV results depicted in Figure 2-6a and Figure 2-11a with a scan rate of 100 $mV \cdot s^{-1}$, which are attributed to CO_2 reduction and H_2 evolution, respectively.
21. **Co(II)TPP** was confirmed to catalyze selective CO_2-to-CO generation with FE of 87%, whereas no H_2 evolution was observed in the CPE experiment in the absence of H_2O.
22. The k_{cat} of **Co(II)BIPC** in the presence of 5 M TFE was determined using the i_{cat} at −2.28 V.
23. According to ref 7b, **Co(II)TPP** does not show current dependence on the concentration of proton sources. Thus, the reaction rate in the absence of a proton source was calculated for **Co(II)TPP**.
24. Demethylated **Co(II)BIPC**, which was prepared according to ref 6a, demonstrated no enhancement of the catalytic activity (Figure 2-18).
25. T. Matsuo, K. Komatsuzaki, T. Tsuji and T Hayashi, *J. Porphyrins Phthalocyanins*, 2012, **16**, 616-625.
26. T. Matsuo, A. Hayashi, M. Abe, T. Matsuda, Y. Hisaeda and T. Hayashi, *J. Am. Chem. Soc*. 2009, **131**, 15124-15125.

Chapter 3
Synthesis, structure and chemical properties of *meso*-dibenzoporphycene

Reproduced in part with permission from [*Angew. Chem. Int. Ed.* 2015, **54**, 6227-6230.]

3-1. Introduction

Porphycene is a constitutional isomer of porphyrin,[1] in which the symmetrically reduced porphyrinoid structure demonstrates notable physicochemical properties such as stronger absorption in the visible region[2] and tautomerization of the inner hydrogen atoms.[3] Investigation of porphycene derivatives indicates that they have potential for use as photosensitizers for photodynamic therapy[4] and as metal ligands in unique catalysts.[5] This has motivated us to prepare new porphycene derivatives with enlarged π-electron peripheries to regulate the electronic and structural features of porphycene. To this end, direct annulation of aromatic units to the porphycene framework is expected to be a useful strategy for extending the π-system, as seen in a series of benzene-fused porphyrins.[6] However, only a few reports for benzene-fused porphycene have been presented,[7] in spite of their expected unique features. Previous examples of annulated dibenzoporphycene and dinaphthoporphycene have been prepared by fusing two benzene and naphthalene moieties to the 3,4,5,6- and 13,14,15,16-positions of the porphycene framework.[8-10] In addition, tetrabenzoporphycene has four benzene-fused moieties at the 2,3-, 6,7-, 12,13-, and 16,17-postions of unsubstituted porphycene (**Pc**) as shown in Chart 3-1a.[11] These benzene-fused porphycenes show characteristic bathochromic shifts. In efforts focused on the 9,10- and 19,20-positions (*meso* positions: *i* and *s* positions in Chart 3-1a) of **Pc** as benzene fusion sites, only the monobenzene-fused derivative has been reported.[7,12] In this case, the low yield of *meso*-monobenzoporphycene prevents detailed evaluation of its physicochemical properties. Moreover, a *meso*-dibenzene-fused derivative has never been prepared and has only been investigated theoretically.[13] Our research group has recently prepared benzo[*i*]porphycene (*meso*-monobenzoporphycene; **mMBPc**, Chart 3-1b) and dibenzo[*i*,*s*]porphycene (*meso*-dibenzoporphycene; **mDBPc**, Chart 3-1c) in good yield by using Suzuki‐Miyaura coupling and intramolecular McMurry coupling reactions. In this paper, the author report the preparation and characterization of the physicochemical properties of these porphycene derivatives.

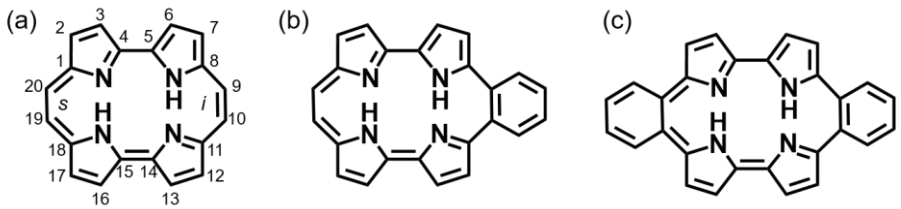

Chart 3-1. Molecular structures of (a) **Pc**, (b) **mMBPc** and (c) **mDBPc**. The *trans* tautmeric forms are represented.

3-2. Results and discussion

Synthesis of mMBPc and mDBPc

The synthesis of **mMBPc** and **mDBPc** is presented in Scheme 3-1. Although a series of porphycene derivatives have been synthesized by the intermolecular double McMurry coupling of two 5,5'-diformyl-2,2'-bipyrrole molecules, **mMBPc** and **mDBPc** were obtained through intramolecular single coupling[14] of diformylated *ortho*-bis-dipyrrolylbenzene derivatives **12** and **13**, respectively. The precursor **11** was prepared from borylated *N*,*N*'-diBoc-2,2'-bipyrrole **10** with *o*-diiodobenzene by Suzuki–Miyaura coupling. A Vilsmeier–Haack reaction of **11** and subsequent Boc deprotection upon heating at 140 °C under vacuum gave the dialdehyde **12**. The intramolecular McMurry coupling of **12** gave **mMBPc** in a 48% yield without oxidation, although the synthesis of porphycene derivatives generally requires the oxidation of the nonaromatic intermediate after cyclization.[7] For the synthesis of **mDBPc**, 3-dimethylaminoacrolein was used as a reagent in the Vilsmeier–Haack reaction to yield the precursor **13**.[15] After deprotection of **11**, the acrolein moiety was introduced into each α-position of the two bipyrrole units. The intramolecular McMurry coupling of **13** provided a mixture of the cyclized products. Further oxidation of the reaction mixture by using *p*-chloranil provided **mDBPc** in a 20% yield based on **13**. Both **mMBPc** and **mDBPc** were fully characterized by ^{1}H and ^{13}C NMR spectroscopy and mass spectrometry (see experimental section for details).

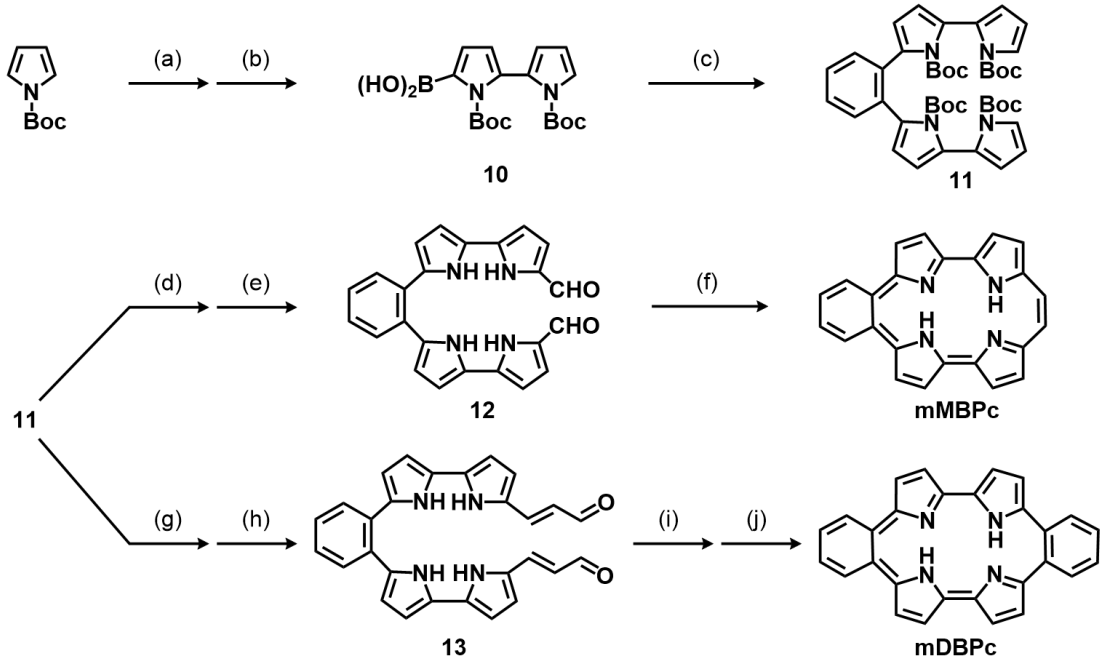

Scheme 3-1. Synthesis of **mMBPc** and **mDBPc**. (a) LTMP, $CuCl_2$, THF, 65%; (b) LTMP, $B(OEt)_3$, THF, 94%; (c) *o*-diiodobenzene, $Pd(PPh_3)_4$, K_2CO_3, H_2O, DMF, 82%; (d) $POCl_3$, DMF, 93%; (e) 140 °C, quant.; (f) Zn, CuCl, $TiCl_4$, THF, 48%; (g) 180 °C, ethylene glycol, 80%; (h) $POCl_3$, 3-dimethylaminoacrolein, CH_2Cl_2, quant.; (i) Zn, CuCl, $TiCl_4$, THF; (j) *p*-chloranil, CH_2Cl_2, 20% in 2 steps. LTMP=lithium 2,2,6,6-tetramethylpiperidide.

UV-vis-NIR absorption spectroscopic and cyclic voltammetric measurements

The UV-Vis-NIR absorption spectra of **Pc**, **mMBPc** and **mDBPc** in CH_2Cl_2 are shown in Figure 3-1. The λ_{max} values of the Q-bands for **mMBPc** appear at 613, 659, and 721 nm in CH_2Cl_2. These bands are red-shifted relative to those of **Pc** (558, 596, and 629 nm). It is significant that the Q-band absorptions of **mDBPc** are located in the NIR region at 648, 884, and 1047 nm. The 418 nm deviation of the lowest-energy Q-band of **mDBPc** from that of **Pc** is much larger than those of previously reported benzene-fused porphycenes (41-135 nm).[8-11] The Soret bands of **mMBPc** and **mDBPc** are also found to be red-shifted relative to that of **Pc** as a result of the benzene fusion. These bathochromic shifts are generally consistent with the theoretical estimations obtained by using DFT-optimized structures (see below and Table 3-3 in experimental section). The redox potentials of **mMBPc** and **mDBPc** were measured by cyclic voltammetry (CV) in CH_2Cl_2 (Table 3-1). The fused benzene moieties of the porphycene framework provide remarkably negative shifts in the oxidation potentials, while the reduction potentials are positively shifted. Considering the symmetry of the molecular orbitals, the HOMO of a butadiene unit, which is regarded as a substituent in each fused benzene moiety, interacts with the HOMO of porphycene to generate a new destabilized HOMO in both of the *meso*-benzoporphycenes (Figure 3-2 and Table 3-4 in experimental section).[13] By contrast, the interaction between the LUMOs of the butadiene unit and porphycene gives a new stabilized LUMO.

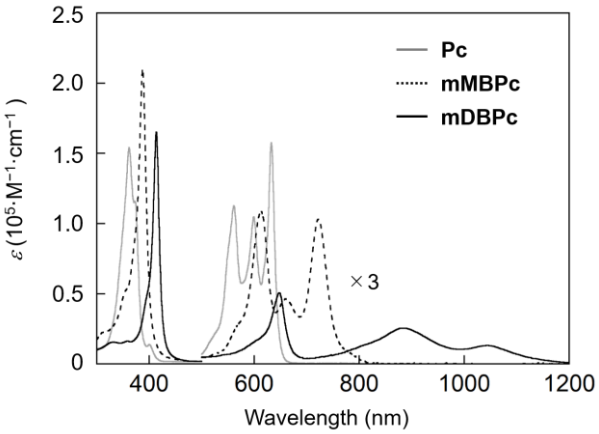

Figure 3-1. UV-vis-NIR absorption spectra for **Pc** (gray solid line), **mMBPc** (black dashed line) and **mDBPc** (black solid line) in CH_2Cl_2 at 25 °C. The absorption spectra in Q-band region (500-1200 nm) are enlarged.

Table 3-1. Comparative oxidation and reduction potentials (V vs Ag|AgCl)[a]

	Oxidation	Reduction
Pc[b]	+1.03	−0.70
mMBPc[c]	+0.68	−0.56
mDBPc[c]	+0.41	−0.40

[a]Potential values were measured through cyclic voltammetry in CH_2Cl_2 containing 0.1 M $TBAPF_6$. [porphycene] = 0.1 mM. [b]Scan rate: 100 mV·s^{-1}. [b]Scan rate: 10 mV·s^{-1}.

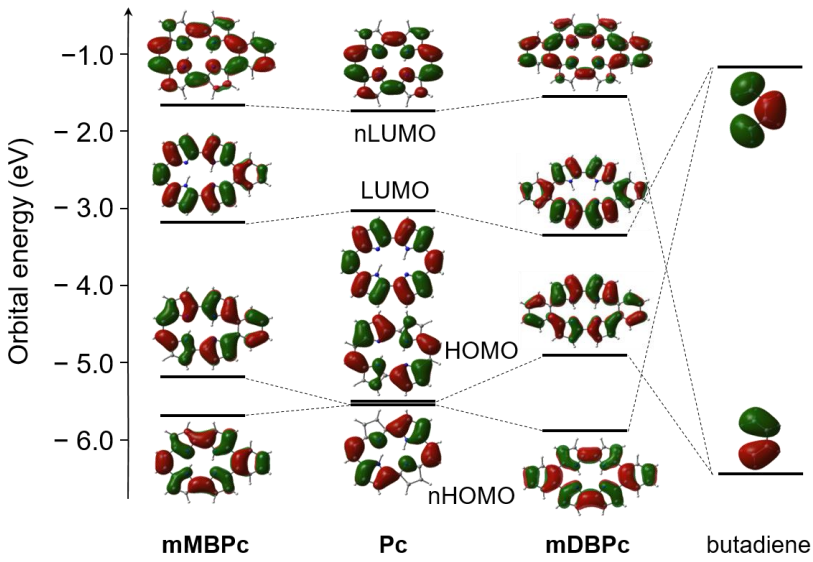

Figure 3-2. Molecular orbitals of **Pc**, **mMBPc**, and **mDBPc** (*cis* form, see below) and their energy levels. The diagram shows the interaction between **Pc** and butadiene units in **mMBPc** and **mDBPc**. Dashed lines indicate the corresponding molecular orbitals for butadiene and the three porphycene molecules.

X-ray crystal structure

The structures of **mMBPc** and **mDBPc** were determined by X-ray crystallography (Figure 3-3). The molecular structures in the crystals display generally planar geometries including the fused benzene moieties. Planar structures in the crystals could be formed by crystal packing, whereas the DFT calculations for **mMBPc** and **mDBPc** demonstrate saddled structures with very small vibrational frequency. This suggests that the frameworks are distorted in solution (Figure 3-4). The bond lengths at the *meso*-positions (C8−C9, C9−C10, and C10−C11 in **mMBPc**; C8−C9, C9−C10, C10−C11, C18−C19, C19−C20, and C20−C1 in **mDBPc**) are longer (>1.43 Å) than those in **Pc** (<1.40 Å)[1] and the bond lengths in each benzene moiety are clearly different, thus indicating electronic interactions between **Pc** and the benzene moieties. The shorter distances between the inner nitrogen atoms (N1−N4 or N2−N3) of **Pc**, **mMBPc** and **mDBPc** are 2.61, 2.59, and 2.54 Å, respectively. The angles C8-C9-C10 and C9-C10-C11 in **mMBPc** and the angles C8-C9-C10, C9-C10- C11, C18-C19-C20, and C19-C20-C1 in **mDBPc** are about 129°, whereas the corresponding angles in **Pc** are about 132°. The shorter N1−N4 and N2−N3 distances and these angles are typical for *meso* substitution in porphycene derivatives.[12a]

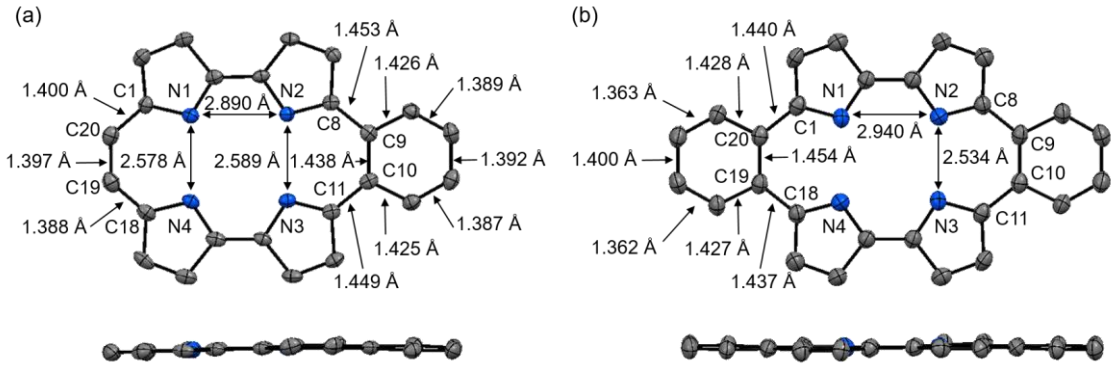

Figure 3-3. Crystal structures of (a) **mMBPc** and (b) **mDBPc** with several important bond lengths shown in ORTEP representation with 50% thermal ellipsoid probability. Top: macrocycle plane view. Bottom: perspective view. For clarity, only selected C and N atoms are numbered and hydrogen atoms are omitted.

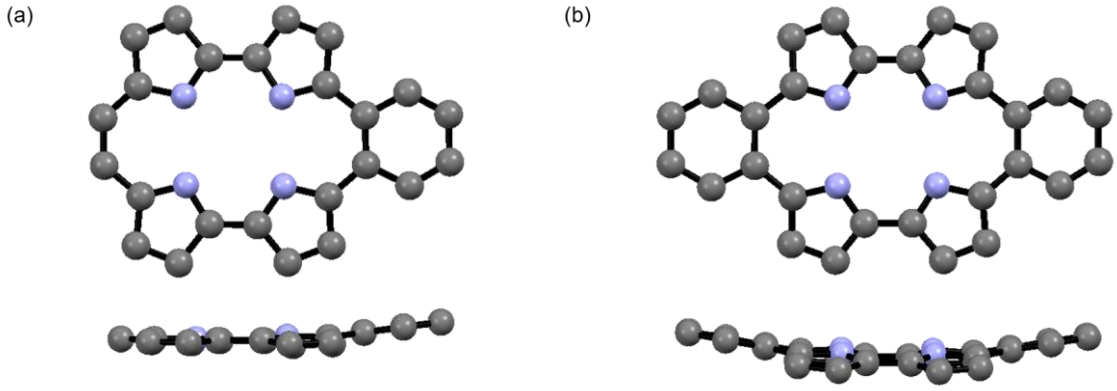

Figure 3-4. DFT(B3LYP/6-311G**)-optimized structures of (a) **mMBPc** (*trans* form) and (b) **mDBPc** (*cis* form). Top: macrocycle plane view. Bottom: perspective view. For clarity, hydrogen atoms have been omitted.

Evaluation of inner NH protons

The inner NH signals of **mMBPc** in the ^{1}H NMR spectrum ($CDCl_3$, 25 °C) appear downshifted at 7.84 ppm and 7.47 ppm, compared with that of **Pc** (3.15 ppm). Interestingly, the corresponding NH signal of **mDBPc** was observed at 8.95 ppm. The remarkable downfield shifts suggest the occurrence of strong intramolecular NH−N hydrogen bonding.[11b,16] The results correlate with the shorter N1−N4 distances in **mMBPc** and **mDBPc** compared to previous reported porphycenes in the crystal structures (Figure 3-5). [9,10,11b,12a,12b,16,17] For further evaluation of the strength of the inner NH‑N hydrogen bonds, an X-ray photoelectron spectroscopic (XPS) study was carried out (Figure 3-6, Table 3-2). In the region of the N1s ionization potentials (IP), two well-resolved peaks were observed for each derivative. The peak with the highest IP value is assigned as the "protonated" nitrogen atoms and the other peak is assigned as the "unprotonated" nitrogen atoms according to the previous report.[17,18] The differences between the IP values of the protonated and unprotonated nitrogen atoms (ΔI_{N1s}) are 1.40 eV (**Pc**), 1.30 eV (**mMBPc**), and 1.15 eV (**mDBPc**). These values show a clear correlation with the N1−N4 distances of the compounds and are

similar to the values from the previously reported data (Figure 3-7). This indicates that the smaller ΔI_{N1s} value is an indication of stronger intramolecular hydrogen bonding.[17] The IP values of *trans* and *cis* forms (Chart 3-2) optimized by DFT calculations and the calculated ΔI_{N1s} values are shown in Table 3-2. In the case of **mDBPc**, the difference between the calculated ΔI_{N1s} values for the two tautomeric forms is relatively large (>0.1 eV) and the experimental ΔI_{N1s} value is mostly consistent with the calculated value for the *cis* form. The present findings support the existence of the *cis* form in **mDBPc**.

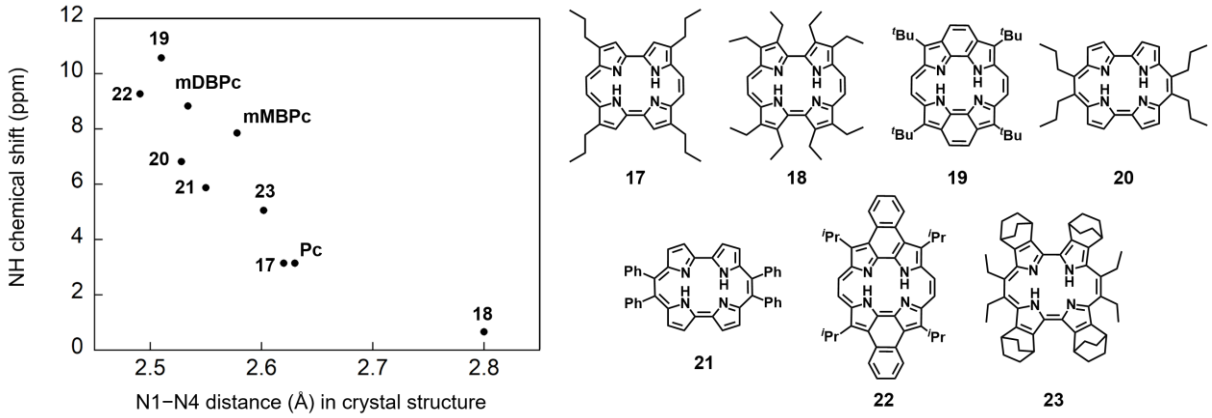

Figure 3-5. Relationship between NH chemical shifts in $CDCl_3$ and the N1−N4 distances of crystal structures in porphycene derivatives.

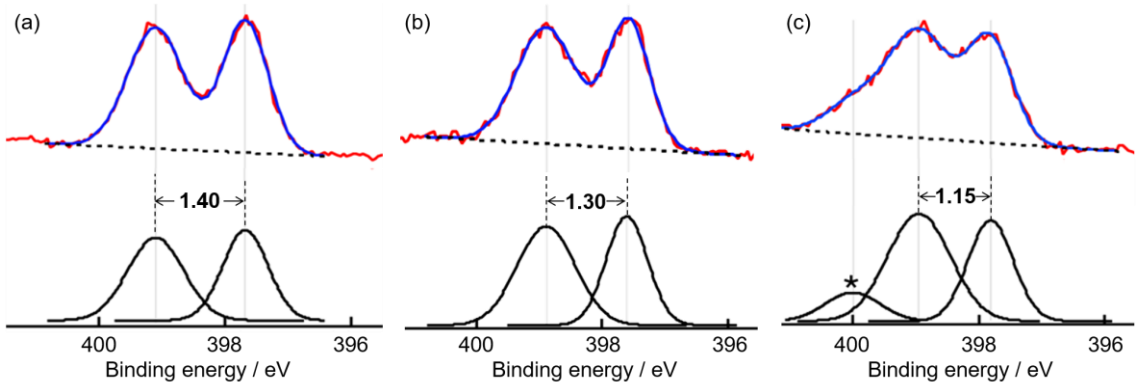

Figure 3-6. XPS spectra for (a) **Pc**, (b) **mMBPc**, and (c) **mDBPc**. Upper spectra: raw spectra and fitted profiles with baselines. Lower spectra: deconvoluted profiles produced by Gaussian fitting. The peak marked with the asterisk is derived from an unassigned impurity.

Table 3-2. XPS peak maxima (eV).[a,b]

	IP	Experimental ΔI_{N1s}	Calculated ΔI_{N1s} *trans* and *cis* forms
Pc	397.70, 399.10	1.40	1.38,[d] 1.46[e]
mMBPc	397.60, 398.90	1.30	1.31,[d] 1.35[e]
mDBPc[c]	397.80, 398.95	1.15	1.28,[d] 1.14[e]

[a]180 W of monochromatized $Al_{K\alpha}$ radiation. [b]Detailed data are summarized in Table 3-6 in experimental section. [c]The unassigned impurity at 400.0 eV was ignored. [d]*trans* form. [e]*cis* form.

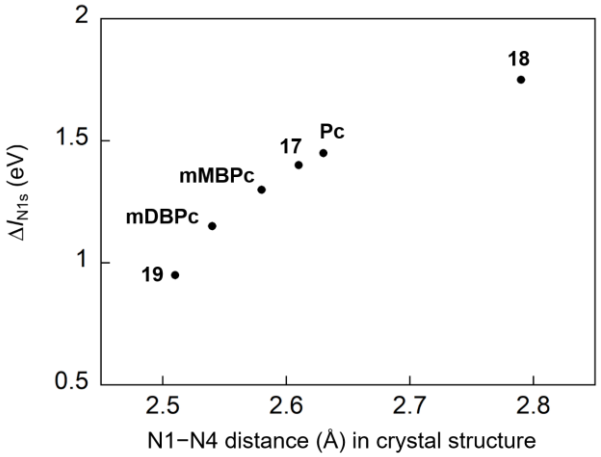

Figure 3-7. Relationship between the ΔI_{N1s} values XPS experiments and the N1−N4 distances of crystal structures in porphycene derivatives.

Generally, porphycene derivatives adopt the stable *trans* form,[2,19,20] as confirmed by experimental and theoretical investigations.[21] As determined for the usual porphycene derivatives, DFT calculations indicate that the *trans* form of **mMBPc** is 1.6 kcal·mol^{-1} more stable than the *cis* form (see Table 3-5 in experimental section). By contrast, Waluk and co-workers reported the tautomerization of *meso*-alkylated porphycenes and demonstrated the existence of two forms (*cis* and *trans* forms) in the gound state by using supersonic jet techniques, although the *trans* form is predominant according to DFT calculations.[2,3a,3b,22] Interestingly, in the case of **mDBPc**, the DFT calculations suggests that the *cis* form is slightly more stable than the *trans* form (0.1 kcal·mol^{-1} in B3LYP/6-311G**, 5.1 kcal·mol^{-1} in ωB97XD/6-311G**). These theoretical data for the tautomeric forms are consistent with the XPS results.

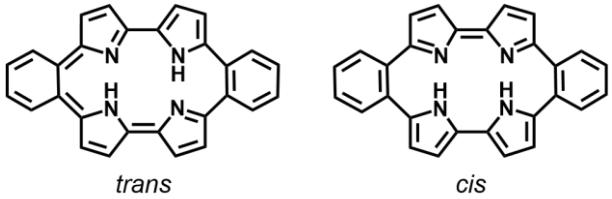

Chart 3-2. Possible tautomeric structures of **mDBPc**.

3-3 Summary

In Chapter 3, **mDBPc** provides very unique characteristics as a result of the simple insertion of two benzene moieties at the ethylene bridges of the porphycene framework. First, the HOMO‑LUMO gap is dramatically reduced as a result of electronic interaction between the fused benzene and porphycene moieties. Second, the theoretical and experimental results indicate that **mDBPc** exists in the *cis* tautomeric form. This is unusual for a series of porphycene derivatives. To the best of our knowledge, this is the first example of the *cis* form of porphycene being more stable than the *trans* form at the ground state. Further spectroscopic studies will contribute to the evaluation of the tautomeric form.

3-4. Experimental section

Materials and methods

UV-vis spectral measurements were carried out with a Shimadzu UV-3700 or UV-3150 double-beam spectrophotometer with a thermostated cell holder. ESI-TOF MS analyses were performed on a Bruker micrOTOF-II mass spectrometer and MALDI-TOF MS analyses were performed on a Bruker autoflex III mass spectrometer. FAB-MS data were measured using a JEOL JMS-700 spectrometer. ^{1}H and ^{13}C NMR spectra were recorded on a Bruker DPX 400 (400 MHz) or Avance III (600 MHz) spectrometer. Chemical shifts were reported in ppm relative to the residual solvent resonances. NMR measurements were carried out at 298 K unless otherwise indicated. XPS spectra were recorded on a Shimadzu KRATOS AXIS-165x spectrometer. Electrochemical studies were carried out using potentiostat (CompactStat, Ivium Technologies) with a platinum wire as a counter electrode, an Ag|AgCl (3 M $NaCl_{aq.}$) electrode obtained from BAS as a reference electrode and a polished platinum disk as a working electrode under anaerobic conditions. Distilled water was demineralized using a Millipore Integral 3 apparatus. Other all reagents of the highest guaranteed grade available were obtained from commercial sources and were used as received unless otherwise indicated.

X-ray Crystallography

A single crystal of **mMBPc** was mounted on a loop. Data from X-ray diffraction were collected at 20 °C by a Rigaku XtaLAB mini imaging plate area detector using graphite monochromated Mo-Kα radiation (0.71075 Å). A single crystal of **mDBPc** was mounted on a loop. Data from X-ray diffraction were collected at −170 °C by a RAXIS RAPID imaging plate area detector using graphite monochromated Mo-Kα radiation (0.71075 Å). All of the crystallographic calculations were performed using the Crystal Structure software package of Molecular Structure Corp. [Crystal Structure, Crystal Structure Analysis Package, version 3.8.1, Molecular Structure Corp. and Rigaku Corp.]. Structures were solved by SIR 2008 and expanded using Fourier techniques. Non-hydrogen atoms were refined anisotropically by full-matrix least-squares on F^2. All structures in the final stages of refinement showed no movement in the atom positions. Hydrogen atoms were attached at idealized positions on carbon atoms

and not refined. Crystallographic parameters are summarized in Table 3-7. CCDC 1046868 (**mMBPc**) and CCDC 1046869 (**mDBPc**) contain the supplementary crystallographic data for this paper.

XPS measurements

Sample powder was dried in vacuo overnight before transfer to a carbon tape on a sample holder. For the XPS measurement, monochromatic $Al_{K\alpha}$ X-ray radiation was used. The power level of the X-ray was 180 W for the narrow scan. The pass energy was 10 eV. Neutralization by the low-energy flood gun with suitable conditions was performed to diminish sample charging during the XPS measurement. The binding energies were calibrated by setting the lowest binding energy component of the C1s electron band to 284.5 eV. This peak was assumed to originate from the C−C component of porphycenes and the 6 surface of carbon tape. The spectra were analyzed by a Multi-Peak Fit package in WaveMetrics Igor Pro 6.22.

DFT calculations

Molecular structures were optimized at the B3LYP[23a]/6-311G** level. Normal mode analysis was performed for the stationary points on the potential energy surface. Concerning the relative stability between *trans* and *cis* forms, structure optimization at the ωB97XD[23b]/6-311G** level was also carried out. The MO diagram in Figure 3-7, excitation energies in Table 3-3, orbital energy levels in Table 3-4, and N1s ionization potentials (IPs) were calculated using the ground-state optimized structure. The N1s IP was calculated using the Koopmans theorem (KT) at the B3LYP/6-311G**//B3LYP/6- 311G** level. Relative IPs with KT were in good agreement with the experimental data. We also checked the basis-set dependence and relativistic effect, but no significant improvement was obtained. A constant shift of Δ=8.65 eV was included, so that the calculated IP for the higher peak of **mMBPc** corresponds exactly to the experimental data. All of the computations were performed with the Gaussian09 program.[24]

Table 3-3. The first and second excited states of **Pc**, **mMBPc** and **mDBPc**[a]

			E_{ex} (calcd.)[b]	E_{ex} (exptl.)[c]	Main configuration (|C|≥0.3)[d]	Osc.[e]
Pc	*trans*	1^1Bu	2.24	1.97	0.61 (nH→L)	0.13
		2^1Bu	2.35	2.22	0.62 (H→L)	0.20
	cis	1^1A1	2.24		0.65 (H→L)	0.14
		1^1B2	2.35		0.64 (nH→L)−0.30(H→nL)	0.17
mMBPc	*trans*	1^1A	1.88	1.72	0.69 (H→L)	0.16
		2^1A	2.27	2.02	0.62 (nH→L)−0.32(nH→nL)	0.15
	cis	1^1A	1.87		0.69 (H→L)	0.16
		2^1A	2.32		0.62 (nH→L)−0.33(nH→nL)	0.14
mDBPc	*trans*	1^1B	1.52		0.72 (H→L)	0.15
		2^1B	2.18		0.61 (nH→L)−0.35(nH→nL)	0.14
	cis	1^1A’	1.50	1.40	0.71 (H→L)	0.14
		1^1A”	2.26	1.91	0.61 (nH→L)−0.35(nH→nL)	0.14

[a]Calculated at B3LYP/6-311G** level. [b]Excitation energy (eV). [c]Experimental excitation energy was derived from absorption spectra. [d]Main configuration with coefficient larger than 0.3. “H”, “L”, “nH” and “nL” denote HOMO, LUMO, next HOMO and next LUMO, respectively. [e]Oscillator strength in atomic unit.

Table 3-4. Molecular orbital energy levels of **Pc**, **mMBPc** and **mDBPc**[a]

	HOMO	LUMO	ΔHOMO[b]	ΔLUMO[b]	ΔE_{ox}[c]	ΔE_{red}[c]
Pc	−5.51	−3.06	0	0	0	0
mMBPc	−5.17	−3.19	0.34	−0.13	−0.35	0.14
mDBPc	−4.90	−3.36	0.61	−0.30	−0.62	0.30

[a]Orbital energy (eV) calculated at B3LYP/6-311G** level. [b]Differential value of HOMO or LUMO orbital energy from that of **Pc**. [c]Differential value of experimental redox potential (V) measured by CV from that of **Pc**.

Table 3-5. Relative potential energy (kcal·mol^{-1}) of *trans*- and *cis*-tautomeric forms of **Pc**, **mMBPc** and **mDBPc**[a]

		trans		TS[b]	*cis*	
		saddle	planar		saddle	planar
Pc	B3LYP	none	0.0 (61.4)	4.5 (1229.3*i*)	none	2.4 (61.0)
	ωB97XD	none	0.0 (59.4)	4.4 (1243.9*i*)	none	1.9 (59.7)
mMBPc	B3LYP	0.0 (25.9)	0.1 (22.1*i*)	3.7 (1199.4*i*)[c]	1.6 (20.5)	1.7 (17.7*i*)
				3.4 (1177.3*i*)[d]		
	ωB97XD	0.0 (36.2)	0.4 (42.6*i*)	4.5 (1243.3*i*)[c]	1.3 (36.5)	1.7 (38.5*i*)
				3.7 (1207.4*i*)[d]		
mDBPc	B3LYP	0.1 (25.2)	0.5 (18.6*i*)	2.6 (1181.8*i*)	0.0 (27.3)	0.6 (25.6*i*)
	ωB97XD	5.1 (30.1)	5.8 (28.7*i*)	7.2 (1183.1*i*)	0.0 (31.4)	2.7 (35.8*i*)

[a]Potential energy of the minimum energy structure was used as reference and 6-311G** basis sets were used. Number in parenthesis is the smallest frequency (in cm^{-1}) obtained with normal mode analysis. [b]Transition state connecting *trans*- and *cis*-forms. [c]Proton transfer between N1 and N4 atoms. [d]Proton transfer between N2 and N3 atoms.

Table 3-6. Calculated N1s ionization potential (IP) values (eV) in porphycenes for XPS experiments

		IP		ΔI_{N1s}	
		KT+Δ[a]	experimental	KT[b]	experimental
Pc	*trans*	397.52, 398.90	397.70, 399.10	1.38	1.40
	cis	397.47, 398.93		1.46	
mMBPc	*trans*	397.55, 397.62	397.60, 398.90	1.31, 1.34	1.30
		398.86, 398.89		(1.31)[c]	
	cis	397.52, 397.60		1.34, 1.38	
		398.87, 398.91		(1.35)[c]	
mDBPc	*trans*	397.62, 398.90		1.28	
	cis	397.71, 398.84	397.80, 398.95	1.14	1.15

[a]IP by Koopmans theorem. "Δ" denotes that the IP values were shifted by 8.65 eV. [b]IP relative to a band with the lowest energy. [c]Difference between averaged IP values of unprotonated and protonated nitrogen atoms.

Table 3-7. Crystallographic data for **mMBPc** and **mDBPc**.

parameters	**mMBPc**	**mDBPc**
emphirical formula	$C_{24}H_{16}N_4$	$C_{42}H_{27}N_6$
formula weight	360.42	615.72
crystal system	orthorhombic	monoclinic
a, Å	4.5787(9)	10.9714(11)
b, Å	17.863(4)	13.8807(14)
c, Å	20.594(4)	18.7322(17)
α, deg	90.0000	90.0000
β, deg	90.0000	100.113(3)
γ, deg	90.0000	90.0000
V, Å^3	1684.4(6)	2808.4(5)
space group	$P2_12_12_1$	$P2_1/c$
Z	4	4
ρ_{calc}, g·cm^{-1}	1.421	1.456
μ(MoKα), cm^{-1}	0.71075	0.71075
temp, K	293	103
data	3849	27289
unique data	2269	6419
$R_1{}^a$	0.0663	0.0622
$wR_2{}^b$	0.1780	0.1741
GOF	0.939	1.010

$^aR1 = \Sigma(|F_o| - |F_c|)/ \Sigma|F_o|$. $^bwR_2 = [\Sigma(w(F_o^2 - F_c^2)^2)/\Sigma w(F_o^2)^2]^{1/2}$.

Synthesis of mMBPc and mDBPc

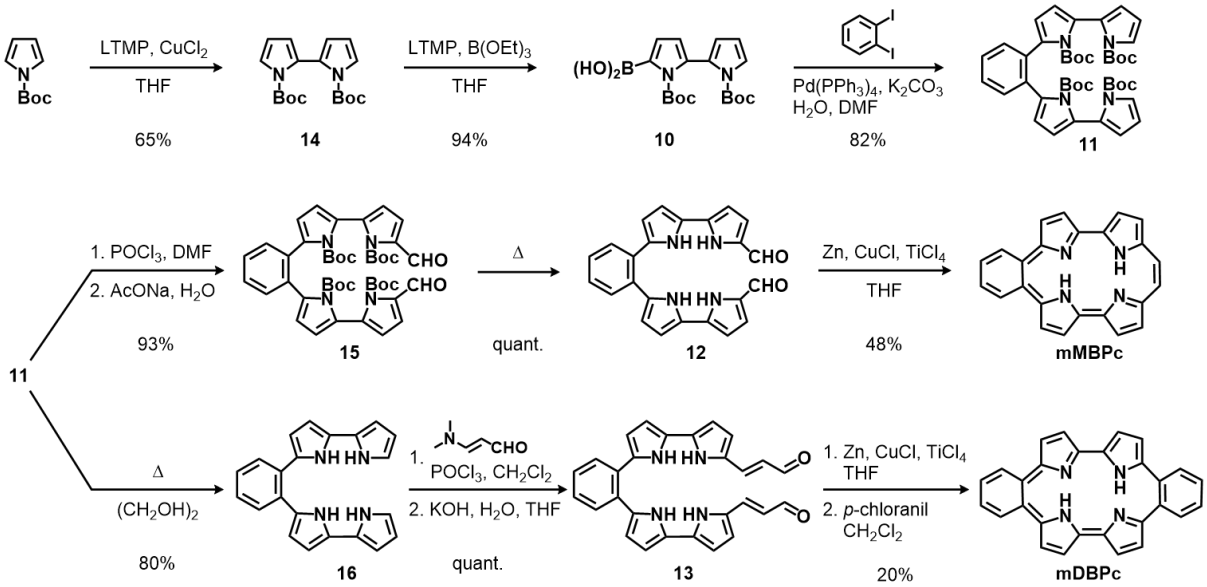

Scheme 3-2. Synthesis of **mMBPc** and **mDBPc**.

N,N'-Di-*tert*-butoxycarbonyl-2,2'-bipyrrole (14)

A hexane solution (22.4 mL) of ^{n}BuLi (35.9 mmol) was added dropwise to a solution of 2,2,6,6-tetramethylpiperidine (5.1 g, 35.9 mmol) in dry THF (20 mL) at –78 °C under an N_2 atmosphere. After stirring for 30 min at –78 °C, *N*-Boc-pyrrole (5.0 g, 29.9 mmol) in dry THF (50 mL) was added dropwise to this solution. The resulting solution was stirred for 3 h at –78 °C. To this solution, $CuCl_2$ (8.04 g, 59.8 mmol) was added and the solution was then stirred for 2 h at –78 °C and then for 18 h at room temperature. The reaction was quenched with sat. $NH_4Cl_{aq.}$ (30 mL). The mixture was extracted with ethyl acetate, and the organic layer was washed with sat. $glycine_{aq.}$ and sat. $NaCl_{aq.}$, and dried over Na_2SO_4. After removal of the solvents under reduced pressure, the product was purified by SiO_2 column chromatography (hexane/ ethyl acetate = 9/1, hexane/CH_2Cl_2 = 3/2) to yield compound **14** as a brown oil (3.2 g, 65%). ^{1}H NMR (400 MHz, $CDCl_3$) δ: 1.37 (s, 18 H, C(C*H*$_3$)$_3$), 6.18 (d, *J* = 2.4 Hz, 4H, pyrrole *βH*), 7.38 (t, *J* = 2.4 Hz, 2H, pyrrole *αH*). ^{13}C NMR (100 MHz, $CDCl_3$) δ: 27.94, 83.27, 110.30, 115.50, 122.12, 126.16, 149.27. HR MS (FAB, positive): *m/z* = 332.1732 $[M]^+$, calculated for $C_{18}H_{24}N_2O_4$ 332.1736.

(*N,N'*-Di-*tert*-butoxycarbonyl-2,2′-bipyrrol-5-yl)boronic acid (10)

A hexane solution (15.1 mL) of ^{n}BuLi (24.1 mmol) was added dropwise to 2,2,6,6-tetramethylpiperidine (3.4 g, 24.1 mmol) dissolved in dry THF (22 mL) at –78 °C under an N_2 atmosphere. After stirring for 30 min at –78 °C, compound **14** (7.13 g, 21.5 mmol) in dry THF (84 mL) was added dropwise to this solution. The resulting solution was then stirred for 3 h at –78 °C. To the solution, triethyl borate (6.39 g, 44.0 mmol) was added slowly and stirred for 30 min at –78 °C and then for 18 h at room temperature. The reaction was quenched with sat. $NH_4Cl_{aq.}$ (20 mL). The mixture was extracted with diethyl ether, washed with sat. $NaCl_{aq.}$ and dried over Na_2SO_4. After removal of the

solvents under reduced pressure, compound **10** was obtained by re-precipitation with hexane/diethyl ether as a pale yellow solid (7.52 g, 94%). ^{1}H NMR (400 MHz, $CDCl_3$) δ: 1.29 (s, 9H, C(C*H*$_3$)$_3$), 1.34 (s, 9H, C(C*H*$_3$)$_3$), 6.15-6.16 (m, 1H, pyrrole *βH*), 6.19-6.20 (m, 1H, pyrrole *βH*), 6.24 (m, 1H, pyrrole *βH*), 6.56 (br, 2H, O*H*), 7.07 (m,1H, pyrrole *βH*), 7.39 (m, 1H, pyrrole *αH*). ^{13}C NMR (100 MHz, $CDCl_3$) δ: 27.67, 27.89, 83.85, 85.20, 110.66, 115.30, 116.67, 122.05, 126.58, 127.11, 132.67, 149.18, 153.05. (It is usually difficult to observe the carbon atom binding to a boron atom in a ^{13}C NMR spectrum due to rapid quadrapole-induced relaxation.)

1,2-Bis(*N,N'*-di-*tert*-butoxycarbonyl-2,2'-bipyrrol-5-yl)benzene (11)

Compound **10** (1.07 g, 2.84 mmol), *o*-diiodebenzene (0.19 g, 0.57 mmol) and K_2CO_3 (1.58 g, 11.4 mmol) were dissolved in DMF (30 mL) and H_2O (3.0 mL). To the N_2-purged solution for 20 min was added $Pd(PPh_3)_4$ (132 mg, 20 mol%). After N_2-purging over 20 min, the solution was stirred at 80 °C for 20 h. The mixture was extracted with ethyl acetate, and the organic layer was washed with sat. $NaCl_{aq.}$ and dried over Na_2SO_4. After removal of the solvents under reduced pressure, the product was purified by SiO_2 column chromatography (hexane/ethyl acetate = 9/1) to yield compound **11** as a pale yellow solid (347 mg, 82%). ^{1}H NMR (400 MHz, CD_2Cl_2) δ: 1.13 (s, 18H, C(C*H*$_3$)$_3$), 1.43 (s, 18H, C(C*H*$_3$)$_3$), 6.00 (d, *J* = 3.2 Hz, 2H, pyrrole *βH*), 6.06 (d, *J* = 3.2 Hz, 2H, pyrrole *βH*), 6.17-6.19 (m, 4H, pyrrole *βH*), 7.26-7.33 (m, 6H, pyrrole *αH*, Ar-*H*). ^{13}C NMR (100 MHz, CD_2Cl_2) δ: 27.20, 27.66, 82.60, 83.21, 110.00, 113.02, 113.85, 115.30, 121.56, 126.52, 126.81, 126.97, 130.19, 134.65, 134.80, 148.88, 149.04. HR MS (FAB, positive): *m/z* = 738.3636 $[M]^+$, calculated for $C_{42}H_{50}N_4O_8$ 738.3629.

1,2-Dis(*N,N'*-di-*tert*-butoxycarbonyl-5'-formyl-2,2'-bipyrrol-5-yl)benzene (15)

To a DMF solution (1.2 mL) of compound **11** (275 mg, 0.37 mmol) was added phosphoryl chloride (285 mg, 1.86 mmol) in 1.2 mL of DMF and the solution was stirred at 0 °C for 1.5 h. After further stirring at room temperature for 19 h, $AcONa_{aq.}$ (8 mL, 4.6 M) was added to the solution at 0 °C. The product was extracted by ethyl acetate and the solution was washed with sat. $NaCl_{aq.}$, dried over Na_2SO_4 and the solvent was evaporated. The residue was passed through the SiO_2 column (hexane/ethyl acetate = 4/1) to yield compound **15** as a brown solid (273 mg, 93%). ^{1}H NMR (400 MHz, CD_2Cl_2) δ: 1.15 (s, 18 H, C(C*H*$_3$)$_3$), 1.45 (s, 18 H, C(C*H*$_3$)$_3$), 6.03 (d, *J* = 3.6 Hz, 2H, pyrrole *βH*), 6.15 (d, *J* = 3.6 Hz, 2H, pyrrole *βH*), 6.23 (d, *J* = 3.6 Hz, 2H, pyrrole *βH*), 7.11 (d, *J* = 3.6 Hz, 2H, pyrrole *βH*), 7.29-7.33 (m, 2H, Ar-*H*), 7.36-7.39 (m, 2H, Ar-*H*), 10.12 (s, 2H, C*H*O). ^{13}C NMR (100 MHz, CD_2Cl_2) δ: 27.21, 27.50, 83.51, 85.46, 113.36, 114.76, 115.17, 119.62, 125.40, 126.98, 130.14, 133.68, 134.34, 135.36, 135.47, 148.53, 148.69, 181.51. HR MS (FAB, positive): *m/z* = 794.3511 $[M]^+$, calculated for $C_{44}H_{50}N_4O_{10}$ 794.3527.

1,2-Bis(5'-formyl-2,2'-bipyrrol-5-yl)benzene (12)

In vacuo, compound **15** (201 mg, 0.25 mmol) was heated at 140 °C for 2.5 h to yield compound **12** as a black solid (106 mg, quant). ^{1}H NMR (400 MHz, CD_2Cl_2/DMSO-d_6) δ: 5.95 (dd, *J* = 3.6 Hz, 2.8 Hz, 2H, pyrrole *βH*), 6.42 (dd, *J* = 4.0 Hz, 2.4 Hz, 2H, pyrrole *βH*), 6.53 (dd, *J* = 3.6 Hz, 2.8 Hz, 2H, pyrrole *βH*), 6.88 (dd, *J* = 4.0 Hz, 2.4 Hz, 2H, pyrrole *βH*), 7.32 (dd, *J* = 6.0 Hz, 3.6 Hz, 2H, Ar-*H*), 7.53 (dd, *J* = 6.0 Hz, 3.6 Hz, 2H, Ar-*H*), 9.30 (s, 2H, C*H*O), 10.92 (br, 2H, N*H*), 11.68 (br, 2H, N*H*). ^{13}C NMR (100 MHz, CD_2Cl_2/DMSO-d_6) δ: 106.84, 109.43, 110.11, 122.90, 124.26, 127.08, 129.28, 130.97, 132.12, 132.73, 134.37, 177.12. HR MS (FAB, positive): *m/z* = 394.1422 $[M]^+$, calculated for $C_{24}H_{18}N_4O_2$ 394.1430.

Benzo[*i*]porphycene (mMBPc)

To a dry THF (150 mL) solution of activated Zn powder (1.56 g, 23.8 mmol) and CuCl (235 mg, 2.37 mmol), $TiCl_4$ (2.30 g, 11.9 mmol) was added dropwise at 0 °C under an N_2 atmosphere. After the reaction mixture was refluxed for 3 h, compound **12** (234 mg, 0.590 mmol) in dry THF (200 mL) was added dropwise over 1.5 h. The solution was refluxed for 30 min. To the solution at 0 °C, 10% $Na_2CO_{3aq.}$ (180 mL) was added dropwise over 1 h before celite filtration. The organic layer was extracted with CH_2Cl_2, washed with water, and dried over Na_2SO_4. After removal of the solvent, the residue was passed through an Al_2O_3 (neutral, grade III) column (CH_2Cl_2) and the collected fractions were recrystallized from hexane/CH_2Cl_2 to yield purple needle crystals (**mMBPc**, 103 mg, 48%). ^{1}H NMR (400 MHz, $CDCl_3$) δ: 7.47 (br, 1H, N*H*), 7.85 (br, 1H, N*H*), 8.32 (dd, *J* = 6.4 Hz, 3.6 Hz, 2H, Ar-*H*), 8.71 (d, *J* = 4.4 Hz, 2H, pyrrole *βH*), 8.95 (s, 2H, *meso-H*), 9.06 (d, *J* = 4.4 Hz, 2H, pyrrole *βH*), 9.15 (d, *J* = 4.4 Hz, 2H, pyrrole *βH*), 9.26 (d, *J* = 4.4 Hz, 2H, pyrrole *βH*), 10.21 (dd, *J* = 6.4 Hz, 3.6 Hz, 2H, Ar-*H*). ^{13}C NMR (100 MHz, $CDCl_3$) δ: 115.57, 122.58, 124.81, 124.95, 125.38, 126.62, 131.03, 131.74, 132.63, 142.45, 147.06, 148.20. HR MS (FAB, positive): *m/z* = 360.1362 $[M]^+$, calculated for $C_{24}H_{16}N_4$ 360.1375.

1,2-Bis(2,2'-bipyrrol-5-yl)benzene (16)

Compound **11** (1.00 g, 1.35 mmol) in ethylene glycol (20 mL) was stirred for 1 h at 180 °C. To the solution, ethyl acetate was added at room temperature and the organic layer was washed with sat. $NaCl_{aq.}$ and dried over Na_2SO_4. After removal of the solvents under reduced pressure, the residue was purified by SiO_2 column chromatography (CH_2Cl_2) to yield compound **16** as a pale green solid (367 mg, 80%). ^{1}H NMR (400 MHz, $CDCl_3$) δ: 6.05 (m, 2H, pyrrole *βH*), 6.16 (m, 2H, pyrrole *βH*), 6.27 (m, 2H, pyrrole *βH*), 6.42 (m, 2H, pyrrole *βH*), 6.69 (m, 2H, pyrrole *αH*) 7.30 (m, 1H, Ar-*H*), 7.53 (m, 1H, Ar-*H*), 8.04 (br, 1H, N*H*), 8.11 (br, 1H, N*H*). ^{13}C NMR (100 MHz, $CDCl_3$) δ:104.38, 104.78, 109.45, 109.67, 118.06, 125.31, 126.81, 127.40, 129.51, 129.95, 130.95. HR MS (ESI, positive): *m/z* = 339.1602 $[M + H]^+$, calculated for $C_{22}H_{19}N_4$ 339.1610.

1,2-Bis(5'-acroleinyl-2,2'-bipyrrol-5-yl)benzene (13)

To a solution of compound **16** (174 mg, 0.514 mmol) and 3-dimethylaminoacrolein (198 mg, 8.73 mmol) in dry CH_2Cl_2 (5.2 mL), $POCl_3$ (393 mg, 2.56 mmol) was added slowly and stirred for 1 h at 0 °C. After removal of the solvents under reduced pressure, the residue was dissolved in $KOH_{aq.}$ (5% w/v, 175 mL) and THF (175 mL). After stirring for 1 h at room temperature, the solution was neutralized with citric acid, and the mixture was extracted with ethyl acetate. The organic layer was dried over Na_2SO_4, and the solvent was removed under reduced pressure. The product was purified by re-precipitation in a diethyl ether/THF solution and compound **13** was obtained as a purple solid (223 mg, quant.). ^{1}H NMR (400 MHz, THF-d_8) δ: 6.06 (m, 2H, pyrrole *βH*), 6.28 (dd, *J* = 7.8, 15.6 Hz, 2H, -CHC*H*CHO), 6.32 (m, 2H, pyrrole *βH*), 6.48 (m, 2H, pyrrole *βH*), 6.55 (m, 2H, pyrrole *βH*), 7.23 (d, *J* = 15.6 Hz, 2H, -C*H*CHCHO), 7.28 (m, 2H, Ar-*H*), 7.51 (m, 2H, Ar-*H*), 9.47 (d, *J* = 7.6 Hz, 2H, C*H*O), 10.1 (s, 2H, N*H*), 10.7 (s, 1H, N*H*). ^{13}C NMR (100 MHz, THF-d_8) δ: 107.36, 107.39, 110.50, 119.00, 121.73, 126.13, 127.46, 129.45, 129.70, 131.93, 132.99, 133.20, 140.84, 191.57. HR MS (ESI, positive): *m/z* = 447.1818 $[M + H]^+$, calculated for $C_{28}H_{23}N_4O_2$ 447.1821.

Dibenzo[*i,s*]porphycene (mDBPc)

To a dry THF (120 mL) solution of activated Zn (1.19 g, 18.2 mmol) and CuCl (178 mg, 1.80 mmol) at 0 °C, $TiCl_4$ (1.75 g, 9.23 mmol) was added dropwise under an N_2 atmosphere. After the reaction mixture was refluxed for 3 h, compound **13** (200 mg, 0.448 mmol) in dry THF (160 mL) was added dropwise over 3.5 h. The reaction mixture was refluxed for 30 min. To the solution at 0 °C, 10% $Na_2CO_{3aq.}$ (272 mL) was added dropwise over 1 h before celite filtration. The organic layer was extracted with CH_2Cl_2, washed with water, and dried with Na_2SO_4. After removal of the solvents, the residue was passed through an SiO_2 column (CH_2Cl_2). The collected fractions were evaporated and the solid was re-dissolved in CH_2Cl_2 (100 mL). To the solution, *p*-chloranil (100 mg, 0.409 mmol) in CH_2Cl_2 (50 mL) was added and then the reaction mixture was stirred for 10 min at room temperature. The residue was passed through an SiO_2 column (CH_2Cl_2) and the green fraction was concentrated. After re-precipitation in a CH_2Cl_2/acetone solution, **mDBPc** was obtained as a dark blue solid (36 mg, 20%).^{1}H NMR (600 MHz, DMSO-d_6, 333 K) δ: 8.34 (dd, *J* = 3.2, 6.4 Hz, 4H, Ar-*H*), 8.83 (s, 2H, N*H*), 9.48 (d, *J* = 4.8 Hz, 4H, pyrrole *βH*), 9.59 (d, *J* = 4.4 Hz, 4H, pyrrole *βH*), 10.23 (dd, *J* = 3.2, 6.6 Hz, 4H, Ar-*H*). ^{13}C NMR (150 MHz, DMSO-d_6, 333 K) δ: 124.83, 126.36, 126.51, 126.64, 131.27, 136.63, 149.28. HR MS (MALDI, positive): *m/z* = 410.1535 $[M]^+$, calculated for $C_{28}H_{18}N_4$ 410.1531.

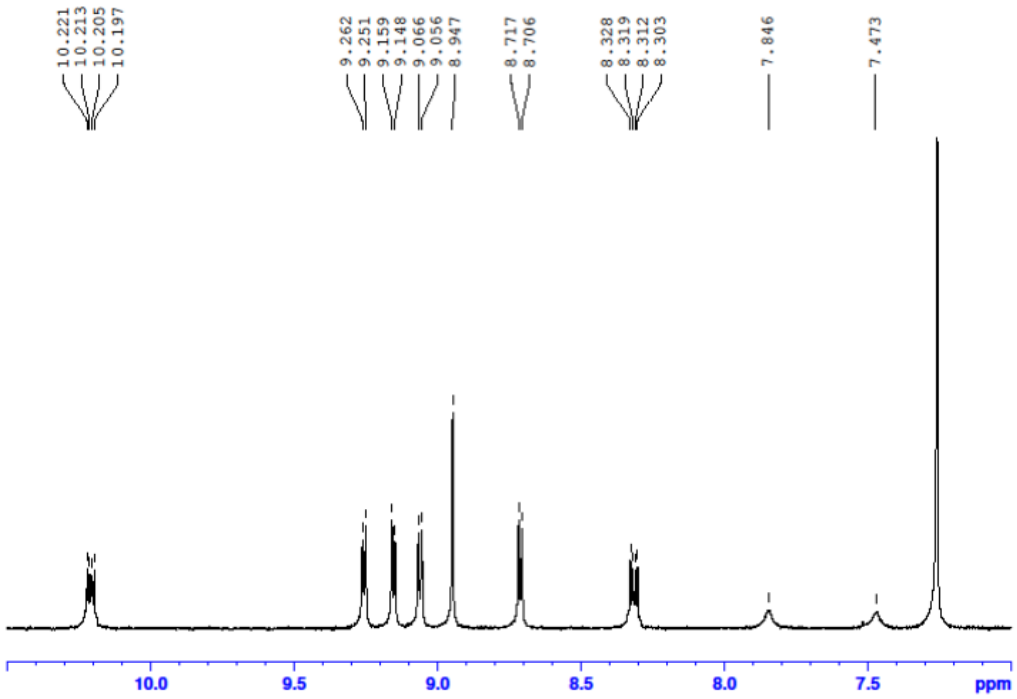

Figure 3-8. ^{1}H NMR spectrum (400 MHz, $CDCl_3$) of **mMBPc**.

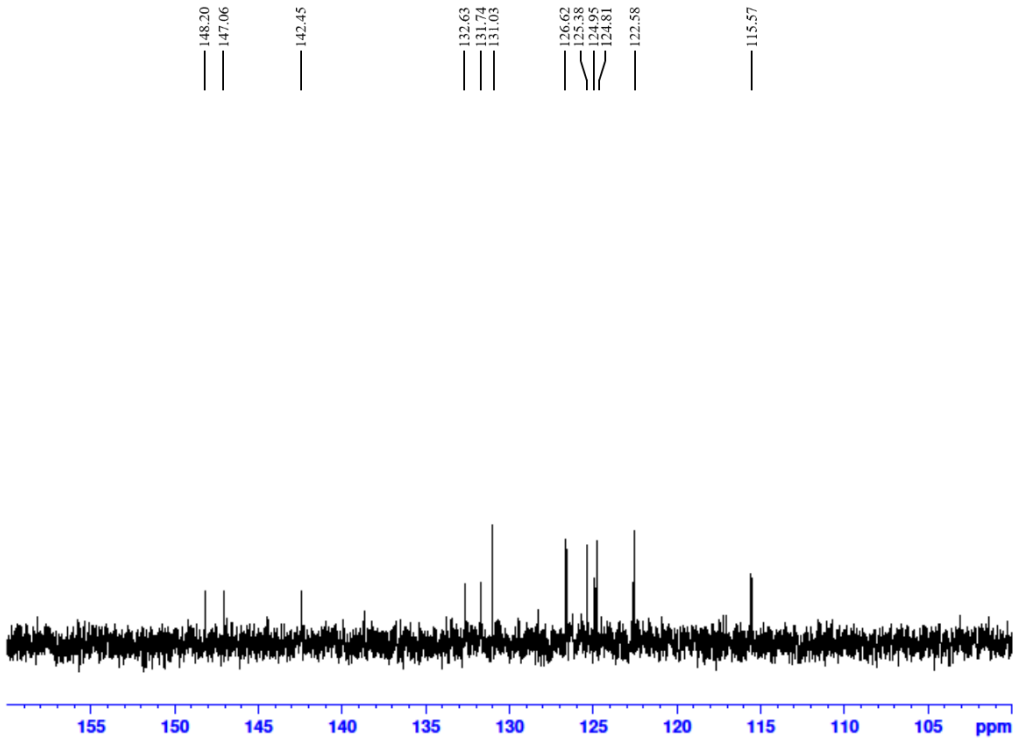

Figure 3-9. ^{13}C NMR spectrum (100 MHz, $CDCl_3$) of **mMBPc**.

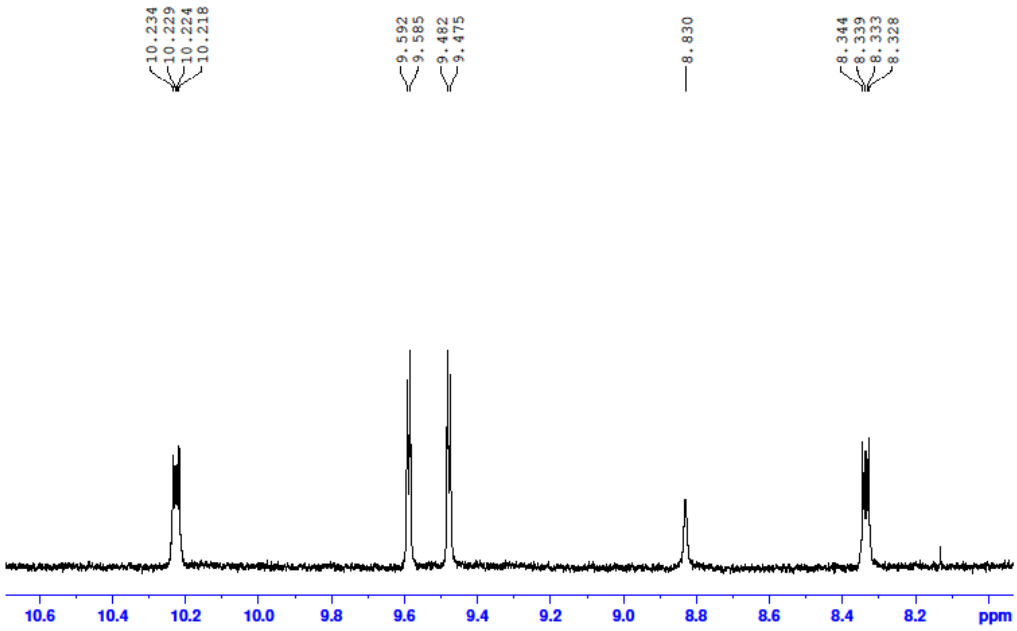

Figure 3-10. ^{1}H NMR spectrum (600 MHz, DMSO-d_6, 333 K) of **mDBPc**.

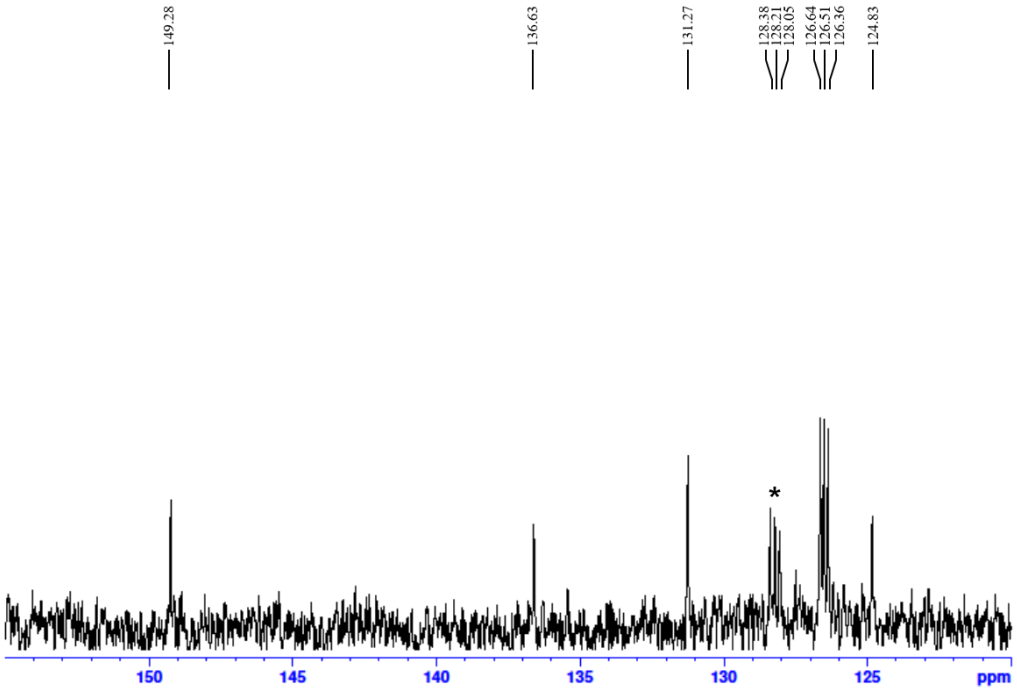

Figure 3-11. ^{1}H NMR spectrum (150 MHz, DMSO-d_6, 333 K) of **mDBPc**. Asterisk (*) is an impurity signal.

References and notes

1. E. Vogel, M. Köcher, H. Schmickler and J. Lex, *Angew. Chem. Int. Ed.* 1986, **25**, 257-259.
2. J. Waluk in *Handbook of Porphyrin Science, Vol. 7* (Eds.: K. M. Kadish, K. Smith and R. Guilard), World Scientific, Singapore, 2010, pp. 359-435.
3. (a) J. Waluk, *Acc. Chem. Res*. 2006, **39**, 945-952. (b) A. Vdovin, J. Sepioł, N. Urbańska, M. Pietraszkiewicz, A. Mordziński and J. Waluk, *J. Am. Chem. Soc*. 2006, **128**, 2577-2586. (c) M. Gil, J. Dobkowski, G. Wiosna-Sałyga, N. Urbańska, P. Fita, C. Radzewicz, M. Pietraszkiewicz, P. Borowicz, D. Marks, M. Glasbeek and J. Waluk, *J. Am. Chem. Soc*. 2010, **132**, 13472-13485. (d) B. Wehrle, H.-H. Limbach, M. Köcher, O. Ermer and E. Vogel, *Angew. Chem. Int. Ed.* 1987, **26**, 934-936.
4. (a) S. E. Braslavsky, M. Müller, D. O. Mártire, S. Pörting, S. G. Bertolotti, S. Chakravorti, G. Koç-Weier, B. Knipp and K. Schaffner, *J. Photochem. Photobiol. B* 1997, **40**, 191-198. (b) J. C. Stockert, M. Canete, A. Juarranz, A. Villanueva, R. W. Horoin, J. I. Borrell, J. Teixido and S. Nonell, *Curr. Med. Chem.* 2007, **14**, 997-1026.
5. (a) K. Oohora, Y. Kihira, E. Mizohata, T. Inoue and T. Hayashi, *J. Am. Chem. Soc*. 2013, **135**, 17282-17285. (b) T. Matsuo, D. Murata, Y. Hisaeda, H. Hori and T. Hayashi, *J. Am. Chem. Soc.* 2007, **129**, 12906-12907. (c) C. J. Fowler, J. L. Sessler, V. M. Lynch, J. Waluk, A. Gebauer, J. Lex, A. Heger, F. Zuniga-Y-Rivero and E. Vogel, *Chem. Eur. J.* 2002, **8**, 3485-3496. (d) T. Hayashi, K. Okazaki, N. Urakawa, H. Shimakoshi, J. L. Sessler, E. Vogel and Y. Hisaeda, *Organometallics* 2001, **20**, 3074-3078. (e) W.-C. Lo, C.-M. Che, K.-F. Cheng and T. W. Mak, *Chem. Commun.* 1997, 1205‑1206. (f) K. Oohora, H. Meichin, L. Zhao, M. W. Wolf, A. Nakayama, J. Hasegawa, N. Lehnert and T. Hayashi, *J. Am. Chem. Soc*. 2017, **139**, 17265-17268.
6. (a) N. Ono, H. Yamada, T. Okujima in *Handbook of Porphyrin Science, Vol. 2* (Eds.: K. M. Kadish, K. Smith and R. Guilard), World Scientific, Singapore, 2010, pp. 1‑102. (b) O. S. Finikova, S. E. Aleshchenkov, R. P. Briñas, A. V. Cheprakov, P. J. Carroll and S. A. Vinogradov, *J. Org. Chem*. 2005, **70**, 4617-4628.
7. D. Sánchez-García and J. L. Sessler, *Chem. Soc. Rev*. 2008, **37**, 215-232.
8. (a) E. Vogel, *Pure Appl. Chem.* 1993, **65**, 143-152. (b) J. Dobkowski, V. Galievsky, A. Starukhin, E. Vogel and J. Waluk, *J. Phys. Chem. A* 1998, **102**, 4966‑4971.
9. V. Roznyatovskiy, V. Lynch and J. L. Sessler, *Org. Lett.* 2010, **12**, 4424‑4427.
10. T. Sarma, P. K. Panda, P. T. Anusha and S. V. Rao, *Org. Lett*. 2011, **13**, 188-191.
11. (a) D. Kuzuhara, J. Mack, H. Yamada, T. Okujima, N. Ono and N. Kobayashi, *Chem. Eur. J.* 2009, **15**, 10060-10069. (b) D. Kuzuhara, H. Yamada, K. Yano, T. Okujima, S. Mori and H. Uno, *Chem. Eur. J*. 2011, **17**, 3376-3383. (c) D. Kuzuhara, H. Yamada, S. Mori, T. Okujima and H. Uno, *J. Porphyrins Phthalocyanines* 2011, **15**, 930-942.
12. The alkyl, aryl and acetoxy substituents of porphycenes at *meso* positions are available: (a) E. Vogel, M. Kocher, J. Lex and O. Ermer, *Isr. J. Chem*. 1989, **29**, 257-266. (b) K. S. Anju, S. Ramakrishnan, A. P. Thomas, E. Suresh and A. Srinivasan, *Org. Lett*. 2008, **10**, 5545-5548. (c) I. Czerski, A. Listkowski, J. Nawrocki, N.

Urbanska, H. Piwonskia, A. Sokołowski, O. Pietraszkiewicz, M. Pietraszkiewicz and J. Waluk, *J. Porphyrins Phthalocyanines* 2012, **16**, 589-602. (d) M. Taneda, A. Tanaka, H. Shimakoshi, A. Ikegami, K. Hashimoto, M. Abe and Y. Hisaeda, *Tetrahedron Lett.* 2013, **54**, 5727-5729.

13. J. Hasegawa, K. Takata, T. Miyahara, S. Neya, M. Frisch and H. Nakatsuji, *J. Phys. Chem. A* 2005, **109**, 3187-3200.
14. W.-M. Dai and W. L. Mak, *Tetrahedron Lett.* 2000, **41**, 10277-10280.
15. Deprotection of **11** was first employed before the Vilsmeier-Haack reaction because the reactivity of 3-dimethylaminoacrolein is relatively low.
16. M. Pietrzak, M. F. Shibl, M. Bröring, O. Kühn, H.-H. Limbach, *J. Am. Chem. Soc.* 2007, **129**, 296-304.
17. A. Ghosh, J. Moulder, M. Bröring and E. Vogel, *Angew. Chem. Int. Ed.* 2001, **40**, 431-434.
18. Although the asymmetric structure of **mMBPc** theoretically generates four distinct signals for the nitrogen atoms in the XPS spectrum, only two resolved peaks were observed because of the low experimental resolution.
19. Under specific conditions, such as porphycene on a Cu(111) surface, the *cis* form was directly observed by STM; T. Kumagai, F. Hanke, S. Gawinkowski, J. Sharp, K. Kotsis, J. Waluk, M. Persson and L. Grill, *Nat. Chem*. 2014, **6**, 41-46.
20. Corphycene and 10-heterocorroles were reported as porphyrinoid compounds with the *cis* tautomeric isomers: a) J. L. Sessler, E. A. Brucker, S. J. Weghorn, M. Kisters, M. Sch.fer, J. Lex and E. Vogel, *Angew. Chem. Int. Ed*. 1994, **33**, 2308-2312. (b) D. Sakow, B. Bcker, K. Brandhorst, O. Burghaus and M. Brcring, *Angew. Chem. Int. Ed.* 2013, **52**, 4912-4915.
21. J. Waluk, M. Muller, P. Swiderek, M. Kocher, E. Vogel, G. Hohlneicher and J. Michl, *J. Am. Chem. Soc*. 1991, **113**, 5511-5527.
22. A DFT calculations (B3LYP/6-31G**) for *meso*-tetramethylporphycene suggest that the *trans* form is more stable by 0.7 kcal·mol^{-1} than the *cis* form.[3b]
23. (a) A. D. J. Becke, *Chem. Phys.* 1993, **98**, 5648-5652. (b) J.-D. Chai and M. Head-Gordon, *Phys. Chem. Chem. Phys.* 2008, **10**, 6615-6620.
24. Gaussian 09, Revision D.01: M. J. Frisch, G. W. Trucks, H. B. Schlegel, G. E. Scuseria, M. A. Robb, J. R. Cheeseman, G. Scalmani, V. Barone, B. Mennucci, G. A. Petersson, H. Nakatsuji, M. Caricato, X. Li, H. P. Hratchian, A. F. Izmaylov, J. Bloino, G. Zheng, J. L. Sonnenberg, M. Hada, M. Ehara, K. Toyota, R. Fukuda, J. Hasegawa, M. Ishida, T. Nakajima, Y. Honda, O. Kitao, H. Nakai, T. Vreven, J. A. Montgomery Jr., J. E. Peralta, F. Ogliaro, M. Bearpark, J. J. Heyd, E. Brothers, K. N. Kudin, V. N. Staroverov, R. Kobayashi, J. Normand, K. Raghavachari, A. Rendell, J. C. Burant, S. S. Iyengar, J. Tomasi, M. Cossi, N. Rega, M. J. Millam, M. Klene, J. E. Knox, J. B. Cross, V. Bakken, C. Adamo, J. Jaramillo, R. Gomperts, R. E. Stratmann, O. Yazyev, A. J. Austin, R. Cammi, C. Pomelli, J. W. Ochterski, R. L. Martin, K. Morokuma, V. G. Zakrzewski, G. A. Voth, P. Salvador, J. J. Dannenberg, S. Dapprich, A. D. Daniels, Ö. Farkas, J. B. Foresman, J. V. Ortiz, J. Cioslowski and D. J. Fox, Gaussian, Inc., Wallingford CT, 2009.

Conclusions

Despite the expected attractive properties, the application of porphyrinoids has not been well-studied because of the synthetic difficulty in chemical modification of the structure. In this context, the author has employed three unique porphyrinoid frameworks as potential candidates: tetradehydrocorrin, bipyricorrole and porphycene. In this thesis, the porphyrinoid modifications were achieved by overcoming the synthetic problems to investigate the reactivity and physicochemical properties.

In Chapter 1, the introduction of an aryl group into each *meso*-position of the tetradehydrocorrin framework was achieved and the corresponding cobalt(II) complex (**Co(II)TDHC**) was utilized as a catalyst for small molecule activation to decrease an overpotential value of the reaction. Electrochemical measurements revealed that a Co(I) species in the complex is significantly stabilized by the monoanionic tetradehydrocorrin ligand relative to that in a cobalt(II) complex of dianionic tetraphenylporphyrin. However, controlled-potential electrolysis experiments with **Co(II)TDHC** promoted a thermodynamically favorable H_2 evolution rather than CO_2 reduction. The present study suggests that large stabilization of the low-valent species is unfavorable for a selective CO_2 reduction reaction, although the strategy to generate a low-valent species by a monoanionic porphyrinoid ligand is effective to produce an electrocatalytically active species with small overpotential.

In Chapter 2, a relatively reactive Co(I) species was successfully generated by employing a monoanionic bipyricorrole ligand, where a bipyrrolic moiety in the tetradehydrocorrin framework is replaced with a bipyridine moiety. The cobalt(II) complex of the bipyricorrole, **Co(II)BIPC**, was found to catalyze a CO_2-to-CO reduction along with negligible H_2 evolution. The pseudo-pH regulation experiments indicate that the difference in the reaction rates between CO_2 reduction and H_2 evolution catalyzed by **Co(II)BIPC** leads to the reaction selectivity. Furthermore, catalytic Tafel plots revealed that the finely designed monoanionic porphyrinoid ligand is useful for decreasing an overpotential value of the electrochemical reaction compared to a dianionic porphyrinoid ligand.

In Chapter 3, a benzene-fused porphycene, *meso*-dibenzoporphycene (**mDBPc**), was synthesized via Suzuki-Miyaura coupling and intramolecular McMurry coupling reactions, which is completely different from the common synthesis of *meso*-unsubstituted porphycene derivatives. **mDBPc** shows significantly red-shifted Q-band compared to unsubstituted porphycene in UV-vis-NIR absorption spectroscopic measurement, which is attributed to a small HOMO-LUMO gap of **mDBPc**. Moreover, it is the first example in porphycene and its derivatives to reveal that the ground state of **mDBPc** adopts the *cis* tautomeric form as a stable isomer.

In conclusion, the author has proved that the porphyrinoid frameworks with appropriate modifications are capable of effectively regulating the reactivity of the metal complex and physicochemical properties. The present findings in this thesis will contribute to the synthesis of an efficient catalyst for small molecule activation and a chromophore to efficiently absorb sunlight energy. Furthermore, the author believes that such progress in porphyrinoid chemistry will open a new way to develop catalysts and materials to address recent requirements especially for realization of an environmentally sustainable society.

List of publications for this thesis

1. Synthesis and Characterization of *meso*-Substituted Cobalt Tetradehydrocorrin and Evaluation of Its Electrocatalytic Behavior Toward CO_2 Reduction and H_2 Evolution
   Ayumu Ogawa, Koji Oohora and Takashi Hayashi
   Inorg. Chem. 2018, **57**, 14644-14652.

2. Electrochemical CO_2 reduction by a cobalt bipyricorrole complex: decrease of an overpotential value derived from monoanionic ligand character of the porphyrinoid species
   Ayumu Ogawa, Koji Oohora, Wenting Gu and Takashi Hayashi
   Chem. Commun. 2019, **55**, 493-496.

3. *meso*-Dibenzoporphycene has a Large Bathochromic Shift and a Porphycene Framework with an Unusual *cis* Tautomeric Form
   Koji Oohora, Ayumu Ogawa, Tamaki Fukuda, Akira Onoda, Jun-ya Hasegawa and Takashi Hayashi
   Angew. Chem., Int. Ed. 2015, **54**, 6227-6230.

Supplementary Publications

4. CuAAC in a Distal Pocket: Metal Active-Template Synthesis of Strapped-Porphyrin [2]Rotaxanes
   Yuta Miyazaki, Christophe Kahlfuss, Ayumu Ogawa, Takashi Matsumoto, Jennifer A. Wytko, Koji Oohora, Takashi Hayashi and Jean Weiss
   Chem. Eur. J. 2017, **23**, 13579-13582.

5. Light Triggers Molecular Shuttling in Rotaxanes: Control over Proximity and Charge Recombination
   Maximilian Wolf, Ayumu Ogawa, Mareike Bechtold, Maxime Vonesch, Jennifer A Wytko, Koji Oohora, Stéphane Campidelli, Takashi Hayashi, Dirk M. Guldi and Jean Weiss
   Chem. Sci. submitted for publication

Acknowledgements

The study presented in this thesis has been carried out at Department of Applied Chemistry, Graduate School of Engineering, Osaka University from April 2012 to March 2015, and from April 2016 to March 2019. The author would like to express his best gratitude to Professor Takashi Hayashi for his continuous guidance, insightful suggestion, constant discussions and warm encouragement throughout this research. The author would like to deeply thank Dr. Koji Oohora for his kind and continuous guidance, valuable suggestions, and helpful discussions. The author also acknowledges Professors Hiroshi Uyama and Takahiro Kozawa for reviewing this thesis and their valuable suggestions.

Acknowledgements are also made to Professor Masahiro Miura and Dr. Yuji Nishii at Department of Applied Chemistry, Graduate School of Engineering, Osaka University for their technical support and valuable discussions on X-ray crystal structural analysis in Chapters 1 and 2.

The author acknowledges Professor Jun-ya Hasegawa at Catalysis Research Center, Hokkaido University for his assistances and helpful discussions on quantum chemical calculations. The author would like to thank Dr. Kyoko Inoue at Analytical Instrument Facility, Osaka University for her kind support and insightful comments for NMR measurements. The author would like to express his gratitude to Professor Shinobu Itoh and Dr. Hideki Sugimoto at Department of Applied Chemistry, Graduate School of Engineering, Osaka University for their technical support on X-ray crystal structural analysis in Chapter 3. The author also acknowledges Simadzu Corporation for their contribution on UV-vis-NIR absorption spectroscopic measurements. The author would like to thank Mr. Kin-ya Katano at Co-Creation Bureau, Osaka University for his technical support and helpful discussions on X-ray photoelectron spectroscopic measurements.

The author would like to express his gratitude to Dr. Akira Onoda for his helpful suggestion and insightful discussion. Acknowledgement is also made to Ms. Kiyomi Lee for her kind help in laboratory life, and all members at Professor Hayashi's group for their discussions, encouragements and friendship.

Finally, the author expresses his great gratitude to his family, Kazuhiko, Kumiko, Izumi, Shiori, and Mii for their heartfelt assistance and encouragements.

Ayumu Ogawa

January 2019